ELECTRONIC RESONANCE ENHANCED COHERENT ANTI-STOKES RAMAN SCATTERING TECHNIQUE FOR DETECTION OF COMBUSTION SPECIES AND BIOLOGICAL MOLECULES

A Dissertation

by

SHERIF FAYEZ HANNA

Submitted to the Office of Graduate Studies of
Texas A&M University
in partial fulfillment of the requirements for the degree of

DOCTOR OF PHILOSOPHY

August 2005

Major Subject: Mechanical Engineering

ELECTRONIC RESONANCE ENHANCED COHERENT ANTI-STOKES RAMAN SCATTERING TECHNIQUE FOR DETECTION OF COMBUSTION SPECIES AND BIOLOGICAL MOLECULES

A Dissertation

by

SHERIF FAYEZ HANNA

Submitted to the Office of Graduate Studies of
Texas A&M University
in partial fulfillment of the requirements for the degree of

DOCTOR OF PHILOSOPHY

Approved by:

Co-Chairs of Committee,	Jerald Caton
	Robert Lucht
Committee Members,	George Welch
	Kalyan Annamalai
Head of Department,	Dennis O'Neal

August 2005

Major Subject: Mechanical Engineering

ABSTRACT

Electronic Resonance Enhanced Coherent Anti-Stokes Raman Scattering Technique for Detection of Combustion Species and Biological Molecules. (August 2005)

Sherif Fayez Hanna, B.S., Cairo University; M.S., Texas A&M University

Co-Chairs of Advisory Committee: Dr. Jerald A. Caton
Dr. Robert P. Lucht

The application of electronic-resonance enhanced (ERE) coherent anti-Stokes Raman scattering (CARS) for the detection of nitric oxide (NO) and acetylene (C_2H_2) is experimentally demonstrated and the effects of various parameters on the ERE CARS signal investigated. In addition, the detection of dipicolinic acid (DPA) using "normal" CARS is demonstrated.

For NO detection, the frequency difference between a visible Raman pump beam and Stokes beam is tuned to a vibrational Q-branch Raman resonance of the No molecule to create a Raman polarization in the medium. The second pump beam is tuned into resonance with the rotational transitions in the (1,0) band of the $A^2\Sigma^+$-$X^2\Pi$ electronic transition at 236 nm, and the CARS signal is thus resonant with transitions in the (0,0) band. A NO gas cell was used for the experiment to detect NO at various pressure levels. A significant resonant enhancement of the NO CARS signal was observed and good agreement between calculated and experimental data was obtained.

For C_2H_2 detection, ERE CARS experiments were performed in a room-temperature gas cell using mixtures of 5000 ppm C_2H_2 in N_2. Visible pump and Stokes

beams were used, with the frequency difference between the pump and Stokes tuned to the 1974 cm^{-1} υ_2 Raman transition of C_2H_2. An ultraviolet probe beam with the wavelengths ranging from 232 nm to 242 nm is scattered from the induced Raman polarization to generate the ERE CARS signal. The effects of probe wavelength and pressure on signal generation are discussed.

CARS was used to detect the 998 cm^{-1} vibrational Raman transition from a sample of polycrystalline DPA. The transition is the breathing ring vibration in the pyridine ring structure in the DPA molecule. The DPA 998 cm^{-1} transition is detected with excellent signal-to-noise ratio and the full-width-at-half-maximum is very narrow, approximately 4 cm^{-1}.

DEDICATION

Dedicated to my dad and mom
For their unconditional love and support over the years

ACKNOWLEDGEMENTS

First, I want to extend my thanks to my research advisor Professor Robert Lucht. I feel greatly indebted to his help, advice and encouragement throughout my research. I am very fortunate for having worked with such a dedicated researcher as well as a wonderful person. It was a true privilege to work in the field of laser diagnostics guided by Professor Robert Lucht, one of the distinguished scientists in this field.

I also want to thank Professor Jerald Caton for his continuous help throughout my Ph.D. studies. His understanding and positive leadership has enabled me to focus on my research without distractions. His support is greatly appreciated.

I gratefully acknowledge the financial support from the Defense Advanced Research Projects Agency (DARPA) and the funding provided by the U.S. Department of Energy, Office of Basic Sciences, Division of Chemical Sciences and the support from the U.S. Army Research Office.

I want to express my appreciation for my friends and coworkers who helped me throughout my research. My first thanks go to Waruna Kulatilaka. We developed the NO ERE CARS experimental system together, and his valuable insights, his great experimental skills as well as theoretical knowledge and sharp observations were invaluable resources for the success of the project. I value him as a coworker as well as a friend.

My thanks go to my colleague and friend Rodolfo Barron-Jimenez. We have worked together on the development of a NO diode laser based sensor. It was a great experience and a true pleasure to work with such an intelligent person. I also extend my

thanks to Thomas N. Anderson. Thomas is an outstanding person with a very promising future. His hard work, dedication and great ideas as well as his great character provide a pleasant atmosphere for team work. On a personal level, he was very supportive during difficult times. I truly appreciate his friendship.

My thanks go also to Mark Gallina. Mark helped me with the data acquisition system by writing a Labview code to hone the CARS experiment into a data acquisition machine. I used this code throughout my research in graduate school. He is a fountain of knowledge in electronics and a very reliable friend. In addition, I want to thank Velur Viswanathan for his contribution in setting up the laboratory and experimental systems and his sincere advice. I appreciate his friendship very much.

I want to thank Kim Moses, who provided me with valuable advice throughout my graduate studies at Texas A&M University. I also want to thank the Mechanical Engineering Department administrative staff, especially Janice Allen and Gina Haddick. Their professional attitude and advice helped me overcome many administrative problems.

On the personal side, the love and support of my dad, my mom and my sisters, Nancy and Mona, can never be overestimated. Their love and support is unconditional and has carried me through the most difficult times and will be always valued and appreciated.

In the end, I want to thank my Lord, Savior and King Jesus Christ for helping me all my life. I firmly trust in Him.

TABLE OF CONTENTS

CHAPTER

LIST OF FIGURES

FIGURE Page

FIGURE Page

FIGURE Page

CHAPTER I

OVERVIEW OVER COHERENT ANTI-STOKES RAMAN SCATTERING (CARS) AND ELECTRONIC-RESONANCE-ENHANCED CARS

The Electronic-Resonance-Enhanced (ERE) Coherent Anti-Stokes Raman scattering (CARS) technique is used in this thesis to detect and experimentally detect nitric oxide (NO) and acetylene (C_2H_2) in Chapters II and III, respectively. The first step towards its application to dipicolinic acid (DPA) involves performing conventional CARS experiments on DPA crystals, as presented in Chapter IV. ERE CARS is a variant of the conventional dual-pump CARS technique and both share many advantages, limitations and basic theory. In this Chapter, the theoretical background of CARS is reviewed with an emphasis on the modifications involved with the ERE CARS technique, the advantages of both techniques are discussed and the experimental considerations of both techniques briefly mentioned in relation to the work presented in this thesis. Eckbreth (1995) and Demtroder (1996) are recommended for in-depth treatments of CARS. In this Chapter, we only outline the more salient aspects of CARS.

1.1. Comparison of CARS with Other Spectroscopic Techniques

The choice of spectroscopic technique for a certain application depends on many factors that have to be evaluated on a case by case basis. In addition to the spectroscopic

---

This dissertation follows the style of *Combustion Science and Technology.*

features offered by each diagnostic technique, the price of experimental system and as well as its complicity play a role in deciding on the system to use. Experimental systems for the CARS technique and its variants are in general more expensive than laser-induced-fluorescence (LIF) or Raman scattering experiments, and more complicated. The spectroscopic features of the CARS technique make it attractive for combustion applications.

Raman scattering and LIF, for example, are incapable of probing the highly luminous particle laden flames, which are typical for many practical combustion applications. This initiated the development of techniques with coherent characteristics, which include CARS. CARS offers major advantages over Raman scattering as briefly outlined in this section The coherent anti-Stokes Raman effect has no threshold. At same conditions, the CARS signals are orders of magnitude stronger than conventional Raman scattering signals. The coherence of the CARS signal permits complete collection and distinguishes it from the background. The demonstrated capability of CARS for measurements in hostile environments as a result of its coherence justifies its utilization. In other conditions, CARS permits single pulse thermometry with laser energies about an order of magnitude smaller than those associated with Raman scattering.

One disadvantage of CARS is its complicated spectroscopic modeling requirements. Compared to Raman scattering, in which spectral synthesis is accomplished easily by an incoherent summation of all transition magnitudes. The spectra acquired by Raman scattering and modeled are relatively insensitive to Raman transition linewidths or precise spectral location. CARS spectra, on the other hand,

exhibits constructive and destructive interference effects and are sensitive to magnitude of the Raman linewidths and the precise spectral locations of the transitions. However, this disadvantage is being overcome with the development of software that emerged commercially in the last year.

One other disadvantage mentioned by Eckbreth (1995) in his treatment of CARS is the line-of-sight optical access. Raman scattering can be detected with a single port, but CARS needs two ports of optical access for signal detection as stated by Eckbreth (1995). We believe that this statement might need reconsideration. In Chapter IV of this thesis, which demonstrates the detection of dipicolinic acid (DPA) by CARS in backscattering configuration, the potential for one optical port use for CARS signal detection is evident.

In comparison with nonlinear Raman techniques, CARS, although not easy, is probably simpler than the other coherent Raman techniques. For example, stimulated Raman gain spectroscopy (SRGS) and Raman-induced Kerr effect spectroscopy (RIKES), encode the signal via beam modulation. In practical media, this approach can be prone to error caused by attenuation from soot, droplets, window fouling or varying refractive effects.

1.2. Theoretical Background

Eckbreth (1995) offered a detailed analysis of the classical treatment for the third order nonlinear CARS susceptibility and the quantum mechanical approach to develop an expression for it. The quantum mechanical approach is summarized in a number of

reviews by Druet and Taran (1981), Barrett and Begley (1981) and Prior (1984) and the main aspects of this treatment as emphasized by Eckbreth (1995) will be reviewed here as well. One general approach is to use time-dependent theory to compute the average dipole moment originating from the third power of the applied macroscopic electric fields. The bulk polarization $P^{(3)}$ is an average over all molecular orientations multiplied by the number density and the third order susceptibility is identified as the coefficient of various cubic field products. This leads to an expression for the susceptibility containing 48 terms. Each term includes the density matrix element times the factor involving a product of four transition moments over all molecular states, illustrated in Fig. 1.1, divided by three frequency factors containing one of the frequencies or combinations of the frequencies of the applied fields. As explained by Fujimoto and Yee (1983), there are actually 1728 possible third order terms in the density matrix that could be reduced to 348 terms if only the terms, in which a given field can interact only once, are considered. These terms can be further reduced if we consider that only 48 terms of these oscillate at $\omega_1 - \omega_2 + \omega_0$.

Terms containing one of the frequencies can produce a very large third order nonlinear CARS susceptibility if one of these resides near a single photon absorption, known as electronic resonance CARS. Combinations of the frequencies can produce third order nonlinear CARS susceptibility $\chi^{(3)}$ enhancements when they coincide with Raman resonances or two photon-absorptions. Terms not containing the appropriate frequencies can produce $\chi^{(3)}$ enhancements when they coincide with Raman resonances or two photon absorptions. Terms not containing the appropriate frequency combinations

can be generally ignored. For CARS there are four processes which can contribute to susceptibility at $\omega_3 = 2\omega_1 - \omega_2$. The nonresonant processes result in a slowly varying contribution known as the nonresonant susceptibility, χ_{nr}, which is generally small but very important to CARS spectroscopy. As will be shown in the experimental scans acquired for NO ERE CARS in the following Chapter of this thesis, the nonresonant background can significantly interfere with the CARS signal and complicate the spectral features.

The two photon process is important as an absorption spectroscopy. The Raman resonance process is the most important aspect of CARS. Omitting the detailed derivation outlined by Eckbreth (1995), one arrives at the following expression for the third order non linear CARS susceptibility

$$\chi^{(3)}_{CARS}(-\omega_3,\omega_1,\omega_1,-\omega_2) = \chi_{nr} + \sum_{ab}\chi^{ab}_{R} \quad \ldots\ldots\ldots\ldots\ldots\ldots \quad (1.1)$$

where χ_R^{ba} is given by

$$\chi_R^{ba} \sim \frac{N}{(\omega_{ba}-\omega_1+\omega_2-i\Gamma_{ab})} \times \sum_{n'}\left(\frac{\mu_{an'}\mu_{n'b}}{\omega_{n'a}-\omega_3-i\Gamma_{na}}+\frac{\mu_{an'}\mu_{n'b}}{\omega_{n'b}-\omega_3-i\Gamma_{n'a}}\right)\times\{\sum_n\left(\rho^{(0)}_{aa}-\rho^{(0)}_{nn}\right)$$

$$\left(\frac{\mu_{bn}\mu_{na}}{\omega_{na}+\omega_2-i\Gamma_{na}}+\frac{\mu_{bn}\mu_{na}}{\omega_{na}-\omega_1-i\Gamma_{nb}}\right)\sum_n\left(\rho^{(0)}_{bb}-\rho^{(0)}_{nn}\right)\times\left(\frac{\mu_{bn}\mu_{na}}{\omega_{nb}-\omega_2+i\Gamma_{nb}}+\frac{\mu_{bn}\mu_{na}}{\omega_{nb}+\omega_1+i\Gamma_{nb}}\right)\cdots$$

$$\ldots\ldots\ldots\ldots\ldots\ldots\ldots\ldots\ldots\ldots \quad (1.2)$$

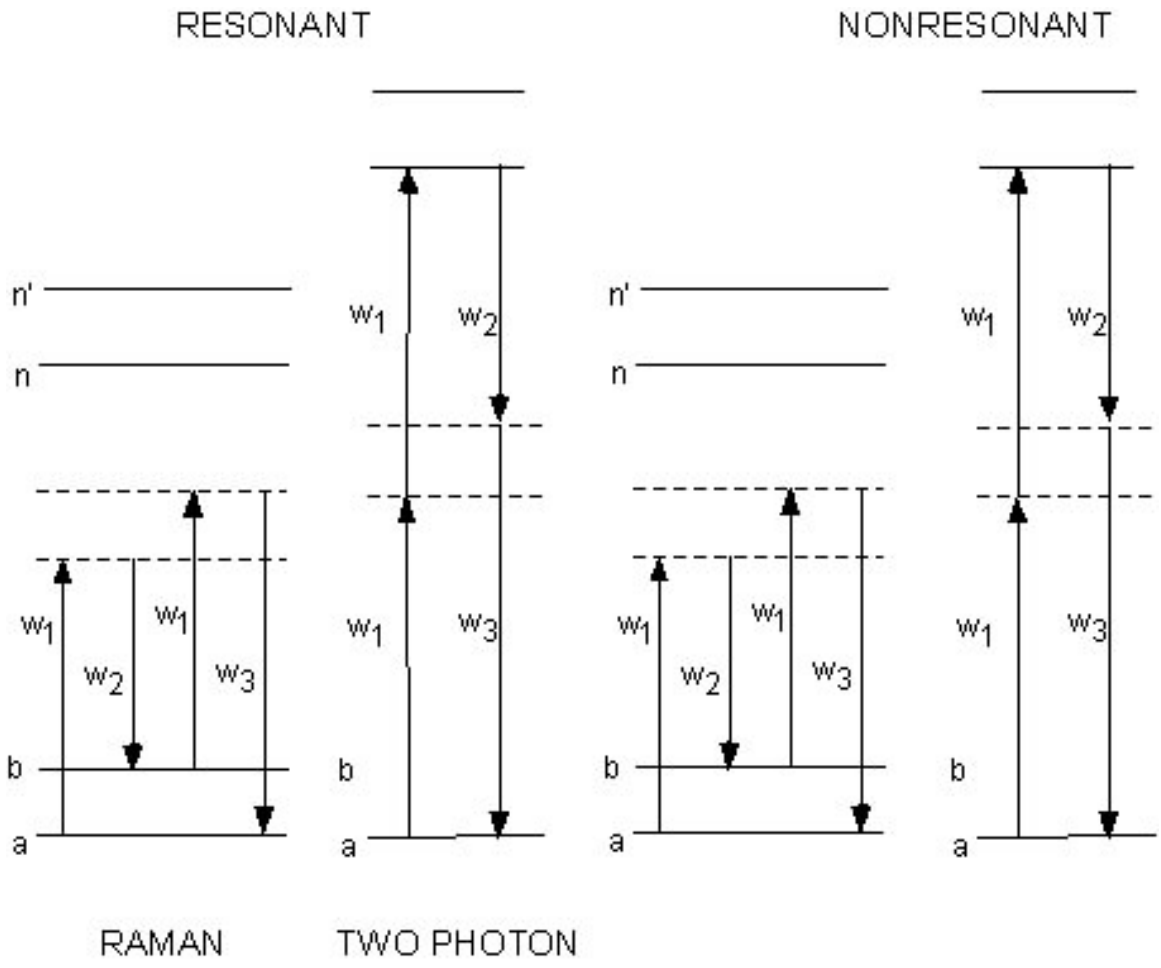

Fig.1.1. Various wave-mixing combinations contributing to CARS. Virtual and real states are indicated by dashed and solid lines (Eckbreth, 1995). Reprinted with permission from *Laser Diagnostics for Combustion Temperature and Species* by Eckbreth, A.C., 2nd Edition, 1995, Gordon and Breach, Amsterdam, The Netherlands. Copyright 1995 by Gordon and Breach.

where N is number density, μ the electric dipole matrix element between the states denoted, ρ the depolarization ratio between two states and Γ is the damping constant and related to the Raman linewidth through $\Delta\upsilon_R = \Gamma / 2\Pi$.

In absence of one-photon electronic resonance, Nibler and Knighten (1979) reduced the above equation for the resonant electronic CARS susceptibility to

$$\chi_{CARS} = \frac{8\pi^2 n_1 \varepsilon_0 c^4 \left(N_a - N_b\right)\frac{\partial\sigma}{\partial\Omega}}{n_2 \hbar \omega_2^4 \left(\omega_j - \omega_1 + \omega_2 - i\frac{\Gamma_{ab}}{2}\right)} \quad \ldots\ldots\ldots\ldots\ldots\ldots\ldots\ldots\ldots\ldots\ldots\ldots\ldots\ldots \quad (1.3)$$

where n is the number density, ε_0 permittivity of free space, ħ Planck's constant / 2Π and $\partial\sigma/\partial\Omega$ is the differential cross section.

The basis for diagnostic utilization becomes apparent in examining equation 1.3 since the susceptibility is both density and temperature dependent. If the detuning of the frequency is defined as $\Delta\omega_j = \omega_j - (\omega_1 - \omega_2)$, equation 1.3 can be rewritten as

$$\chi_{CARS} = K_j \frac{\Gamma_j}{2\Delta\omega_j - i\Gamma_j} \quad \ldots\ldots\ldots\ldots\ldots\ldots\ldots\ldots\ldots\ldots\ldots\ldots\ldots\ldots\ldots\ldots\ldots\ldots \quad (1.4)$$

where $K_j = \frac{(4\pi)^2 n_1 \varepsilon_0 c^4 N \Delta_j}{n_2 \hbar \omega_2^4 \Gamma_j}\left(\frac{\partial\sigma}{\partial\Omega}\right)_j$ ……..…….... (1.5)

with Δ_j defined as the fractional population difference between the states involved in the wave mixing. At resonance $\Delta\omega_j = 0$. Considering the fact that there are a multitude of Raman resonance transitions and accounting for the nonresonant susceptibility, the full CARS susceptibility may be expressed as

$$\chi_{CARS} = \sum_j \frac{K_j \Gamma_j}{2\Delta\omega_j - i\Gamma_j} + \chi_{nr} \quad \ldots\ldots\ldots\ldots\ldots\ldots\ldots\ldots\ldots\ldots\ldots\ldots\ldots\ldots\ldots\ldots\ldots\ldots\ldots\ldots \quad (1.6)$$

Yarkoni and Prior (1984) termed the CARS susceptibility in equation 1.6 the population susceptibility which can only be used for wave mixing frequencies far from electronic transitions. In the vicinity of electronic resonances, the 48 term expression must be employed; fortunately, just a few terms are predominant. To investigate electronic resonance CARS we have to examine equation 1.2. The effect of detuning into various electronic resonances is quite apparent in this equation. The Raman and anti-Stokes electronic resonances multiply the term in brackets containing the state population densities. The pump laser ω_1 resonance with ω_{na} is very important due to the weighting of the $\rho_{aa}^{(0)}$ than the Stokes laser ω_2 resonance with ω_{nb} which detracts from the susceptibility and is weighted by the upper vibrational level population, $\rho_{bb}^{(0)}$ in the ground electronic state. These resonances simplify the spectroscopy since a few dominant lines emerge in the CARS spectrum from all the transitions possible. Druet et al. (1978) emphasized that the perturbation expression for the third order susceptibility in equation 1.2 will not be applicable if the pump and Stokes intensities give rise to saturation and corrective terms may be applied. Except for the enhancement in the susceptibility, all of the features of resonance CARS are similar to conventional CARS. The equation of growth, treated in depth by Eckbreth (1995), and the requirement to phase match the process are the same.

1.3. Experimental Considerations

There is no formal intensity threshold for generating the CARS signal and as such, the experiments can be performed using continuous-wave (cw) laser sources as

demonstrated by Gustafson et al. (1982). With pulsed lasers, there is an imposed threshold, since a measurable number of signal photons needs to be generated during the pulse duration. In time-resolved measurements, the photon count needs to be statistically significant. Although a certain signal generation threshold is absent, high-intensity laser sources are required to generate CARS signals at higher intensity levels than the various sources of interferences. However, there are a number of factors which limit the laser irradiances used to generate the CARS signal. Eckbreth (1995) investigated the wave equation for the Stokes laser beam and examined the growth of the Stokes field. The stimulated Raman gain in which the Stokes wave is amplified via a Raman resonance by an intense pump beam can perturb the Stokes laser amplitude profile and lead to distorted spectra. This effect is generally unimportant at atmospheric pressure and below, but can become a significant factor at elevated pressure levels and should be avoided.

Another limitation on the laser irradiances involved in CARS experiments is the perturbation of the population difference via stimulated Raman pumping between the two quantum states. This is treated in depth by Regnier and Taran (1974). State perturbation will be perturbed if the characteristic time for population pumping is less than or comparable to the laser pulse width. Because the expression for calculating the characteristic time for population pumping involves a product of the pump and Stokes laser irradiances, there is an upper limit imposed on the combination of both irradiances.

Optical breakdown by intense electrical fields of the incident light waves also limits the laser beam energies. This factor is significant in particle-laden combustion

media such as in soot flames, where the focal fluxes cannot exceed a few tens of gigawatts per square centimeter.

The selection of the laser source is an important factor in CARS experiments. Most CARS systems employ a frequency-doubled neodymium: YAG lasers for various reasons. They can be operated at high repetition rates up to 50 Hz, which expedites data collection and permits use of boxcar averagers. At repetition rates higher than 10 Hz, the experiment is nearly cw in behavior. This permits the improvement of the optical alignment of the laser beams at the CARS probe volume while the apparatus is running, a very important feature due to the critical alignment condition of CARS experiments. In addition, because most CARS experiments employ the Nd: YAG laser to generate the Stokes beam as well by pumping a dye laser, the 532-nm output of the Nd: YAG laser can pump very efficiently in the 550 to 700-nm region of the spectrum. Compared to ruby lasers, the CARS radiation from the Nd: YAG resides in a region of higher detection quantum efficiency than does the CARS generated from the 694.3-nm line of ruby.

The Stokes beam may be employed in either narrowband or broadband mode depending on the spectral resolution, sensitivity or temporal resolution desired. For high spectral resolution a tunable, narrowband dye laser is used to generate the Stokes beam. The dye laser is scanned across the Raman transition to generate the CARS spectrum piecewise. The spectral resolution in this case is limited by the linewidths of the laser sources. However, some applications require broadband Stokes beam utilization. In nonstationary and turbulent combustion diagnostics, spectral scanning will result in

distorted spectra weighted towards the high-density, low-temperature excursions due to the nonlinear dependence of the CARS signal in such media on temperature and density. As such, true time average cannot be obtained. To overcome such problems, a broadband Stokes beam source can be used. Although the Stokes beam intensity in the broadband case is less, resulting in weaker CARS signals, it generates the entire CARS spectrum with each pulse. This permits instantaneous measurements of medium properties and the from a time series of instantaneous measurements, the probability function of a given parameter can be assembled and the true time average and magnitude of turbulent fluctuations can be obtained.

Excimer lasers have been used in CARS systems as demonstrated by Marowsky et al. (1986). Their high repetition rates and pulse energies make them attractive to employ, yet the poor beam quality of excimer lasers limits its use to generating the CARS beams rather than being directly used in the CARS generation process. It is used as a pumping source for two dye lasers, one which serves as the pump beam and the other serves as Stokes beam.

Alignment of the three laser beams is critical to the success of the CARS experiment. If the three beams are aligned parallel to each other before being focused in the CARS probe volume, they will cross at the focal point of the lens by definition. However, due to wavefront sphericity and chromatic aberration, the beams will not waist at the crossing point. Adjustable telescopes in the path of two beams, if three different wavelengths are used, are necessary for adjusting the position of the waist. A pinhole of smaller diameter than the smallest beam waist is used as a preliminary alignment tool to

ensure that the three beams cross at the focal point. The telescopes also permit the focal diameter to be varied. In unsteady and turbulent media, the Stokes beam diameter should match or even exceed the pump beam diameter to account for beam steering.

Other factors that influence the CARS experiment and have to be taken into account are the normalization of the CARS signal and single pulse statistics. Normalization of the CARS signal is used to account for effects of pulse-to-pulse laser power fluctuations, long term power drifts, spectral variations of dye power due to decaying dye solution and temporal changes in the optical alignment on the CARS spectrum. Single pulse statistics are used to account for multimode operation of the lasers. Eckbreth (1995) offers a detailed treatment of these factors.

1.4. Dissertation Outline

This dissertation is divided into five chapters. After this brief introduction to coherent anti-Stokes Raman scattering (CARS) in Chapter I, Chapter II presents the results obtained by performing nitric oxide ERE CARS experiments and a detailed discussion of its significance. The numerical and experimental results are compared to show the success of the experiment. The experimental investigation of ERE CARS for acetylene detection is presented in Chapter III, followed by the detection of dipicolinic acid by conventional CARS in Chapter IV and a detailed discussion of its potential for biological agents' detection. The dissertation is concluded in Chapter V with summary of the results and recommendations for future research.

CHAPTER II

ELECTRONIC–RESONANCE–ENHANCED (ERE) COHERENT ANTI-STOKES RAMAN SCATTERING (CARS) SPECTROSCOPY OF NITRIC OXIDE

A three-laser electronic-resonance-enhanced (ERE) coherent anti-Stokes Raman scattering (CARS) technique for the measurement of minor species concentration in combustion processes has been demonstrated by Hanna et al. (2003). The frequency difference between the visible Raman pump beam and Stokes beam is tuned to a vibrational Q-branch Raman resonance of the nitric oxide (NO) molecule to create a Raman polarization in the medium. The ultraviolet probe beam is tuned to a resonance with rotational transitions in the (1,0) band of the $A^2\sum^+$-$X^2\Pi$ electronic transition around 236 nm, and the CARS signal is thus resonant with transitions in the (0,0) band. Significant resonant enhancement of the NO CARS signal was demonstrated and good agreement between theory and experiment was obtained.

2.1. Motivation

Development of new spectroscopic methods for detection of the NO molecule has gained a lot of attention in the last few years. Since the passage of the Clean Air Act in 1970, levels of five of the six most harmful pollutants have decreased in the atmosphere. The concentration levels of the different nitric oxides (NO_x), in contrast,

have increased since that time according to recent reports from the U.S. EPA Office for Air Quality Planning and Standards (2000).

NO and NO_2 molecules are emitted during combustion processes, with NO being the major species in terms of concentration (Colls, 2002). As such, most concentration measurement techniques focus on the NO molecule. In very small quantities, NO plays a significant role in biological processes in human body. An entire journal, NO, is devoted to the study of NO involvement in the different vital body processes. In large quantities, around 50 ppm, NO exposure can slightly agitate the mucous membranes. Between 60-150 ppm the unhealthy effects of exposure to the NO molecule include coughing, shortness of breath, and burning of throat. Above these levels NO can be lethal and deadly, even for short exposure times. The NO molecule also has devastating effects on the environment as it oxidizes to NO_2 which in turn reacts to form ozone and nitric acid, which constitutes the major component of acid rain.

Considering its effects, many regulations have been developed to restrict the emission of NO in combustion streams. This in turn necessitated the advancement of different technologies to detect NO, measure its concentration and to reduce it to an acceptable level. The emission of NO from gas turbines is limited to 9 ppm in many states, for example. One of the major advantages of laser-based technologies is the non-intrusive nature of the methods and the real-time capability of the measurements.

A significant advantage of the ERE CARS technique is its enhanced selectivity due to the requirement of simultaneous vibrational and electronic resonance for signal generation. In our research, a three-color laser technique is used. The probe beam is an

ultraviolet laser beam with the frequency tuned into electronic resonance with specific transitions in the NO molecule. The first pump and the Stokes beam are visible laser beams with frequencies far from resonance with the $A^2\sum^+$-$X^2\Pi$ electronic transition. The wide separation of the frequencies of the pump beam and probe beam is a major advantage for this technique compared to previous ERE CARS experiments that featured the same laser frequency for both the pump and probe beams and with both the pump and Stokes beams at or near the electronic resonance. These previous experiments are well represented by Attal-Tretout et al. (1977), Doerk et al. (1995) and Doerk et al. (1997b).

Another motivation for this research is the need for developing ERE CARS techniques for probing hydrocarbon species. The NO ERE CARS experiments is the first step in developing this technique and gaining experience with the experimental system, as well as evaluate a theoretical model with a well studied molecule like NO. The enhanced selectivity feature becomes more emphasized in detecting hydrocarbon species.

Moreover, the detection for NO by ERE CARS is the first step in developing a detection method for biological spores such as anthrax. Because NO is a well studied molecule and the literature contains numerous papers with its spectroscopic data, it serves as an excellent probe molecule for developing this technique for detection of biological molecules, as discussed in Chapter IV. Scully et al. (2002) propose the use of FAST CARS to detect anthrax, and NO ERE CARS is the first step in this direction.

2.2. Previous Related CARS Research

The ERE CARS technique described in this thesis is a variant of the dual-pump CARS technique developed for the simultaneous detection of two species. Lucht (1987) demonstrated the use of a three-laser CARS technique for simultaneous detection of spectra from two species. In this study, a narrow-band tunable dye laser was used to produce one of the CARS pump beams. The frequency difference between the spectra of the two species was adjusted by changing the frequency of the dye laser pump beam, enabling the spectra to be displayed on the same intensified diode array detector. This in turns permits the determination of the temperature and mole fractions simultaneously. An advantage of this technique is that the relative intensity of the CARS signals is not dependent on the relative intensity of the pump and Stokes beams or on the geometry of beam overlap in the CARS probe volume. Dual-pump CARS is especially attractive for investigating flames with severe temperature gradients and high species concentrations changes.

Lucht et al. (2003) demonstrated the application of dual-pump CARS in measuring the temperature and carbon dioxide concentration in laboratory flames, in a gas cell at room temperature and on an engine test stand in the U.S. Air Force Research Laboratory, Wright-Patterson Air Force Base. A modeless dye laser, a single-mode Nd: YAG laser and an unintensified back-illuminated charge-coupled device digital camera were used to perform these measurements. The CARS measurements were performed on a single-laser-shot basis. The standard deviations of the temperatures and CO_2 mole fractions determined from single-shot dual-pump CARS spectra in steady laminar

propane/air flames were approximately 2% and 10% of the mean values at 2000 K and 0.1, respectively. The precision and accuracy of single-shot temperature measurements and of CARS temperature measurements were comparable to the findings in various literature sources. The application of dual-pump CARS for single-shot measurements in a swirl-stabilized combustor was also demonstrated.

The advantage of the ERE CARS technique presented in this thesis, which features wide separation of the frequencies between the two pump beams and between the Stokes and first pump beam and the resonance, is evident when compared to previous research. These experiments were performed with same laser frequency for both pump beams and with the pump and Stokes beams near electronic resonance. Attal-Tretout et al. (1977) discuss the implementation of the electronically enhanced CARS technique in gases and report the first experimental observation of this effect in I_2 vapor at 1 millibar.

Doerk et al. (1995) applied resonance enhanced CARS with narrow separation of frequencies of the beams to the CH radical produced in a microwave excited Ar/CH_4 plasma. The electronic $A^2\Delta$-$X^2\Pi_r$ transition of the CH radical was probed and rotational lines up to N=15 and υ=2 were measured. Good agreement with previous measurements by application of LIF technique was observed. The study suggested the re-evaluation of the assumption of quadratic density dependence of the integrated CARS signal to account for uncertainties in their measurements. These uncertainties could have been the result of saturation that at the time was roughly accounted for in literature. Due to the relatively good agreement between the rotational temperatures measured with resonant

CARS by Doerk et al. (1995) and LIF measurements in similar environment, the experimental error seems to be tolerable.

Doerk et al. (1997a) extended the investigations mentioned above to test their resonant CARS results more precisely by comparing the results with LIF measurements on the same transition. These measurements delivered a calibration of the resonant CARS system and therefore enabled absolute density determination. One important conclusion of this comparison is the suitability of LIF and resonant CARS for the diagnostics of minor species, and the preference of one technique over the other depends on the experimental limitations. For successful application of LIF, the emission in the spectral region of the LIF signal has to be significantly lower than the LIF signal itself. The saturation of the detection system, in this research a photomultiplier tube, by the luminescence from the plasma or flame, has to be avoided. The quenching effects have to be negligible as well. If conditions are suitable, LIF offers about one order of magnitude higher sensitivity. However, in luminescent flames and plasmas, where LIF is not suitable, resonant CARS is superior.

In other experiments utilizing ERE CARS, the three laser beams frequencies were all in or near electronic resonance. Attal-Tretout et al. (1990) used a resonant CARS system to obtain spectra of the OH radical in high pressure flames. Three separately tunable lasers were used to achieve optimal enhancement, and the spectra observed were fit by using numerical computations. This permitted the estimation of the collisional broadening parameters for one-photon, ground and excited electronic state vibrational Raman transitions. The technique was also used by Attal-Tretout et al. (1990)

for temperature measurements by slight detuning of a single pump laser frequency. The technique proved promising for high pressure flames as concluded from this study.

2.3. Spectroscopic Research on the NO Molecule

The importance of the NO molecule has prompted different research venues in the combustion community to detect the molecule, study its spectroscopic properties or invent methods to reduce its concentration. In this section, we discuss the some notable previous research projects concerning the NO molecule. Many findings published in these research projects were used in our research project. In addition, a general overview over the current NO research will be presented.

The reduction or elimination of the non-resonant background is necessary for detection of minor species using CARS. Rahn et al. (1979) obtained background-free CARS spectra of carbon monoxide in a rich methane-air flame. The principles of background-free CARS were derived and the different polarization techniques used to suppress the background were discussed. The original intent of their research was to demonstrate the capabilities of CARS for measuring minor species concentrations together with temperature when the background is suppressed. These new capabilities were based on manipulation of polarization-dependent properties of CARS signal. Suppressing the non-resonant background led to an increase of signal-to-noise ratio by a factor of two hundred. The method used was applicable in crossed beam, phase-matched geometries and thereby offered at the time the potential of precise spatial resolution. This technique was used later in our experimental system to suppress the non-resonant

background, which led to a significant increase in signal-to-noise ratio as will be discussed.

Laane and Kiefer (1980) theoretically investigated interference effects in the high resolution CARS spectra of gases by calculating the CARS spectra of two individual lines and of the diatomic molecules O_2, N_2 and NO for a number of different linewidths. In high-resolution CARS spectra of the Q-branches of diatomic molecules, considerable interference between the lines occurs due to the contribution of the real part of the susceptibility, causing asymmetry in the band profiles. This interference is subject to variation with the pressure broadening of the linewidths at high and medium pressures and it also depends on the Doppler broadening at low pressures.

Lempert et al. (1984) experimentally measured self-broadened NO Q-branch spectra in the pressure region ranging from 20 to 100 KPa. The J- and Ω- dependent pressure broadening coefficients were determined. The observed collisional narrowing was analyzed using a relaxation matrix theory, in which previous experimental results were incorporated together with theoretical values of NO rates. Assuming the near equivalence of off-diagonal relaxation matrix elements to rates, the fitting law approach was used to reproduce all available spectroscopic data for the NO molecule. Good agreement between experiment and theory was observed. The results obtained by Laane and Kiefer (1980) and Lempert et al. (1984) for the NO molecule were used in this thesis to provide the spectral data needed for performing least-square fits of theoretical spectra to the experimental spectra obtained using ERE CARS.

Huo et al. (1985) observed a large optical Stark effect in the two-photon spectrum $X^2\Pi \rightarrow A^2\Sigma^+$ in the NO molecule. It was explained as a near-resonant process in which the upper state of the two-photon transition is perturbed by interactions with higher-lying electronic states coupled by the laser field. A theoretical method has been developed that should be uniquely applicable to near-resonant Stark effects. Several aspects of the model were found to be essential to reproduce the features in the NO spectra. The time-dependent Schrödinger equation was solved directly since perturbation methods were unsuccessful. Similar observations were made in the ERE CARS results as will be discussed later. It is worth mentioning that Huo et al. (1985) did not discuss different results previously reported in literature by Johnson and coworkers. Further Stark effect studies in the NO molecule were performed by Deng et al. (1997), who measured Stark shifts and broadening on several multiphoton resonant rotational-vibronic levels in NO. The levels and wavelengths were chosen so that the number of ions produced was minimized and complications due to space charge were avoided. The study concluded that the Stark effects are independent of pressure. The same conclusion was previously reported by Pratt (1989) in a lower pressure range. In contrast to former results published in literature, Pratt (1989) reported a constant ac-Stark-broadened linewidth for pressures between 2×10^{-4} and 10 Torr. Pratt (1989) addressed the discrepancy between his results from those of Johnson and coworkers, and attributed the difference to saturation effects.

Pott et al. (1998) used a CARS system to study the reduction of NO by microwave-generated N_2 plasma under atmospheric pressure. The detection of NO at

atmospheric pressure by CARS was limited to 2500 ppm. Using polarization-sensitive background reduction techniques as outlined by Rahn et al. (1979), the detection limit was reduced to 200 ppm.

Doerk et al. (1997b) used folded BOXCARS to detect NO in the atmosphere. The observed NO CARS spectra included the first hot band in temperature range from 300 K to 800 K. The detection limit of NO reported is 25 % in nitrogen under atmospheric pressure. For reasons not fully explained, the down scaling of the signal by polarization techniques was not successful. The weakness of the signal was attributed to the presence of NO_2, which disturbed the measurement because of the strong absorption suffered by the laser beams in the plasma medium. It is worth mentioning that the spectra reported by Doerk et al. (1997b) and Pott et al. (1998) were just barely discernable from the background signal, a problem that we overcame as reported in this thesis and by Hanna et al. (2003).

Collisional studies for the NO molecule were performed by Chang et al. (1992). They investigated the $A^2\Sigma^+$-$X^2\Pi$ electronic transition in the NO molecule, measuring collision-broadening and pressure-shift coefficients in the NO (0,0) band at 226 nm. Data were obtained for nitrogen and argon colliders for variety of different rotational quantum numbers. The results confirmed that the room-temperature broadening coefficient for the NO ultraviolet transitions is very large, approximately a factor of three greater than for ultraviolet transitions of OH. Their measurement of pressure shifts indicated that these too are quite significant and must be considered for high-pressure diagnostic applications. Measurements were performed at room temperature and 2800 K

and in all the profiles, evidence of collision-induced lineshape asymmetries was observed.

Other NO electronic transitions in the ultraviolet have been studied by various researchers. Ebata et al. (1983) used two tunable dye lasers to measure the double-resonance-enhanced four-photon ionization spectra and fluorescence dip spectra of nitric oxide, simultaneously. The spectra showed clear rovibronic structure for the $^2\Sigma^+$ and $^2\Pi$ states in the third-photon region between 65,000 and 70,000 cm^{-1}. Laser power florescence dip and ionization signals were analyzed using kinetic rate equations. The absorption cross sections for various transitions were obtained. In addition, by varying the delay time between the pulses from the first and second dye lasers, Etaba et al. (1983) observed collision-induced rotational relaxation in the $A^2\Sigma^+$ state. The relaxation rate was found to be comparable to the electronic quenching rate.

Piper and Cowles (1986) measured the branching ratio for the NO γ bands. They showed that the electronic transition moment for the NO ($A^2\Sigma^+$-$X^2\Pi$) transition varies by about 40% over the r-centroid range of 1.13-0.97 Angstroms. Combining this transition-moment variation with radiative lifetime measurements they provided a complete set of Einstein coefficients for NO (A-X) transitions for υ' = 0-2.

Wysong et al. (1989) studied the spectral overlap between the O atom two-photon transitions and one-photon O_2 and NO transitions near 226 nm. They were investigating the effect of excitation of photodissociating O_2 levels on measurement of O atoms concentration in flames. They conclude that excitation of O^3P_1 will minimize the photochemical interference in the O-atom measurements.

Wang et al. (1996) excited the gamma system $A^2\Sigma^+$-$X^2\Pi_r$ of nitric oxide isotopomers using an anode glow of a two column hollow cathode discharge tube and recorded the spectra in the spectral region 214 – 273 nm with medium resolution. They reported the gamma system of $^{15}N^{18}O$ and several bands of $^{14}N^{18}O$ for the first time. In addition, the rotational structure of the 0-1, 0-2 and 0-3 bands of $^{15}N^{18}O$ of this system was also recorded with high resolution. The results were analyzed with a global fit using the wavenumbers for the above mentioned states, the infrared vibration-rotation absorption bands of the $X^2\Pi_r$ state from the literature, and an effective Hamiltonian method for the $^2\Pi$ state.

Paul (1997) provides a summary of relations and spectroscopic parameters required for the accurate prediction of transition frequencies and rotational line strengths of the gamma bands of NO. These relations and parameters take into account the effects of finite centrifugal distortion, higher order spin-orbit coupling and lambda-doubling. The magnitude of the correction is found to increase with rotational number to levels of 5-15 % for values of J › 50. The corrections are more important for the satellite as compared to the main branch transitions.

Luque and Crosley (1999a) used dispersed fluorescence scans of the A-X (4, v") and D-X (0, v") progressions of nitric oxide, after two-photon excitation, to determine the electronic transition moments of these band systems. The measured collision free lifetimes of 206 +/- 7 ns for the $A^2\Sigma^+$, v'=0 and 18+/- 1 ns for $D^2\Sigma^+$, v'=0 were used to place transition probabilities on an absolute basis and estimate various cross sections and branching ratios. The two-photon excitation of A–X (4,0) had an unusual intensity

distribution, probably due to interference between the intermediate states in the excitation or due to anomalies associated with photoionization.

Laser-induced-fluorescence (LIF) has been used extensively to measure the concentration of the NO molecule in flames, combustion exhaust streams and in combustion devices, and to obtain additional spectroscopic data for the NO molecule. The group of Prof. Laurendeau and coworkers at Purdue University has performed a series of experiments to probe NO with LIF and selected publications are discussed in this paragraph. Cooper and Laurendeau (2000) report spatially resolved, linear LIF measurements for NO in high pressure spray flames. The laser was tuned to the Q_2 (26.5) transition of the γ (0, 0) band. The resulting fluorescence was detected in a 2-nm region centered on the γ (0, 1) band. The objective of the study was to assess the possible interferences due to oxygen and to evaluate the application of LIF in high pressure flames. Quantitative radial NO profiles were measured at different pressures and analyzed to understand the operation of lean-direct injectors for gas turbines combustors. An empirical relation was obtained from downstream NO measurements in LDI flames to correlate the NO concentration with overall pressure.

Charleston-Goch et al. (2001) performed NO concentration measurements using LIF in flames fueled with synthesized coal-gas, The flame temperatures varied from 1535 to 1790 K and the pressures were between 1.0 and 12 atm. Detailed analysis to establish the relation between the NO concentration and the air-to-fuel ratio, type of fuel, flow rate and axial distance was performed in the burnt gas for a series of laminar, premixed, low calorific value gas flames containing H_2, CO and CH_4 as the combustible

species. The results were compared to the results of two different kinetic mechanisms to examine the validity of these mechanisms for the regimes investigated.

Naik and Laurendeau (2002) measured the NO concentration using the LIF technique in counter-flow diffusion flames at atmospheric pressure, utilizing methane as the fuel. Different levels of nitrogen were injected into the fuel stream or into the oxidizer stream and the flames were investigated at a 20 s^{-1} strain rate. The NO molecule was excited at 224.45 nm in the γ (0,0) band. The results were modeled using OPPDIF with GRI Mech-3.0. The excitation scans indicate no significant change in the background for oxygen-rich as compared to air-rich flames with no notable interference from other species. Axial profiles of NO were also obtained. Good agreement between model and experiment was obtained for temperatures below 2600 K. Above this temperature the agreement between model and experiment was not as good due to radiative heat loss and soot formation, suggesting the need for a combined soot formation and radiation model for these flames.

Khadiya and Glumac (2001) obtained NO profiles in $H_2/O_2/NH_3$ stagnation point flames using LIF measurements for a wide range of equivalences ratios and substrate temperatures. The flames were stabilized against platinum substrates. The NO LIF measurements were used to investigate and optimize gas-phase and surface chemical models of NO destruction. The experimental results were compared with a one-dimensional stagnation flow model that incorporates full gas-phase chemistry, multicomponent transport and detailed surface chemistry. Good agreement was obtained

for a limited range of operating conditions. At low temperatures, the mechanism underpredicts the NO removal rate, while at high temperatures it does the opposite.

Bessler et al. (2002) used planar laser-induced fluorescence (PLIF) images to measure NO concentrations in premixed laminar flames from 1-60 bar by exciting the A-X (0,0) band. The effects of various factors on LIF measurements of NO concentrations such as the gas composition, oxygen molecule interference, variation of local temperature and laser attenuation were studied. The interference from the oxygen molecule was found to produce an error of 25% in a lean 60 bar flame, which brings into question the effectiveness of the supposedly minimum O_2 – LIF contribution scheme used for NO detection. The dependence of the NO concentration on the temperature was found to be lower than 15%, which was attributed to the fact that different effects cancel out. Bessler et al. (2002) reported a 40% error in NO concentration due to laser and signal attenuation by interacting gases such as CO_2 and by water vapor, despite the small scale of the flame in their experiment. The latter finding has prompted research to understand the dynamic range of the correction needed to minimize errors.

2.4. Sensor Technology and UV Generation Methods

Due to strict environmental regulations regarding the emission of NO from combustion processes and the continuous development of new versions of gas turbines, the need for on-site sensors for continuous NO concentration measurements and the measurement of pollutant concentration as a whole, much research activity has been devoted to the development of NO sensor technology. A good overview of the main types

of NO sensors can be found in a Vaught Engineering Corporation report (1999). Anderson (2003) provides an excellent overview of the advantages of diode-laser-based technologies. Diode-laser-based sensors offer the potential for continuous, real-time measurements of pollutants concentration. This feature makes this sensor technology easy to incorporate into control schemes to optimize the combustion process and minimize emissions, as demonstrated by Furlong et al. (1999). The disadvantage of this technology is that it is expensive in comparison with competing technologies. However, the price of diode lasers has been constantly declining due to the interest of the telecommunication community in diode lasers and the widespread use of these lasers in fiber optic communication.

Compared to CARS or DFWM, diode-laser-based sensor technology is much cheaper and simpler, yet it lack the accessibility to spectral features of NO that is provided by these laser diagnostics methods. Absorption based sensors operating in the IR domain were first used to probe the NO molecule. Many research groups have made measurements in the second overtone (3, 0) absorption band of NO. Sonnenfroh and Allen (1997) used an experimental distributed feedback (DFB) laser operating a 1.8 μm to measure NO in several media. The spectral lines probed were chosen carefully to minimize water vapor interference with the NO spectra. An absorption cell was used for the room temperature measurements, and a hydrogen/air flame, imbedded with NO flow, was used for the high temperature measurements. Although water vapor showed significant interference at the wavelength probed, the sensitivity reported in these experiments was 140 ppm per meter. Several other groups also reported NO measurements using this same wavelength [Kessler

at al. (1997) and Mihalcea et al. (1998)]. These studies differed in flames used and spectral lines probed, selected specifically to minimize water vapor interference, and the sensitivity varied according to the proper selection of spectral lines.

Oh and Stanton (1997) acquired NO spectra in the first overtone (2, 0) absorption band of NO at 2.65 μm. Using a single-mode diode laser cooled by liquid nitrogen at 183 K, they performed sub atmospheric measurements of NO in an absorption cell, probing the Λ-doublet components of the $^2\Pi_{3/2}$ R (16.5) transition of NO in the (2, 0) band. These lines were used to avoid water vapor interference. The detection limit reported was 15 ppm per meter, which was achieved by using modulation spectroscopy.

With the development of quantum cascade (QC) lasers, the range of NO detection shifted to the fundamental absorption band of NO in the mid-IR. The detection limit in these experiments was reduced to low as 3 ppb in a100-m path as demonstrated by Menzel et al. (2001). These low detection limits were achieved only in NO absorption gas cells. The QC lasers also used for cavity ringdown spectroscopy (CRDS) as demonstrated by Kosterev et al. (2001). These low detection limits were achieved only in NO absorption gas cells.

The IR detection of the NO molecule has the advantage of simplicity for the optical system, because no frequency conversion is needed. However, this simplicity compromises the spectral features of the scans for many reasons. The spectra acquired in the IR region for NO suffer from interference with water vapor and CO_2. These are the major components of combustion exhaust streams and therefore isolated NO lines have to be located and probed. Even then, the absorption lines of the other molecules usually

overlap with the isolated line due to high concentrations that broadens the lines. In addition, the IR transitions are relatively weak, especially for overtone transitions.

These shortcomings of IR NO sensors prompted us to develop an NO sensors working in the UV range. Strong energy level transitions in the UV as opposed to weak IR transitions offer higher sensitivity, and the absence of molecules that interfere with the NO spectra in the UV domain enhances selectivity and eliminates interferences. Because no readily available diode laser source for UV radiation exists, different frequency conversion processes have been utilized. Second harmonic generation (SHG) was chosen for the ERE CARS experiment to produce a 236 nm UV beam by frequency doubling the dye laser output at 472 nm. SHG has been previously used by Hancock et al. (2002) to generate UV radiation at 430 nm to probe excited argon atoms. The output of an 860-nm diode laser was doubled in a $KNbO_3$ crystal to obtain this wavelength. Ray et al. (2001) used frequency-quadrupling of a 1064 external cavity diode laser to study the OH molecule at 266 nm. The first stage of frequency-doubling of the 1064 nm radiation to produce 532 nm radiation was performed using a periodically poled lithium niobate (PPLN) crystal, and a beta-barium borate (BBO) crystal was subsequently used to generate 266 nm radiation to allow OH absorption scans at this wavelength. Koplow et al. (1998) measured NO at 215 nm using frequency-quadrupling of a DFB diode-laser-seeded tapered amplifier output at 860 nm, a very expensive device.

However, the need for other frequency techniques presented itself because simple SHG could not produce UV radiation at other wavelengths to probe specific lines such as the 226 nm NO line. Tunable diode lasers (or any compact size lasers) are not available to

scan a wide range. In the ERE CARS experiment, the compact size was not a priority and therefore, the radiation of a dye laser was used and frequency-doubled. In sensor technology however, compact size is key. Another non-linear technique, sum frequency generation (SFG), was utilized to access other NO spectral lines. Corner et al. (2002) probed the OH molecule at 309 nm by sum frequency mixing of a 404-nm diode laser with a 1320-nm DFB laser in a BBO crystal, producing 0.8 nW of UV radiation. Alnis et al. (2000) utilized a BBO crystal to generate 254-nm radiation for detection of mercury atom by sum frequency mixing of the 404-nm and 688-m outputs of separate diode lasers. They report that 0.9 nW of 254-nm radiation were produced.

Lucht and coworkers at Texas A&M University and at Purdue University have used sum-frequency-generation to produce 226-nm radiation for the detection of NO in the UV region. Hanna et al. (2002) developed and demonstrated an all-solid-state continuous-wave laser system for ultraviolet absorption measurements of nitric oxide (NO) molecule. The single-mode, tunable output of a 10-mW, 395-nm external-cavity diode laser (ECDL) was sum-frequency-mixed with the output of a 115-mW, frequency-doubled, diode-pumped Nd: YAG laser in a beta-barium-borate crystal to produce 40 nW of tunable radiation at 226.8 nm. The wavelength of the 395-nm ECDL was then scanned over NO absorption lines to produce fully resolved absorption spectra. Initial results from mixtures of NO in nitrogen in a room temperature gas cell were reported and the estimated NO detection limit of the system for the demonstrated absorption sensitivity of 2×10^{-3} is 0.2 ppm per meter of path length for 300 K. The estimated accuracy of the measurements is +/- 10%.

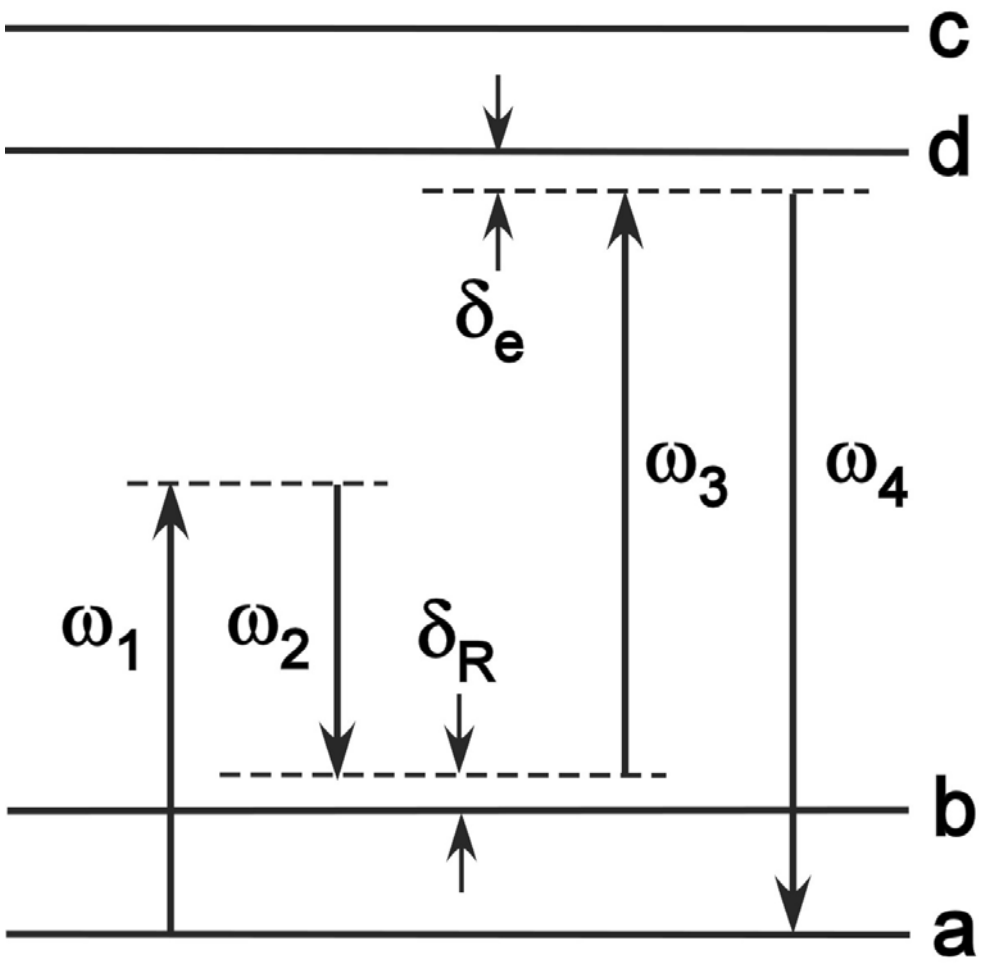

Fig.2.1. Energy level schematic diagram of the dual-pump ERE CARS process.

Anderson et al. (2005) built on the above encouraging results and demonstrated the use of the above NO sensor for field measurements in the exhaust streams of a gas turbine and a well-stirred reactor. Increasing the power to 325 +/- 75 nW of ultraviolet radiation at 226.8 nm, corresponding to the (υ'=0 and υ''=0) band of the $A^2\Sigma^+$-$X^2\Pi$ electronic transition of NO, they were able to demonstrate the full capability of the sensor to resolve the absorption spectrum and accurately measure the NO concentration in actual combustion environments. The sensitivity was estimated to be 0.23% corresponding to a detection limit of 0.8 ppm in 1 m for 1000 K gas. These results are very encouraging and show that the sensor technology for NO detection is very promising. Currently the same group at Purdue is developing a variety of sensors for various combustion species.

2.5. Energy Diagram for ERE CARS for NO Molecule Detection

Figure 2.1 represents the schematic level diagram of the electronic resonance enhanced (ERE) CARS system for NO molecule detection. The first pump beam at ω_1 and the Stokes beam at ω_2 are visible laser beams with frequencies far from resonance with the $A^2\Sigma^+$-$X^2\Pi$ electronic resonance. The second pump beam at frequency ω_3 is at or near electronic resonance. As mentioned before, the wide separation of the frequencies of the first pump and second pump beams distinguishes this experiment from previous ERE experiments. The Raman polarization in the medium is established when the Stokes laser is tuned so that the frequency difference between the first pump beam at ω_1 and Stokes beam at ω_2 is equivalent to a Raman resonance of the NO molecule. The second pump beam at ω_3 scatters from the Raman induced polarization to produce the CARS signal at

$\omega_{CARS.}$ δ_R and δ_e are the detuning from the Raman resonance and the electronic resonances, respectively. The wavelengths of the Stokes beam and the second pump beam are varied to scan the resonance. One wavelength is scanned at a time while the other beam's wavelength is held constant. The wavelengths for NO ERE CARS are approximately 532 nm for the first pump beam, 236 nm for the second pump beam, and 591 nm for the Stokes beam to produce a CARS signal at 226 nm.

2.6. Experimental System

A schematic of the experimental system is shown in Fig 2.2. The laser source for the first pump beam at ω_1 was a Continuum model 9010 injection-seeded, Q-switched Nd: yttritium-aluminum-garnet (YAG) laser with a repetition rate of 10 Hz, pulse length of approximately 7 ns, and pulse energy for the second harmonic production at 532 nm of approximately 750 mJ. During the acquisition of the high-pressure NO ERE CARS scans, the seeder was not working in a consistent manner and its operation had to be monitored regularly on an oscilloscope to judge its performance and its effect on the scan. The 532-nm pump beam was directed through a series of reflections from 532-nm mirrors to the CARS probe volume. Along this path, 85% of the energy of the 532-nm beam was reflected by a beamsplitter to pump a Continuum ND6000 narrowband, tunable dye laser to produce the Stokes beam at ω_2. Before passing through the 15-85% beamsplitter, the output of the 532-nm laser beam was directed through a half-waveplate and polarizer combination to control the energy of both the first pump beam and the Stokes beam.

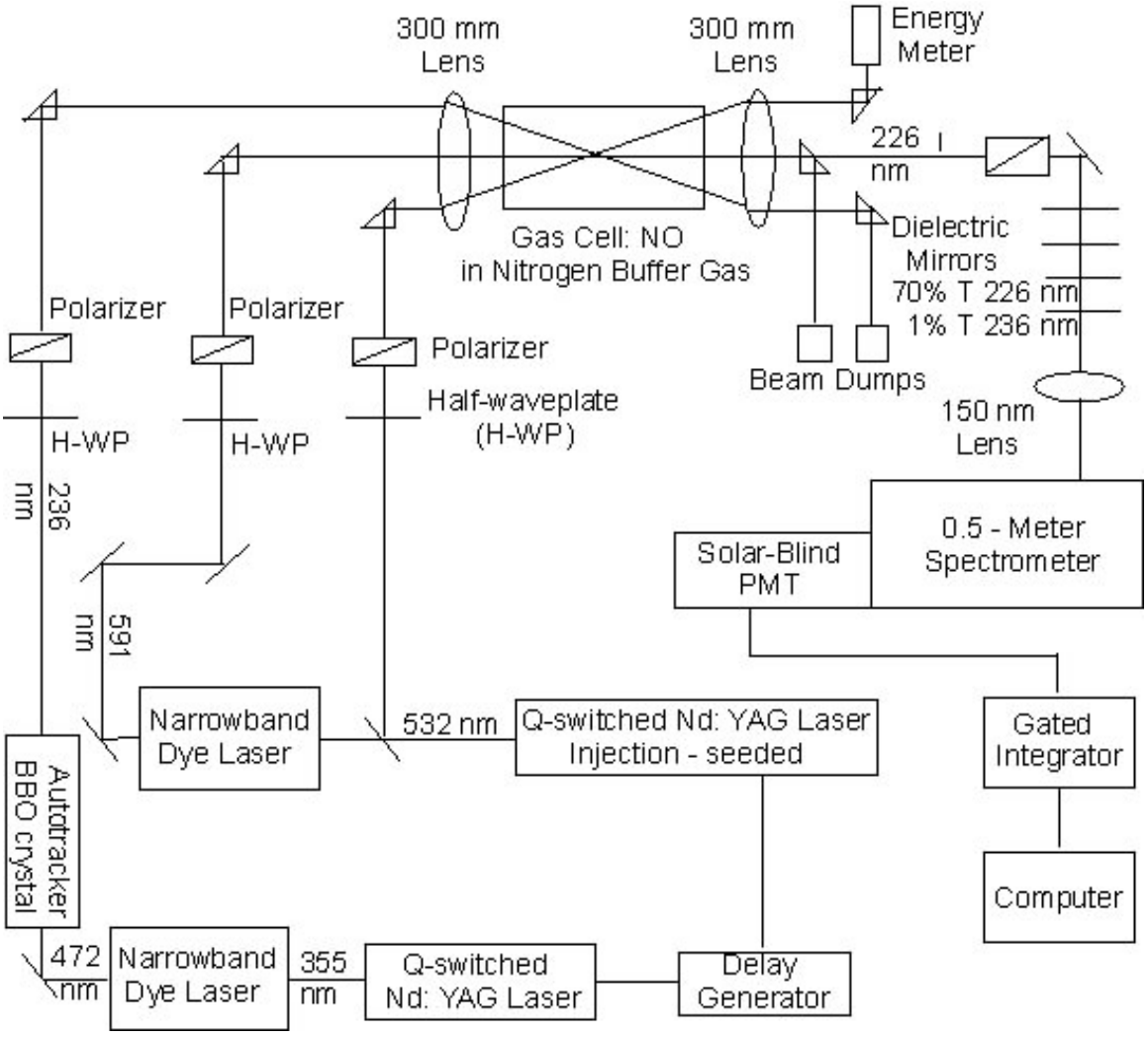

Fig.2.2. ERE CARS system schematic for measurements of NO.

It was necessary to control the laser power in case of breakdown of the medium or saturation of the transition. In addition, separate control of the pulse energy for the 532-nm pump beam was provided through another combination of half-waveplate and polarizer after its passes through the beamsplitter. The 532-nm beam, after passing through the polarizer, becomes linearly polarized with the polarization axis at 60 degrees to the vertical as shown in Fig. 2.3. This polarization is necessary for minimization of the non-resonant background. The first pump beam also passes through a delay line to ensure that all three beams are overlapped in time at the CARS probe volume.

A Continuum ND6000 narrowband, tunable dye laser is pumped by a portion of the 532-nm output from the 9010 Nd: YAG laser to produce the Stokes beam at ω_2 with about 10% efficiency. The laser dye used was Rhodamine 610 (Rh 610), purchased from Exciton, and dissolved in methanol. The concentration of Rh 610 in the oscillator was 214 mg/l and in the amplifier it was 37 mg/l. This dye solution provided excellent durability, efficient conversion of energy and wide tuning range that proved advantageous in the first stages of the experiment, when the wavelength of the Stokes beam for resonance was not precisely determined. The output of the Stokes dye laser was near 591 nm with a frequency bandwidth of approximately 0.08 cm^{-1}. The Stokes beam was directed through multiple reflections by AR-coated prisms to the probe volume. Along the path, it was directed through a half-waveplate and polarizer combination to control its power and to be linearly polarized at 60 degrees to the vertical as shown in Fig. 2.3. This, as mentioned above, polarization was used to suppress the non-resonant background.

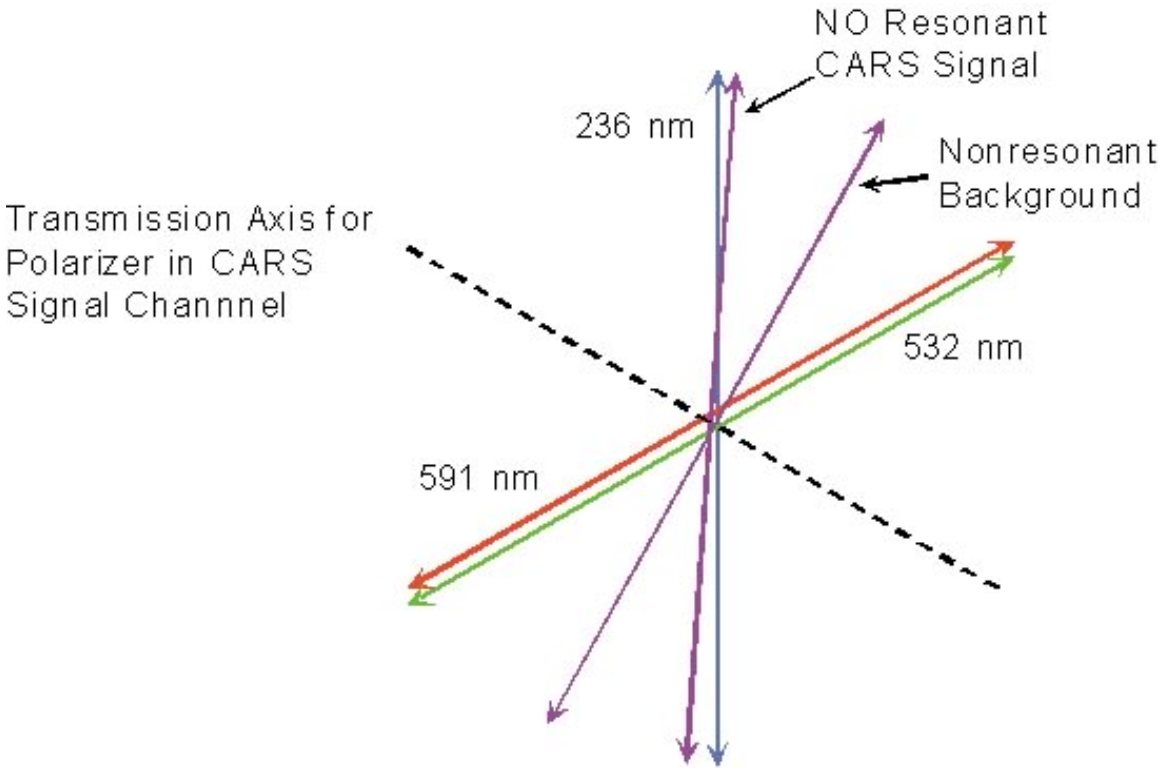

Fig.2.3. Polarization suppression of the nonresonant CARS background contribution.

The second pump beam at 236 nm was generated by frequency-doubling the output of the second narrowband Continuum ND6000 narrowband dye laser. The third harmonic output from a Continuum model 8010 Nd: YAG laser at 355 nm with a pulse energy 350 mJ was used to pump a second Continuum ND6000 dye laser to produce a 472 nm beam. The dye solution used for the dye laser was a solution of LD 490 in methanol. The concentration used for the oscillator was 560 mg/l and the concentration used for the amplifier was 80 mg/l. The LD 490 dye has moderate solubility in methanol and a short lifetime (an hour for pumping energy typical for this experiment) which required multiple changes of dye for multiple CARS scans. For LD 490, according to the data sheet supplied by the supplier Exciton, the wavelength 472 nm lies on the border of the lasing range when pumped with a 355 nm beam, whereas it peaks around 486 nm. This resulted in a poor energy conversion for the dye laser of about 5% and the output at 472 nm was approximately 15 mJ. In spite of the poor energy conversion ratio and the short life time, it provided much superior beam shape, more pulse energy, and longer dye life time than the only other available alternative, the Coumarin dyes.

The frequency-doubling of the 472-nm beam to produce the 236 nm pump beam was accomplished using an INRAD Autotracker III with a beta barium borate (β-BBO) crystal. The estimated frequency bandwidth of the UV pump beam generated was 0.2 – 0.3 cm^{-1}. The 472 nm beam from the dye laser was down-collimated using a two-lens telescope before it entered the Autotracker. The BBO crystal tuning angle was varied through a feedback control system to maintain optimal frequency-doubling as the fundamental dye laser wavelength was scanned. The UV power fluctuations are controlled

through this process, yet not fully eliminated. The speed of changing the BBO tuning angle by the control loop in the Autotracker has to be synchronized with the speed of the dye laser scan.

The UV beam that emerged from the Autotracker was collinear with the fundamental beam at 472 nm. A 243-nm mirror was used to reflect the UV beam at 236 nm and transmit the 472 nm into a beam dump. The UV beam was also directed through a half-wave plate/polarizer arrangement so that the UV beam was vertically polarized for nonresonant background suppression. In the high-pressure NO scans, acquired a year after the low-pressure spectra, this arrangement was also used to keep the UV beam energy steady as the fundamental dye laser power declined during the experiment. The UV energy was set to a low value at the beginning of the scan to avoid saturation of the electronic transition. The half-waveplate was rotated to maintain the UV energy constant as the dye laser power declined. The UV energy was measured using a Molectron Joulemeter and displayed on a Labview program.

The CARS signal was generated using a three-dimensionally phase-matched geometric arrangement. The pulse energies for the 532, 590 and 236-nm beams at the CARS probe volume were on average 30, 20 and 0.1 mJ, respectively. The three beams were focused into the CARS probe volume using a 300-mm lens. To ensure signal generating phase-matching conditions, both Nd:YAG lasers were synchronized using a delay generator and the timing of the three beams at the CARS probe volume was constantly monitored using a digital oscilloscope. The initial alignment of the three beams in the CARS probe volume was performed by modifying the ERE CARS system. A

normal CARS system was used first to detect room nitrogen and the nitrogen CARS signal was maximized. This required a change of dye from Rh 610 to Rh 640 in the Stokes dye laser to produce the 607-nm output necessary to establish the Raman resonance for the nitrogen molecule. It also required the use of beamsplitter on a kinematic mount to produce the second of two 532-nm beams. One of the green beams was passed through the fused silica optics in the UV pump beam path into the CARS probe volume and the three beams were directed through a 100 μm pinhole. This ensured good overlap between the 532 nm pump beam and the Stokes beam. The gas cell was then placed, filled with nitrogen, in the CARS probe volume and misalignment of the beams due to the gas cell windows was corrected. Marking the position of the gas cell, it was removed together with the dual pump CARS optics and the UV beam was focused using the same pinhole to overlap the other two beams. The gas cell was then placed again in its marked position, filled with NO/N_2 gas mixture. The Stokes and UV wavelengths required for resonance were determined after multiple trials.

The gas cell used for this experiment was 0.3 m in length and machined from aluminum. It has two fused silica windows to provide optical access. The overlap of the three beams inside the gas cell was moved close to the exit window to minimize the absorption of the ERE CARS signal at 226-nm by NO.

The ERE CARS beam at 226-nm emerged from the cell above the UV beam and was collimated using a 300-mm lens. The 532-nm beam and the Stokes beam were both directed by prisms into beam dumps. The UV pump beam was directed into a pyroelectric Joulemeter to measure the pulse energy on a shot-by-shot basis. The signal from the

Joulemeter was used to normalize the ERE CARS spectra to account for the UV beam energy fluctuation. Scattering from the 236-nm UV pump beam was a major contributor to the noise in the spectra acquired and had to be minimized. Two 226-nm mirrors in the signal channel were used to raise the ERE CARS beam path to the level of the spectrometer entrance slit, and in the process any scattered light at 532-nm from the first pump beam or at 591-nm from the Stokes beam along the ERE CARS beam path was eliminated. To eliminate UV scattering, apertures were used both along the signal beam path and the 236-nm beam path before the CARS probe volume. In addition, four dielectric mirrors coated for reflection of 215-nm at 45 degrees were placed in the signal channel before the spectrometer. The 215-nm mirrors were used at 0 degrees incidence and had approximately 70% transmittance at 226 nm but less than 1% transmittance at 236-nm. These mirrors served as spectral filters and significantly reduced the background from the 236-nm scattered light. This came at the expense of the ERE CARS signal level, but the drastic increase in the signal-to-noise ratio proved to be an experimental breakthrough in acquiring the ERE CARS spectra that had been dominated by UV scattered light in earlier stages of the experiment. Previously, optical filters from various companies, nominally specified to eliminate the scattered light while transmitting the ERE CARS signal, were tested, but were found to be ineffective in reducing the scattered light.

The ERE CARS signal beam was then focused using a 150-mm lens onto the entrance slit of a 0.5-m spectrometer, and a solar-blind photomultiplier was used to detect the 226-nm ERE CARS signal. The ERE CARS signal and the UV pulse energy were recorded on a shot-by-shot basis using gated integrators while either the Stokes dye laser

wavelength or the 472-nm dye laser was scanned under computer control. A Lab view program was used to acquire the spectra and perform the dye laser scans.

In addition to eliminating the UV scattering, suppression of the non-resonant CARS background proved necessary to obtain meaningful data at low NO concentrations. Polarization techniques were used to suppress the nonresonant four-wave mixing background signal as discussed by Rahn et al. (1979). The polarization arrangement shown in Fig. 2.3 was used. Both the 532-nm pump beam and the 591-nm Stokes beam were linearly polarized with the polarization axis at 60 degrees to the vertical. The ultraviolet pump beam was vertically polarized. The resonant CARS signal generated with this polarization arrangement has a nearly vertical polarization, while the nonresonant background is linearly polarized at 30 degrees to the vertical. An α–BBO polarizer was placed in the ERE CARS signal channel with its transmittance axis perpendicular to the polarization of the nonresonant background, thus drastically reducing the intensity of the nonresonant background. The ERE CARS signal intensity was also reduced, but the signal-to-noise ratio for the ERE CARS signal was significantly increased.

2.7. Results and Discussion

For initial comparison purposes between experimental and theoretical data the Sandia CARS code, developed at the Combustion Research Facility at Sandia National Laboratories for analysis of CARS spectra acquired in combustion experiments and published by Palmer (1989), was used to simulate typical experimental conditions.

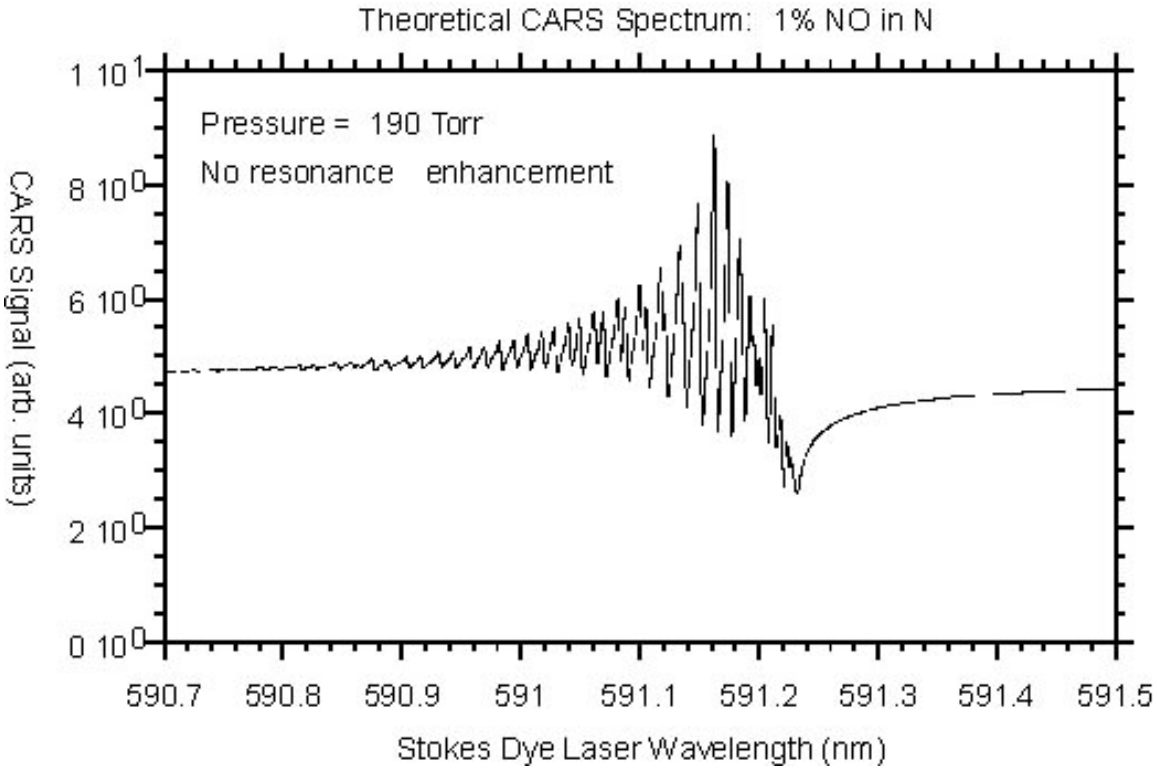

Fig.2.4. Theoretical NO CARS spectrum obtained by Sandia CARS code.

Fig. 2.4 depicts a theoretical spectrum calculated using the Sandia CARS code for a Stokes dye laser scan in the wavelength range shown. The medium is 1% NO gas in nitrogen buffer gas at a pressure of 190 Torr. Electronic resonance is not included in this spectrum and therefore the CARS resonant signal is comparable to the nonresonant four-wave mixing background signal. Because of noise sources present in the experiment, the detection limit in the absence of the electronic resonance enhancement process is estimated to be 1 %.

The effect of electronic resonant enhancement is illustrated by the dramatic change in the NO CARS spectrum as the wavelength of the ultraviolet pump beam is changed from 237.3 nm to 237 nm, as demonstrated in Fig. 2.5 and Fig. 2.6, respectively. At the ultraviolet pump wavelength of 237.3 nm, the NO CARS signal is barely evident and modulated by a nonresonant background of comparable intensity. When the ultraviolet wavelength is changed to 237 nm, a very strong resonant signal is observed. Both spectra were acquired by fixing the ultraviolet wavelength at the given mentioned wavelengths and scanning the dye laser wavelength across the Raman transition. The NO concentration used was 1% NO in nitrogen buffer gas at room temperature and at 295 Torr and 159 Torr, respectively.

The energy level schematic in Fig. 2.1 indicates that ERE CARS spectra can be recorded as a function of the Raman detuning δ_R by scanning the Stokes dye laser wavelength for fixed ultraviolet wavelength or as a function of electronic detuning δ_e by scanning the ultraviolet wavelength for fixed Stokes wavelength. The results of a spectral scan of the ultraviolet pump beam frequency at fixed Raman shift is shown in Fig. 2.7.

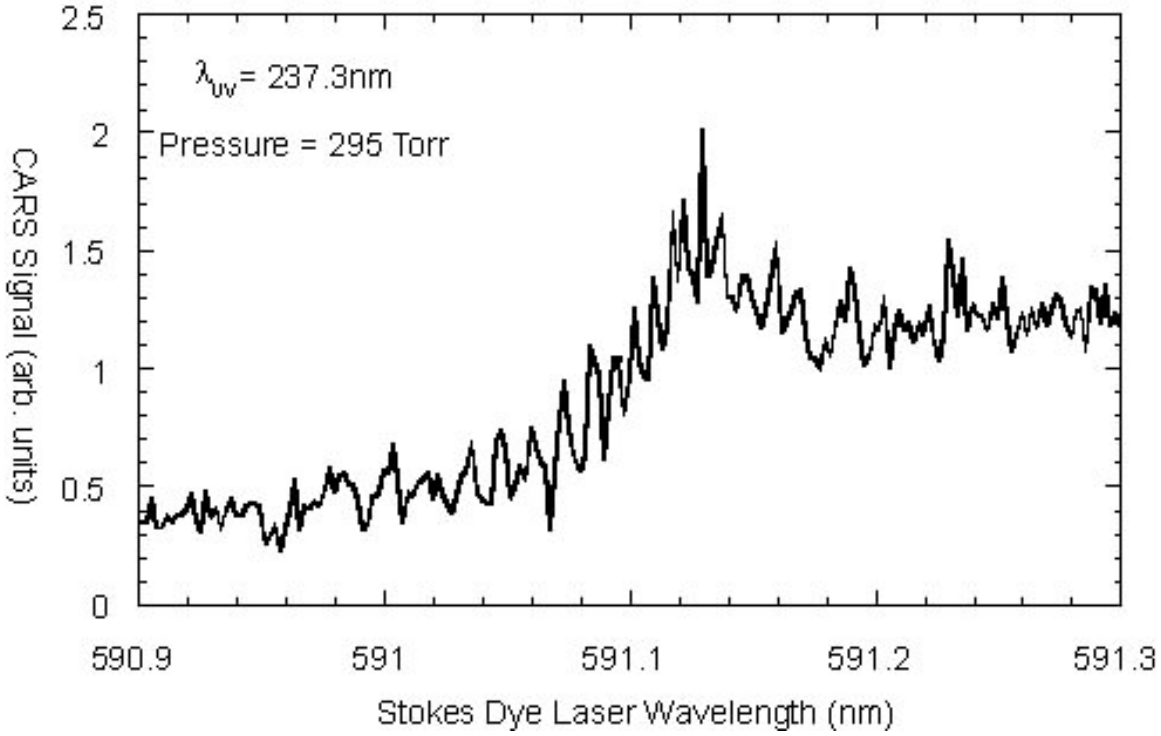

Fig.2.5. NO ERE CARS spectrum recorded at ultraviolet wavelength of 237.3 nm.

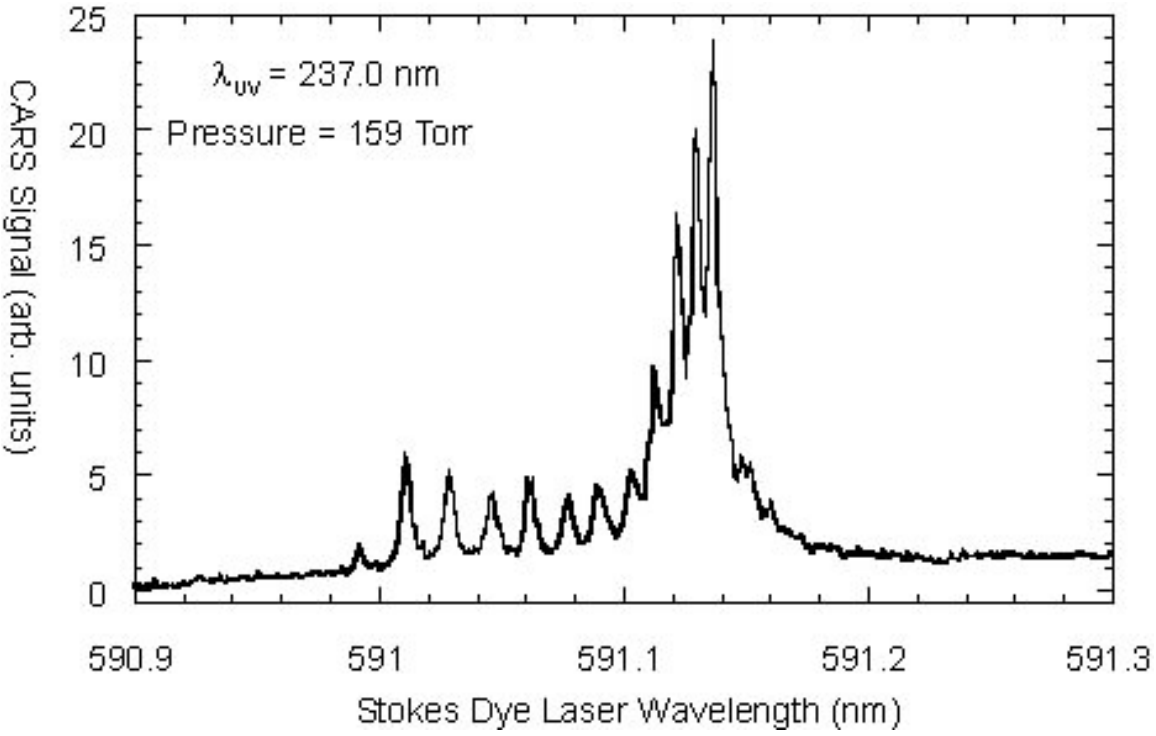

Fig.2.6. NO ERE CARS spectrum acquired with ultraviolet pump wavelength of 237 nm.

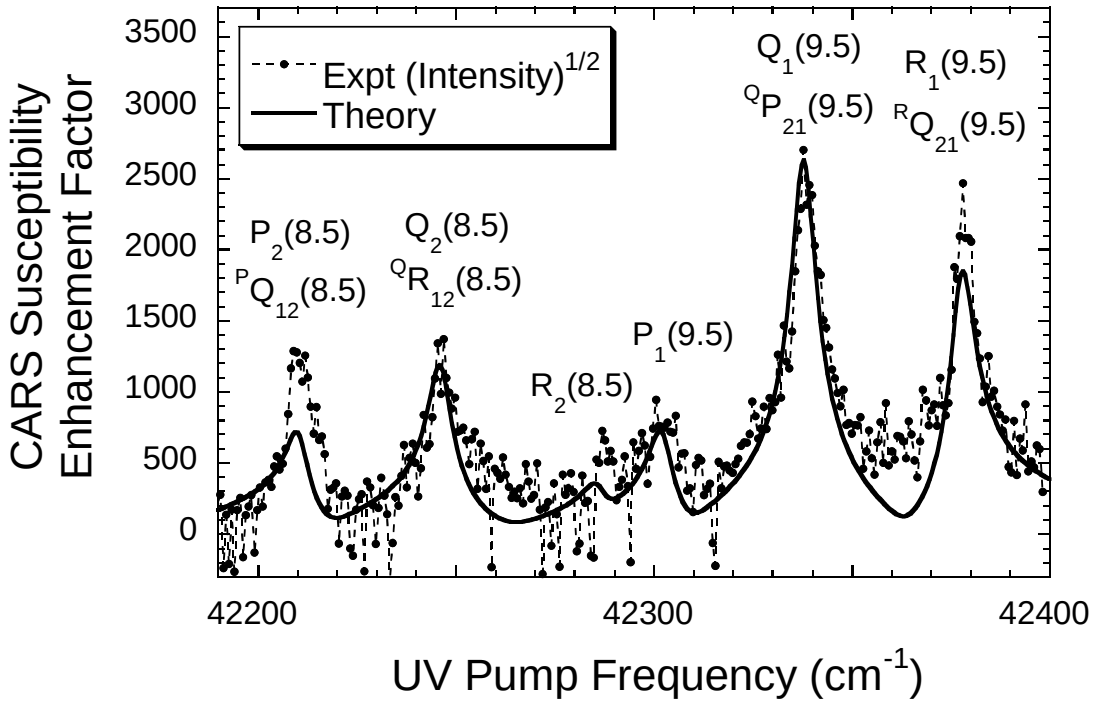

Fig.2.7. ERE CARS spectra obtained by scanning the ultraviolet pump beam with the Stokes beam frequency fixed at 1874.35 cm^{-1}. The NO concentration was 1000 ppm and the cell pressure was 13.0 kPa.

The experimental scan was performed using a mixture of 1000 ppm of NO in a buffer gas of nitrogen. The gas cell was at room temperature, approximately 300 K, and at a pressure of 13.0 kPa. The modeling of the scan was performed using a perturbative ERE CARS analysis previously used by Attal-Tretout et al. (1977), Doerk et al. (1995), Doerk et al. (1997b) and Attal-Tretout et al. (1990). The basic equation for the CARS susceptibility, as given by Druet and Taran (1981), can be written as

$$\chi_{CARS}\left(\omega_4:\omega_1,-\omega_2,\omega_3\right) = \frac{N}{\hbar^3}\sum_{a,b,c,d}\left\{\left[\frac{1}{\omega_{ba}-\left(\omega_1-\omega_2\right)-i\Gamma_{ba}}\right]\left[\frac{\mu_{4ad}\mu_{3db}}{\omega_{da}-\omega_4-i\Gamma_{da}}\right]\right.$$
$$\left.\times\left[\left(\frac{\rho_{aa}^{(0)}\mu_{1bc}\mu_{2ca}}{\omega_{ca}+\omega_2-i\Gamma_{ca}}\right)+\left(\frac{\rho_{aa}^{(0)}\mu_{2bc}\mu_{1ca}}{\omega_{ca}-\omega_1-i\Gamma_{ca}}\right)-\left(\frac{\rho_{bb}^{(0)}\mu_{2bc}\mu_{1ca}}{\omega_{cb}-\omega_2+i\Gamma_{cb}}\right)-\left(\frac{\rho_{bb}^{(0)}\mu_{1bc}\mu_{2ca}}{\omega_{cb}+\omega_1+i\Gamma_{cb}}\right)\right]\right\}^{\cdots} \quad \text{(2.1)}$$

where the $\chi_{CARS}\left(\omega_4:\omega_1,-\omega_2,\omega_3\right)$ is the CARS susceptibility, $\mu_{1ac}=\vec{\mu}_{ac}\bullet\hat{e}_1$, where $\vec{\mu}_{ac}$ (C-m) is the electric dipole moment matrix element for states *a* and *c*, $\hat{e}_1$ is the unit polarization vector for the electric field of pump 1, $\rho_{aa}^{(0)}$ is the initial population of state *a*, *N* is the total number density (m^{-3}) of resonant molecules, $\hbar$ is Planck's constant (J-s), Γ_{ab} is the dephasing rate (s^{-1}) for the electric dipole transition between states *a* and *b*, and other parameters are defined in a similar fashion. The first term in the equation above in square brackets is the Raman resonance detuning term for the CARS process, the second term in square brackets is the electronic resonance enhancement term, and the final term in square brackets is the term that accounts for the strength of the Raman transition.

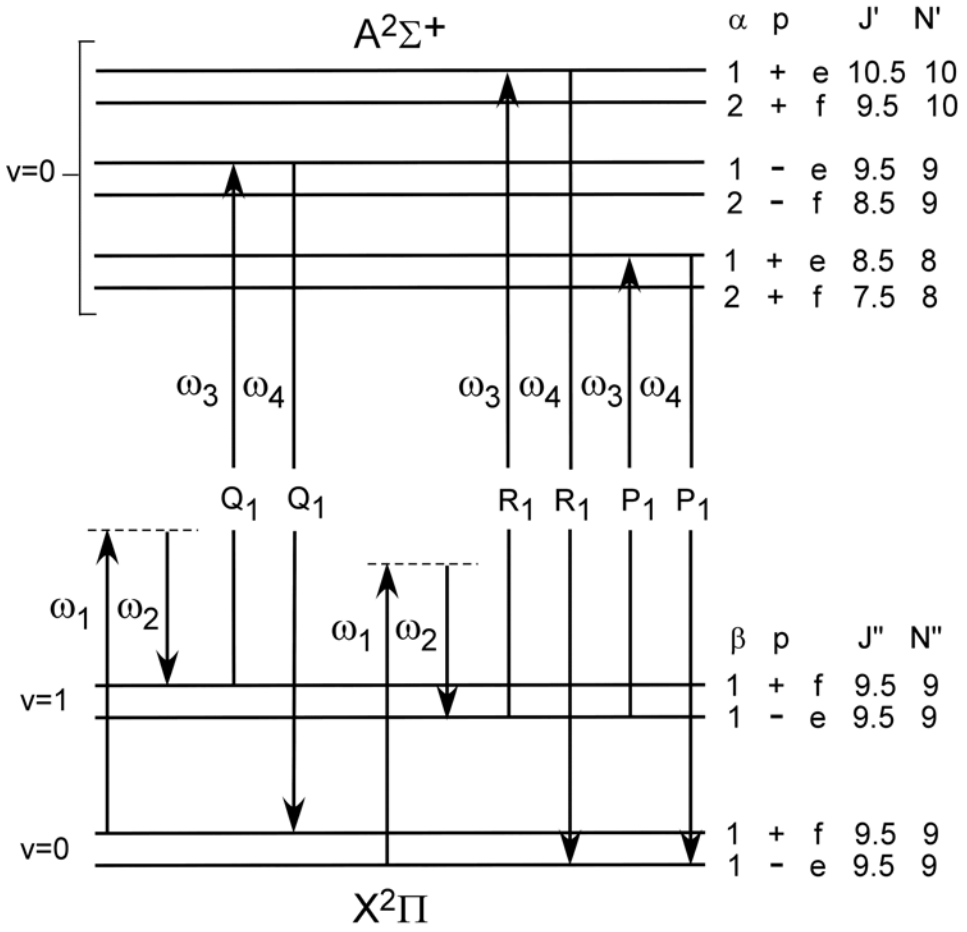

Fig.2.8. Detailed energy level diagram showing the origin of the ERE CARS effect of the Q (9.5) Raman Q-transition. The ultraviolet pump beam is tuned to the Q_1 (9.5), R_1 (9.5) or P_1 (9.5) transitions in the (0, 1) band of the $X^2\Pi - A^2\Sigma^+$ electronic transition.

The Sandia CARS code was modified for the ERE CARS calculations by incorporating electronic resonance terms from the equation above. NO spectral data were obtained from the spectroscopic database code LIFBASE by Luque and Crosley (1999b) and from previous high-resolution NO CARS measurements such as Laane and Kiefer (1980) and Lempert et al. (1984).

The square root of the CARS intensity is plotted in Fig. 2.7 versus the theoretical enhancement factor. The enhancement factor is the square root of the calculated CARS intensity for the ultraviolet pump frequency divided by the square root of the calculated CARS intensity for λ_3 = 532 nm. There is good agreement between theory and experiment and an enhancement factor of nearly 200 at the peak of the Q_1 (9.5) line can be observed. The spectral line assignment for the NO ERE CARS spectrum in Fig. 2.7 is based on the ERE CARS energy diagram in Fig. 2.8. Fig. 2.8 is specialized to the case where the Raman resonance frequency is tuned to the Q-branch resonances between the J" = 9.5 in the (1, 0) Raman band. The three main-branch transitions, Q_1 (9.5), R_1 (9.5) and P_1 (9.5), through which the electronic resonance enhancement occurs are shown in the diagram; satellite transitions are not shown in Fig. 2.8 for the sake of simplicity. The main–branch electronic resonances, Q_1 (9.5), R_1 (9.5) and P_1 (9.5), will be predominant in the spectrum when the Raman Q-branch transition between the J = 9.5 = N + 0.5 levels in the (1, 0) band in the $X^2\Pi$ state is probed. The occurrence of the Q_2 (8.5), R_2 (8.5) and P_2 (8.5) lines in the same scan indicates that the Raman Q-branch transition between the J = 8.5 = N – 0.5 levels in the (1, 0) band occurs at nearly the same Raman shift.

Comparison between theory and experiment is complicated by the noise in the spectrum resulting from the multi-mode frequency structure of the 236-nm and 591-nm beams. It is also negatively influenced by the short lifetime of the LDS 490 laser dye that was used to produce the 472-nm beam, resulting in a continuous decrease in the 236-nm pump beam energy and the level of the NO ERE CARS signal. The NO ERE CARS spectrum was normalized by dividing by the UV beam energy, but the influence of the UV beam energy decrease could not be fully eliminated. Despite this, the major features of the experimental data were reproducible for a very wide range of ultraviolet laser scans with fixed Stokes frequency, using only two minor and constant frequency offset parameters for the Stokes and ultraviolet pump beams.

There appears to be significant saturation of the ultraviolet transition, because it is necessary to increase the ultraviolet spectral width to 6 cm^{-1} to obtain good agreement between the experimental and theoretical width of the resonance line. The increase in ultraviolet pump spectral width decreased the theoretical susceptibility enhancement factor by more than a factor of 10.

When scanning the Stokes dye laser to obtain the NO ERE CARS spectra, good agreement was observed as well between the experimental scan and the modeling. Signal-to-noise ratios in excess of 10 were obtained from mixtures of 100 ppm NO in nitrogen buffer gas, as shown in Fig. 2.9. The combination of polarization suppression of the nonresonant background and the electronic resonance enhancement results in a significant decrease in the CARS detection limit. Polarization CARS measurements of NO in plasmas have been reported by Doerk et al. (1997b) and by Pott et al. (1998).

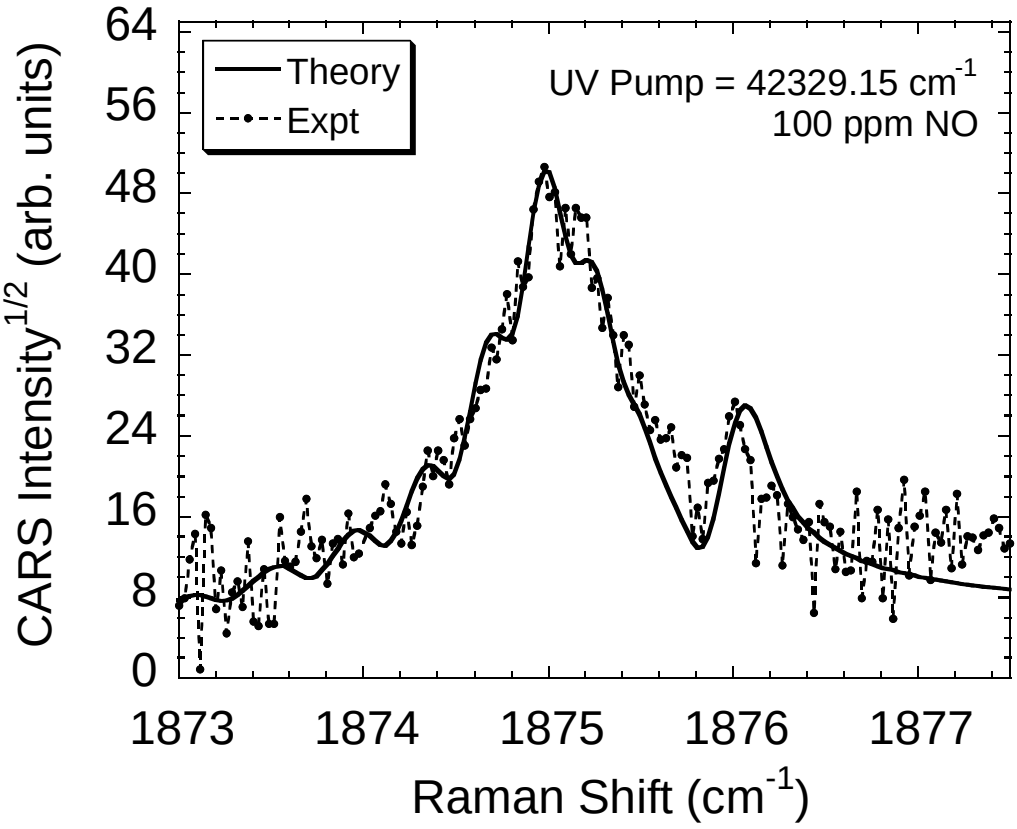

Fig.2.9. ERE CARS spectra obtained by scanning the Stokes beam with the ultraviolet pump frequency fixed at 42329.15 cm^{-1}. The NO concentration was 100 ppm and the cell pressure was 71.1 kPa.

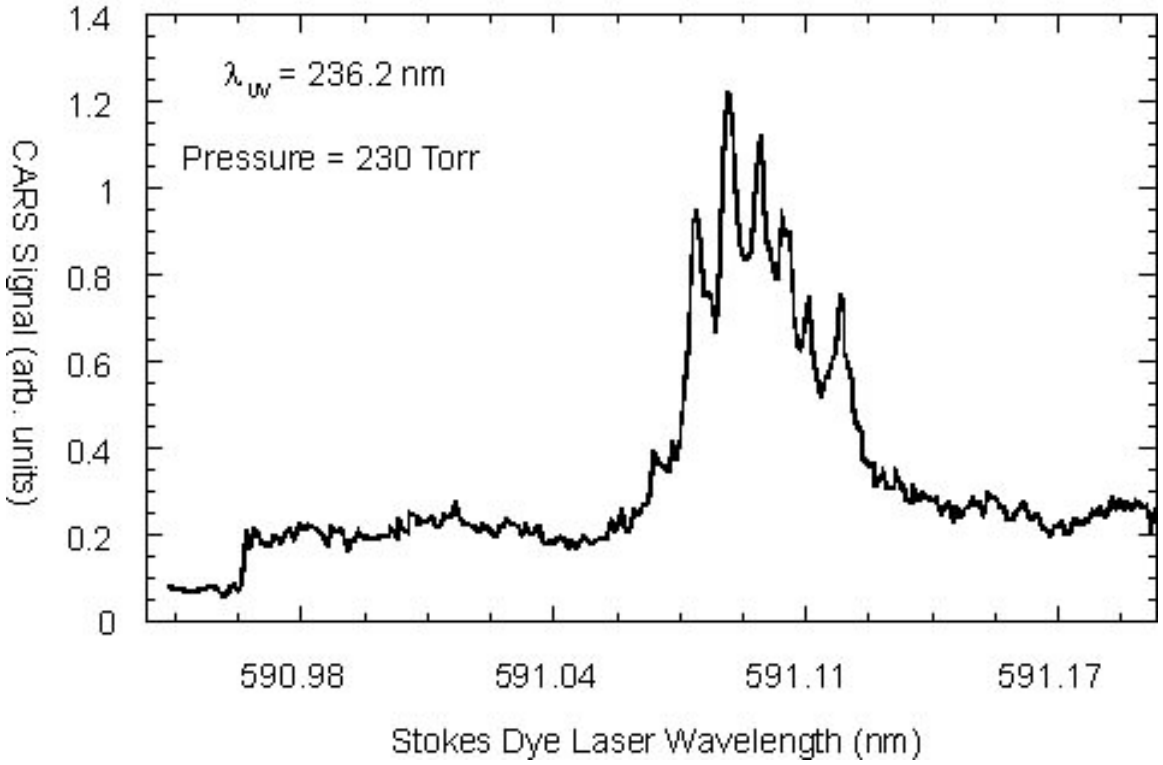

Fig.2.10. Experimental NO ERE CARS spectrum for 1000 ppm NO in nitrogen buffer gas without nonresonant background suppression.

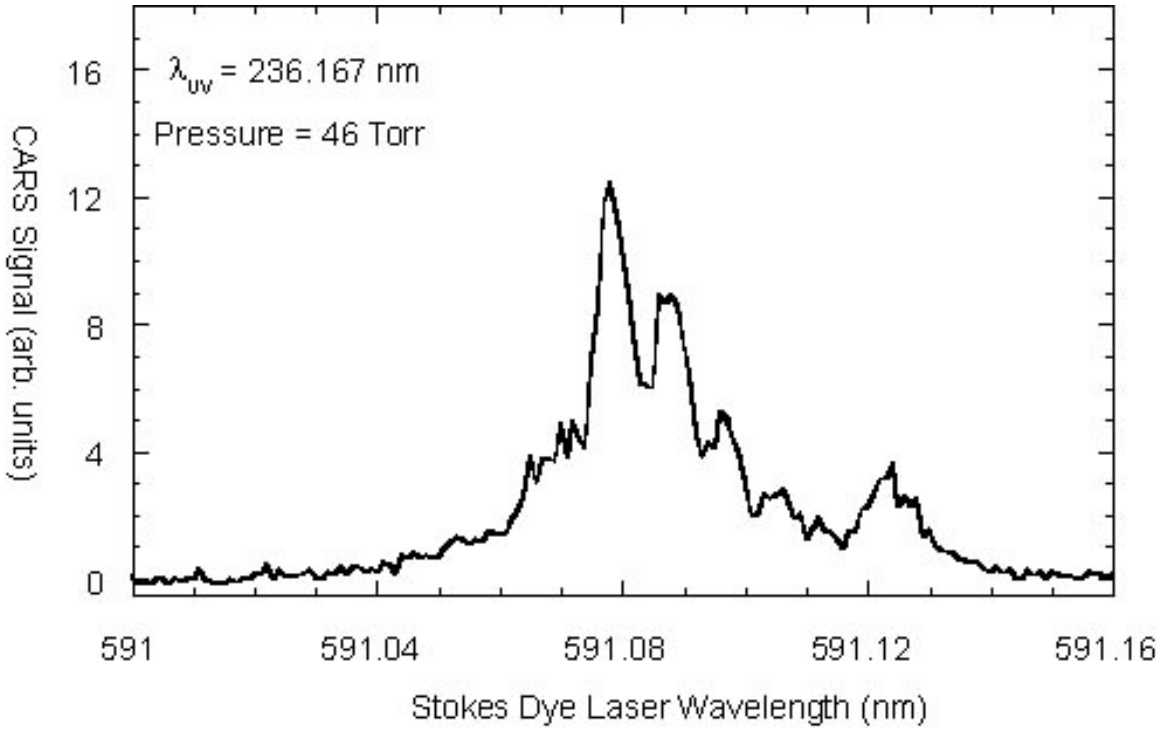

Fig.2.11. Experimental NO ERE CARS spectrum for 1000 ppm NO in nitrogen buffer gas suppression of nonresonant background.

It is worth mentioning that Pott et al. (1998) reports a detection limit of 200 ppm of NO at room temperature and atmospheric pressure, yet the published CARS spectrum for the above mentioned conditions is dominated by background signal which complicated the spectrum and suppresses the detection limit.

The effect of polarization techniques on the NO ERE CARS scans is more amplified by comparing Fig. 2.10, acquired without background suppression techniques, with Fig. 2.11, taken after the elimination of the background was accomplished. The scans were taken at an early stage of the experiment and are presented only to indicate the effect of the nonresonant background suppression on ERE CARS scans, and they were performed before the signal strength was maximized by various techniques discussed above. The ERE CARS scan for NO in Fig. 2.10 was acquired by scanning the Stokes dye laser wavelength across the Raman active (v'=1, v''=0) vibrational band of the NO molecule. The NO gas cell was maintained at 230 Torr. The wavelength of the UV pump beam was kept at 236.2 nm and the UV energy was observed to vary within 10% of its average value. The ERE CARS signal for NO is resonant with transitions in the strongest part of the NO molecule ultraviolet electronic band at 226.2 nm. Electronic resonance enhancement is evident and the resonant ERE CARS signal dominates the spectrum, but is complicated by the nonresonant background. The Stokes laser beam was blocked at a Stokes wavelength of 590.9 nm to assess the relative intensities of scattered UV light and the nonresonant background. Fig. 2.11 was acquired with the same NO concentration in nitrogen but at 46 Torr pressure in the gas cell. The UV pump beam wavelength was fixed at 236.167 nm and polarization techniques for background suppression were used. The

nonresonant background is barely evident and the NO resonant CARS signal dominates the spectrum with a significant increase in the signal-to-noise ratio and the emergence of spectral features and lines, previously dominated by the nonresonant background, is evident as well.

All the above scans were performed at sub atmospheric pressure. The gas cell was fitted with an Omega pressure transducer and the pressure was regulated through a needle valve on the suction line of a DS-202 Varian vacuum pump. NO ERE CARS scans were also performed at high pressures to examine the applicability of the technique to detect NO at high pressure. This is very relevant to high pressure flames and combustion processes in combustion devices. In the high pressure scans, the UV pump beam energy was kept constant within 10 % of the average value and the decline due to the dye solution decay was overcome by coupling the half-waveplate in the UV beam path with a polarizer. Starting the scan with moderate UV energy, the half-waveplate was rotated to increase the UV power and compensate for the loss of intensity as the scan progresses.

The signal-to-noise ratios of high pressure scans were degraded significantly from inconsistent injection seeding for the Continuum Nd: YAG 9010 laser. Many factors affect the operation of the seeder, such as uniform temperature and seeder diode power, as well as the alignment with fundamental laser beam. Small temperature changes of a few degrees can cause multimode operation for the seeder, and therefore a chilled water cooling system is necessary for the minimization of temperature fluctuations in the laser system. The diode was producing sufficient power to maintain single-mode operation, and the optical alignment of the seeder was in order.

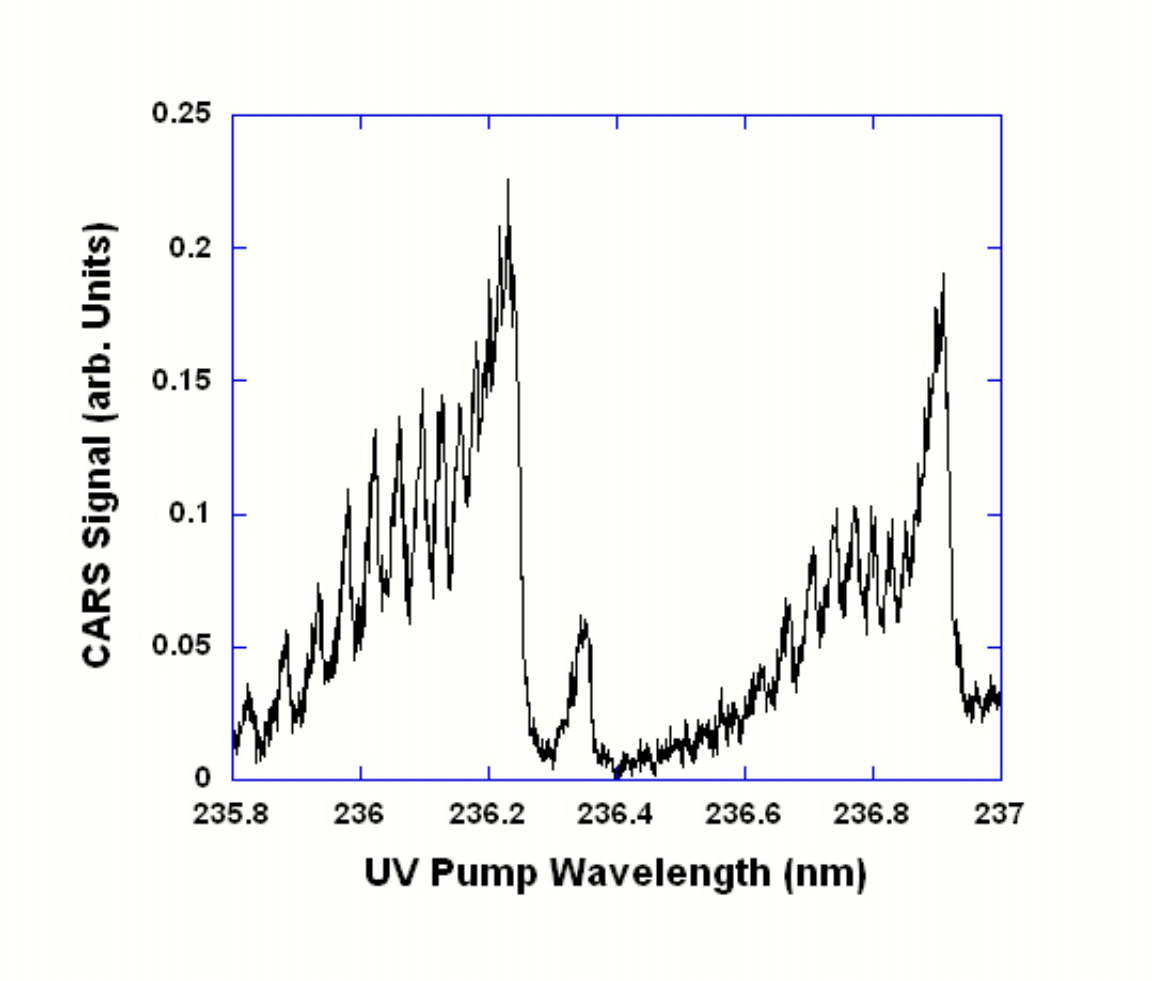

Fig.2.12. NO ERE CARS spectra obtained by scanning the ultraviolet pump beam with the Stokes beam wavelength fixed at 591.05 nm with single mode 532-nm beam operation. The NO concentration was 1000 ppm and the cell pressure was 500 Torr. The Continuum Nd: YAG laser injection seeder was maintained a single mode operation during the scan.

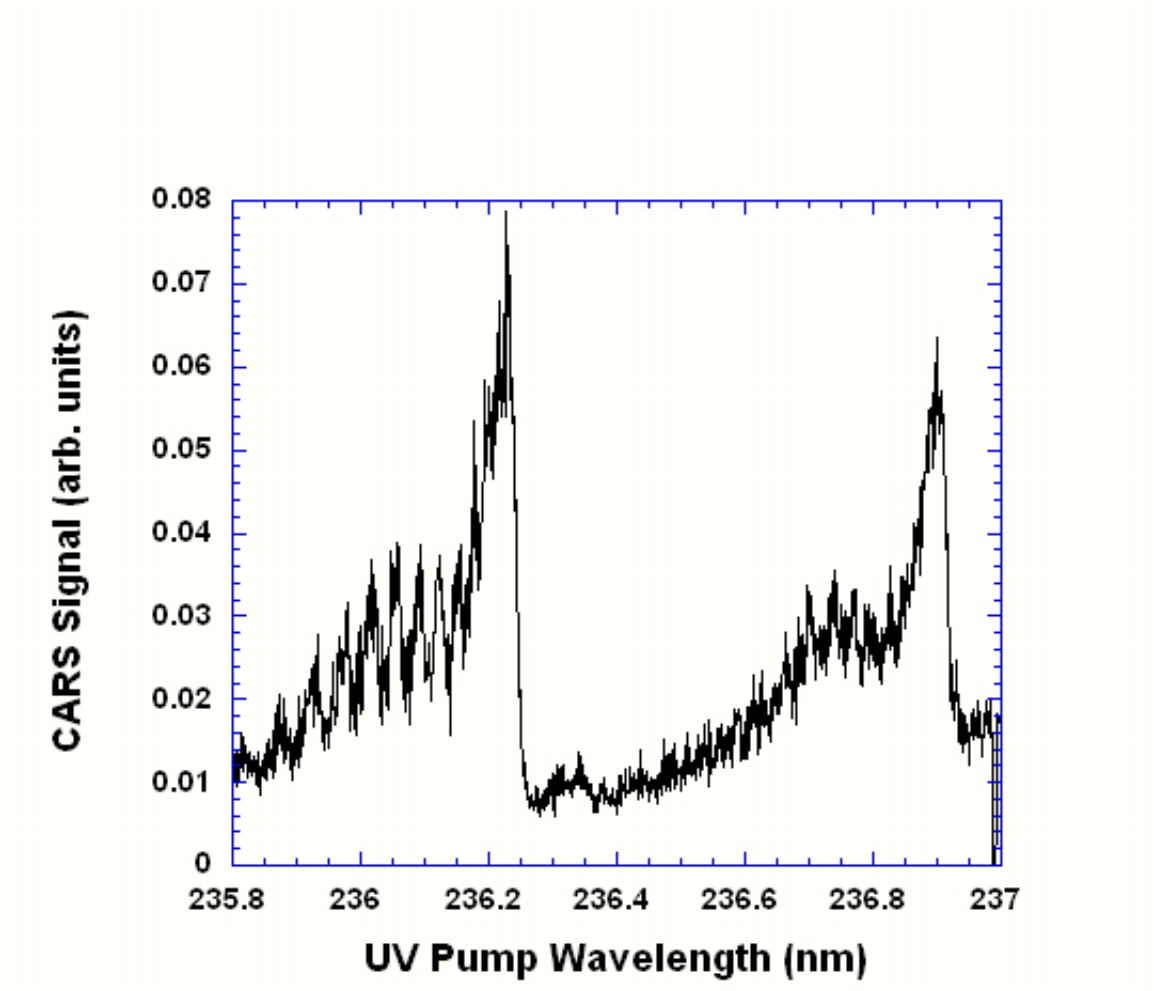

Fig.2.13. NO ERE CARS spectra obtained by scanning the ultraviolet pump beam with the Stokes beam wavelength fixed at 591.05 nm with multimode 532-nm beam operation. The NO concentration was 1000 ppm and the cell pressure was 500 Torr. The Continuum Nd: YAG laser injection seeder did not maintain a single-mode operation during the scan.

However, we did not realize for a long time that our laser was hooked up to the normal water supply rather than the chilled water supply. Once we realized this, we switched the laser cooling water to the chilled water line. The seeder output was monitored on an oscilloscope.

Comparison of Fig. 2.12 with Fig. 2.13 reveals the effect of seeder inconsistency on the results. Both of these NO ERE CARS spectra were obtained by scanning the ultraviolet pump beam with the Stokes beam wavelength fixed at 591.05 nm. The NO concentration was 1000 ppm and the cell pressure was 500 Torr. In Fig. 2.12 the seeder was operating in a single-mode condition, and therefore the spectrum shows excellent spectral resolution between the different spectral lines and well defined spectral features. In Fig. 2.13 the seeder was fluctuating between single-mode and multimode operation as evident in the noise that complicates the spectrum.

Numerical simulation for the high pressure is currently performed by Prof. R.P. Lucht, the School of Mechanical Engineering, Purdue University and collaborators. Preliminary simulations revealed that the UV linewidth for the high pressure data simulation is smaller than the linewidth of the previous low pressure scans by a factor of 3. This is attributed to the fact that the UV beam energy in the high pressure scans was maintained at a much lower level than the low pressure scans to be able to maintain it nearly constant as explained above.

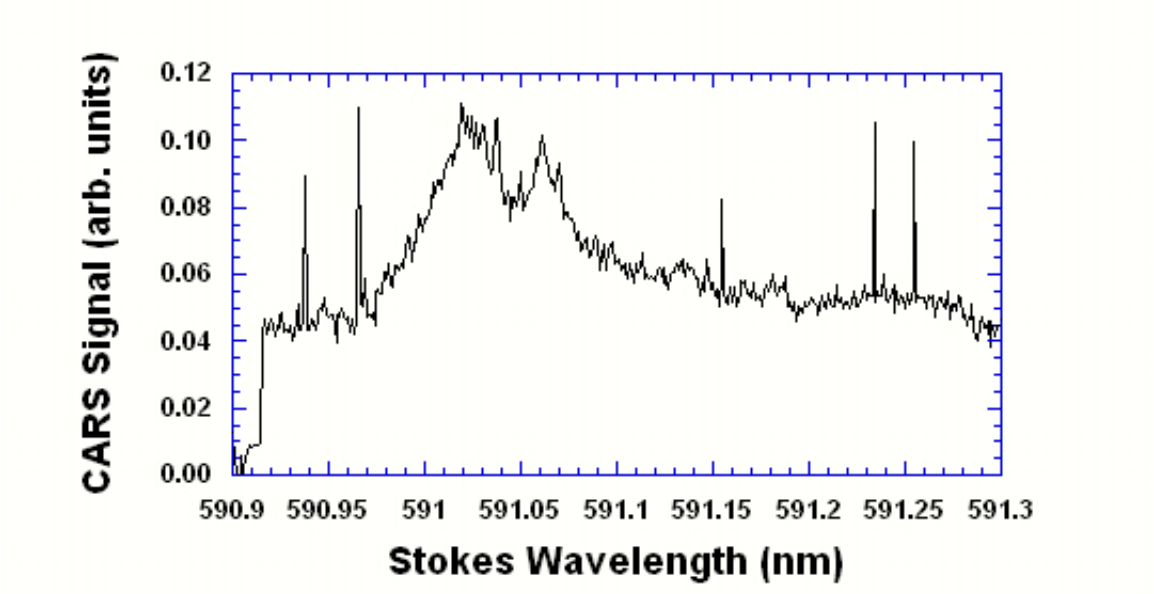

Fig.2.14. NO ERE CARS spectra obtained by scanning the Stokes beam with the UV pump beam fixed at 236.188 nm. The NO concentration was 1000 ppm and the cell pressure was 3 atm.

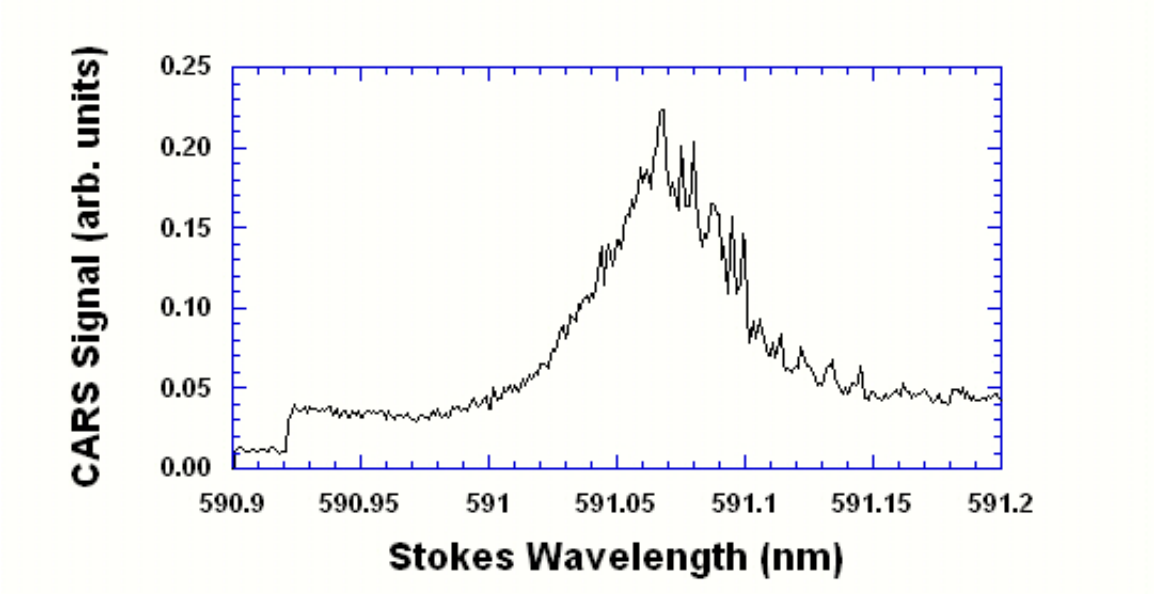

Fig.2.15. NO ERE CARS spectra obtained by scanning the Stokes beam wavelength while the UV pump beam wavelength is fixed at 236.24 nm. The NO concentration was 1000 ppm and the cell pressure was 3 atm.

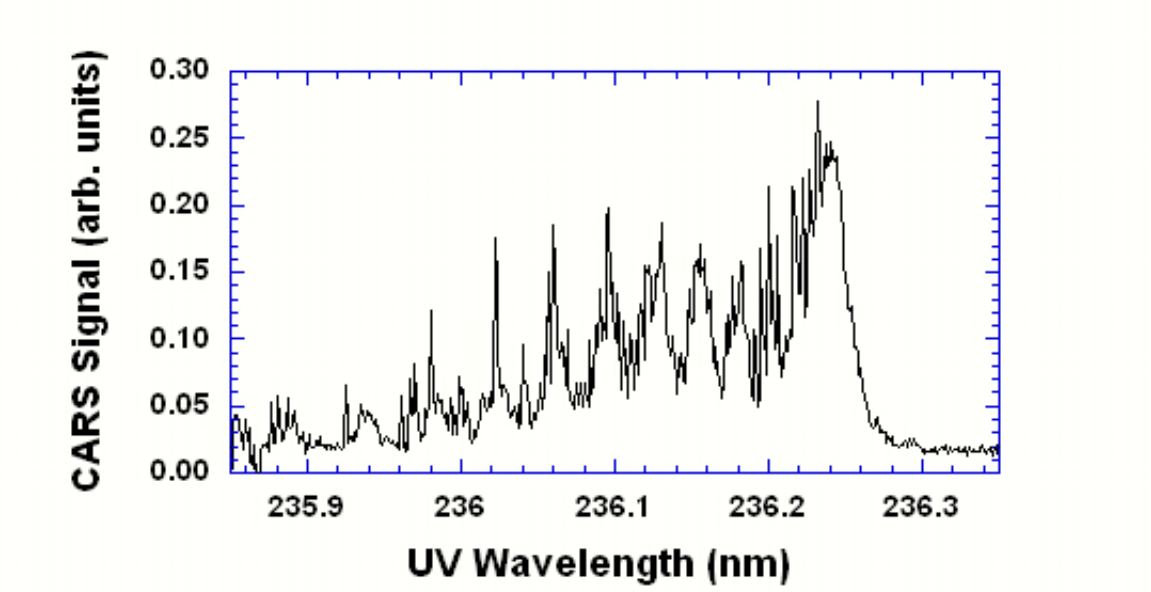

Fig.2.16. NO ERE CARS spectra obtained by scanning the ultraviolet pump beam wavelength with the Stokes beam wavelength fixed at 591.06 nm. The NO concentration was 1000 ppm and the cell pressure was 1 atm.

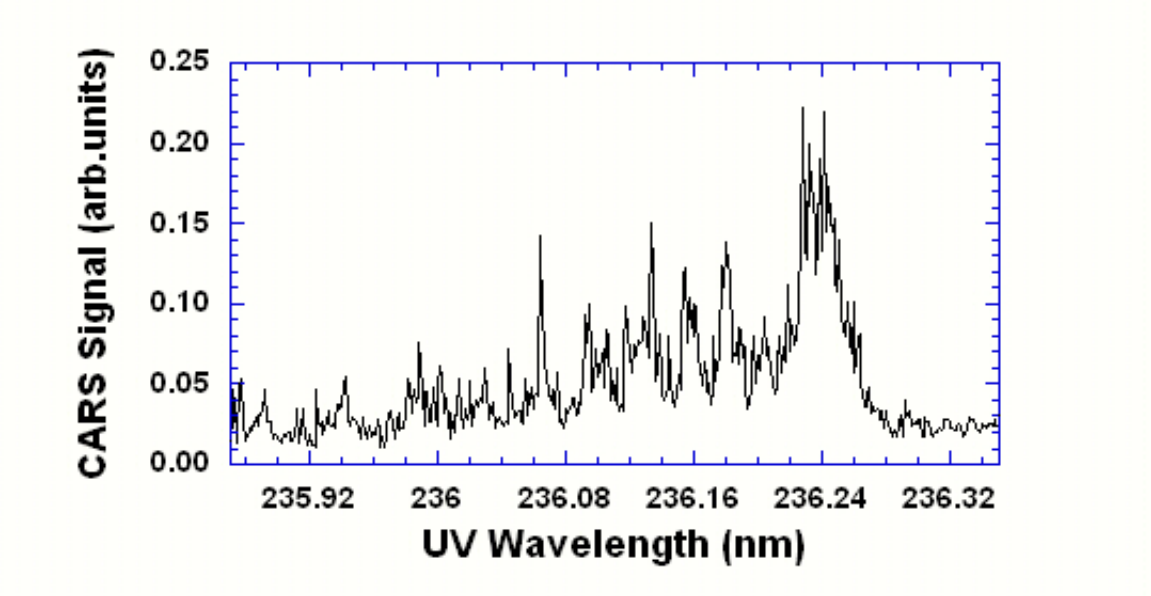

Fig.2.17. NO ERE CARS spectra obtained by scanning the ultraviolet pump beam wavelength with the Stokes beam wavelength fixed at 591.07 nm. The NO concentration was 1000 ppm and the cell pressure was 1 atm.

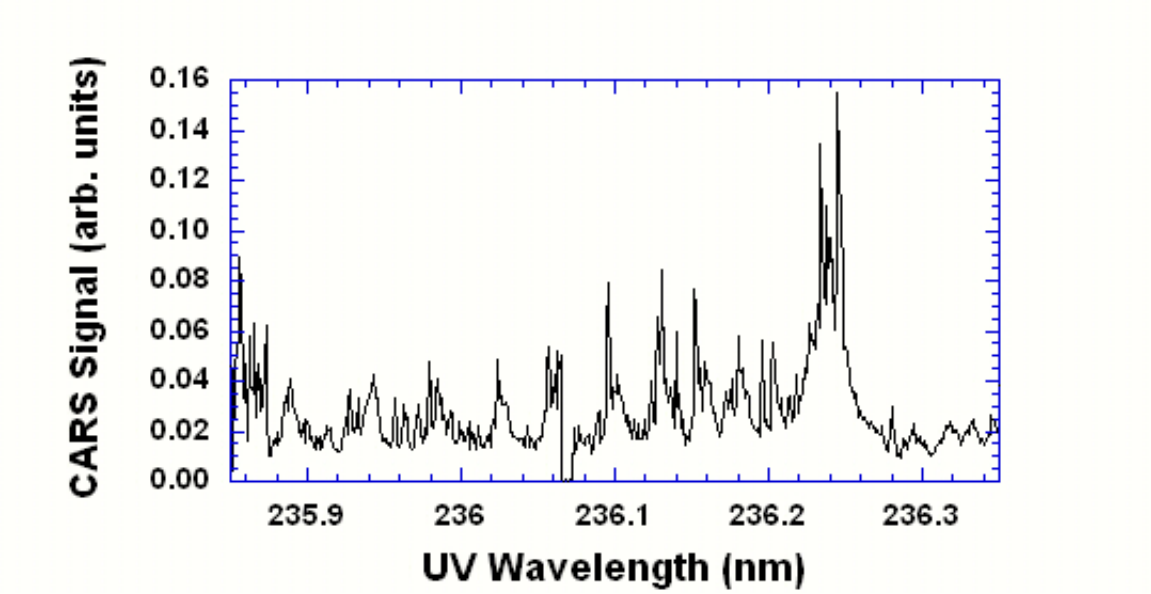

Fig.2.18. NO ERE CARS spectra obtained by scanning the ultraviolet pump beam wavelength with the Stokes beam wavelength fixed at 591.08 nm. The NO concentration was 1000 ppm and the cell pressure was 1 atm.

The effect of varying the UV pump beam wavelength on the NO ERE CARS spectrum is illustrated in Fig. 2.14 and Fig. 2.15. NO ERE CARS spectra were obtained by scanning the Stokes beam with the UV pump beam fixed at 236.188 nm and 236.24 nm, respectively. The NO concentration was 1000 ppm and the cell pressure was 3 atm. The signal-to-noise ratio is higher in Fig. 2.15 and a pressure shift took place. The nonresonant background in both cases is higher than in low pressure experiments as expected due to pressure increase. It is more difficult to suppress the nonresonant background using polarization techniques for high-pressure scans due to birefringence of the cell windows.

The effect of varying the Stokes beam wavelength on the NO ERE CARS spectrum is illustrated by comparing Fig. 2.16, Fig. 2.17 and Fig. 2.18. NO ERE CARS spectra in these figures were obtained by scanning the ultraviolet pump beam wavelength with the Stokes beam wavelength fixed at 591.06 nm, 591.07 nm and 591.08 nm, respectively. The NO concentration was 1000 ppm and the cell pressure was 1 atm for the three scans. The ERE CARS signal depicted on the vertical scale was normalized by the UV pump beam energy to ensure similar conditions for all cases. The Stokes beam wavelength variation did not influence the Stokes beam power, which was almost constant in this range. The ERE CARS signal intensity is reduced by increasing the wavelength of the Stokes beam.

Two sets of data, each containing three ERE CARS scans for NO at pressures of 2, 3 and 4 atmosphere, illustrates the effect of changing the pressures on ERE CARS spectra at constant Stokes wavelength. The first set contains figures 2.19, 2.20 and 2.21,

and the second set includes figures 2.22, 2.23 and 2.24. These NO ERE CARS spectra were obtained by scanning the ultraviolet pump beam wavelength with the Stokes beam wavelength fixed at 591.06 nm for the first set and at 591.07 nm for the second set. The NO concentration was 1000 ppm and the cell pressure was 2, 3 and 4 atm for each set, respectively. As expected, the CARS signal increases with increasing pressure, and linewidth broadening is experienced, yet it seems that there was partial saturation of the transition at higher pressures. More insight will be provided when the numerical simulation is finished and the spectral parameters are calculated. Of particular interest is Fig. 2.19, which shows excellent spectral resolution of the spectral lines as well as well defined other features. The single-mode operation of the seeder was monitored throughout this scan and it was steady in its operation without multimode structures introduced.

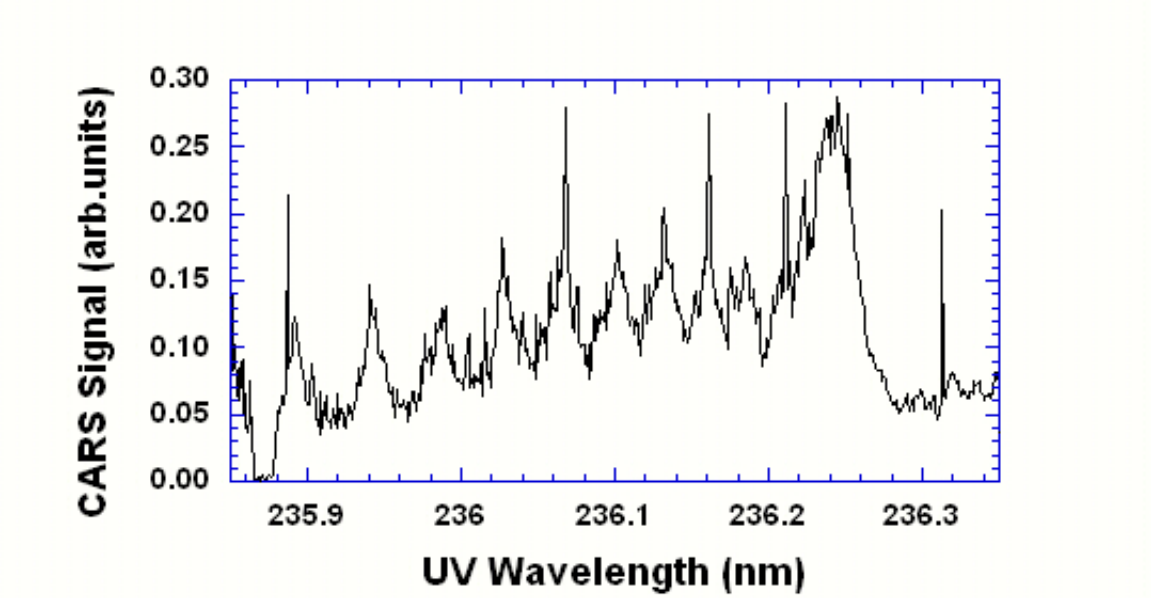

Fig.2.19. NO ERE CARS spectra obtained by scanning the ultraviolet pump beam wavelength with the Stokes beam wavelength fixed at 591.06 nm. The NO concentration was 1000 ppm and the cell pressure was 2 atm.

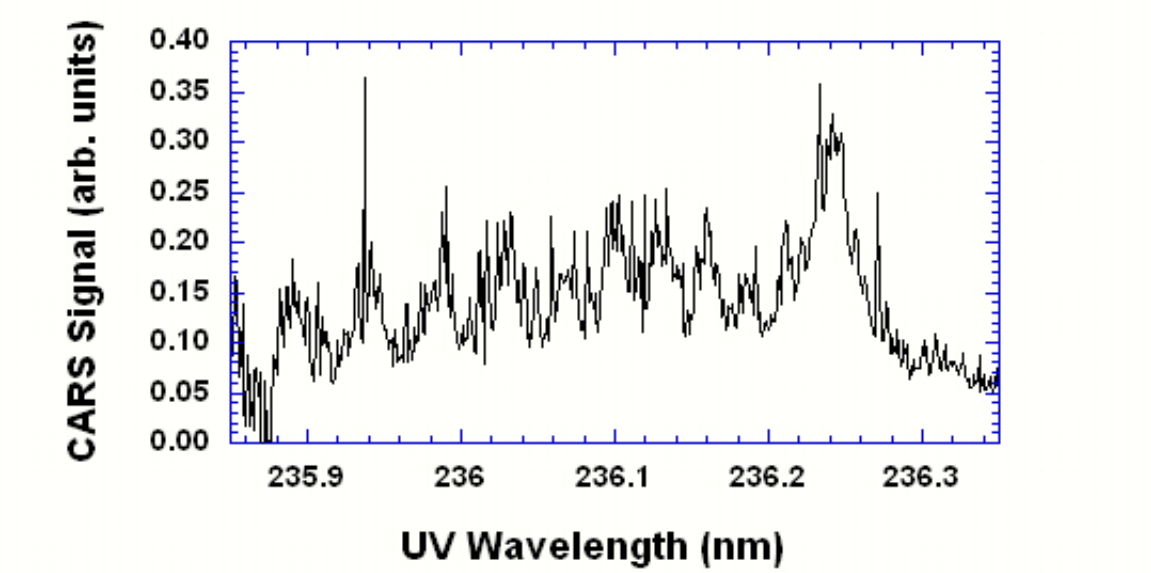

Fig.2.20. NO ERE CARS spectra obtained by scanning the ultraviolet pump beam wavelength with the Stokes beam wavelength fixed at 591.06 nm. The NO concentration was 1000 ppm and the cell pressure was 3 atm.

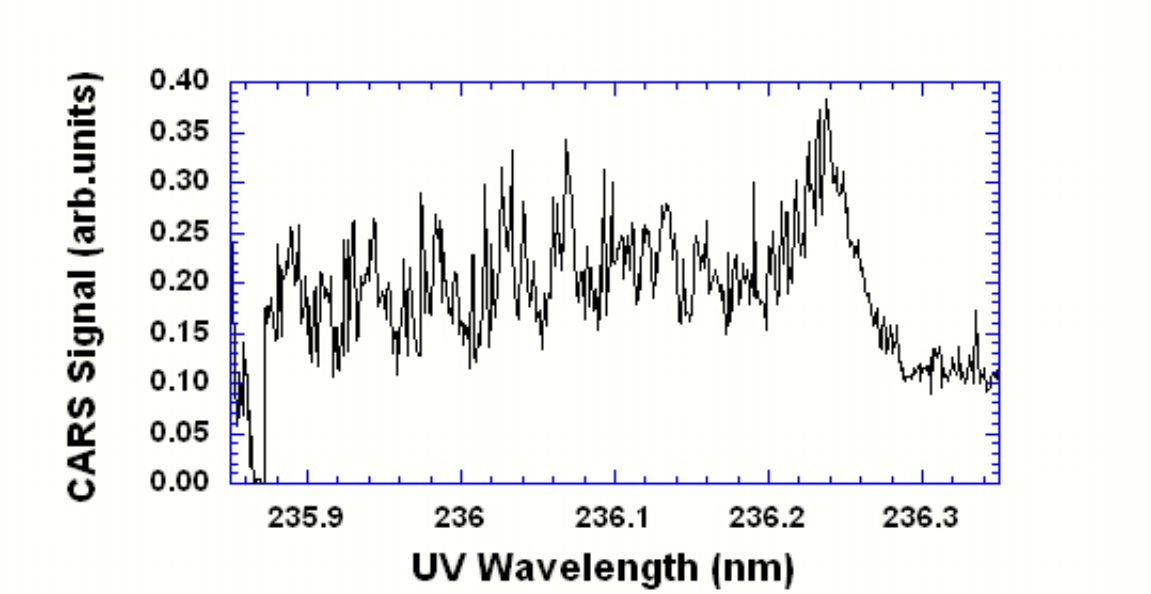

Fig.2.21. NO ERE CARS spectra obtained by scanning the ultraviolet pump beam wavelength with the Stokes beam wavelength fixed at 591.06 nm. The NO concentration was 1000 ppm and the cell pressure was 4 atm.

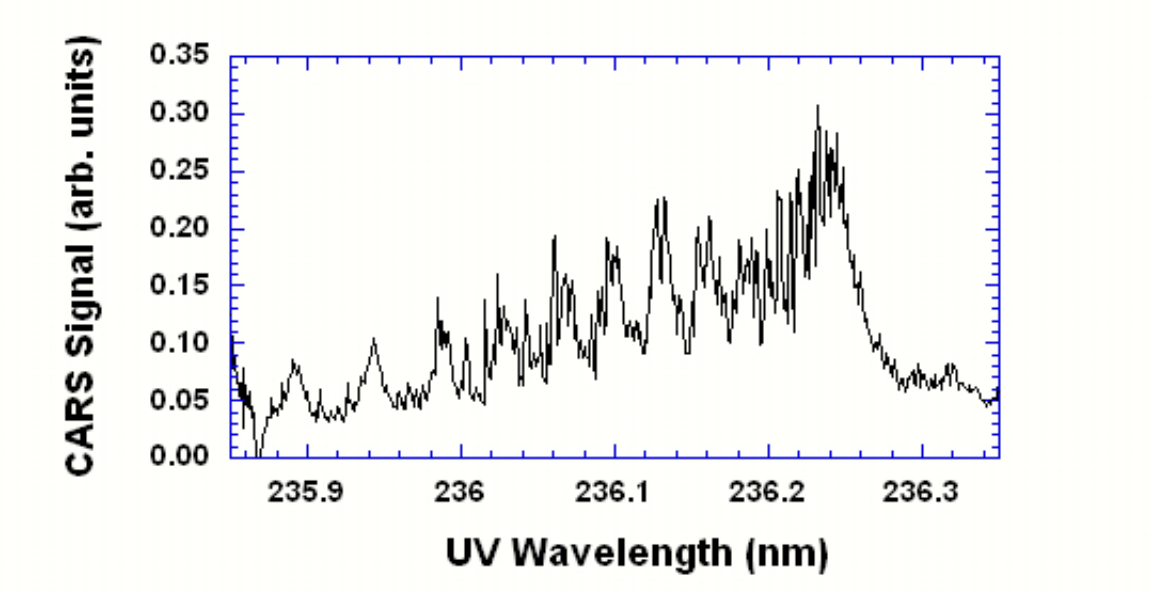

Fig.2.22. NO ERE CARS spectra obtained by scanning the ultraviolet pump beam wavelength with the Stokes beam wavelength fixed at 591.07 nm. The NO concentration was 1000 ppm and the cell pressure was 2 atm.

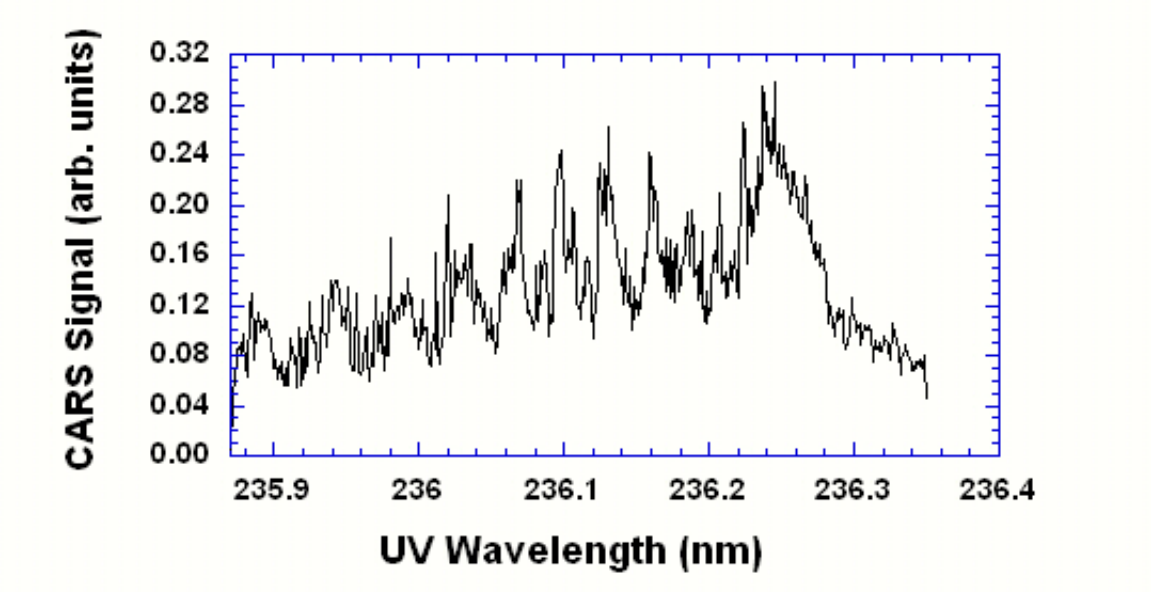

Fig.2.23. NO ERE CARS spectra obtained by scanning the ultraviolet pump beam wavelength with the Stokes beam wavelength fixed at 591.07 nm. The NO concentration was 1000 ppm and the cell pressure was 3 atm.

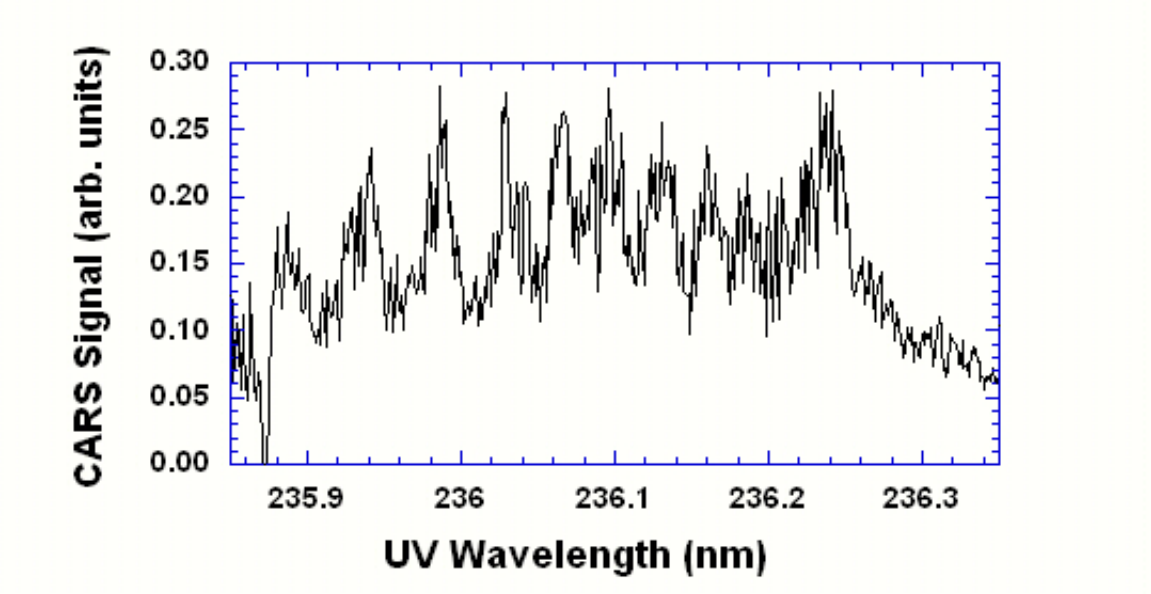

Fig.2.24. NO ERE CARS spectra obtained by scanning the ultraviolet pump beam wavelength with the Stokes beam wavelength fixed at 591.07 nm. The NO concentration was 1000 ppm and the cell pressure was 4 atm.

CHAPTER III

ELECTRONIC–RESONANCE-ENHANCED (ERE) COHERENT ANTI-STOKES RAMAN SCATTERING (CARS) SPECTROSCOPY OF ACETYLENE

The detection of acetylene (C_2H_2) by electronic-resonance-enhanced (ERE) coherent anti-Stokes Raman Scattering (CARS) was demonstrated by Hanna et al. (2004). The ERE CARS experiment discussed in Chapter II was modified slightly for the C_2H_2 measurements. Experiments were performed using room-temperature gas cell with mixtures of 5000 ppm C_2H_2 in N_2. Visible pump and Stokes beams were used, with the frequency difference between the pump and Stokes tuned to the 1974 cm^{-1} υ_2 Raman transition of C_2H_2. An ultraviolet probe beam with wavelengths ranging from 232 nm to 242 nm was scattered from the induced Raman polarization to generate the ERE CARS signal. The effects of probe wavelength and pressure on ERE CARS signal generation for C_2H_2 are discussed.

3.1. Introduction and Motivation

In the three-laser ERE CARS technique presented in this Chapter for detection of acetylene, the probe beam is an ultraviolet laser beam with a frequency tuned into electronic resonance with ultraviolet transitions in the C_2H_2 molecule. The technique used here is a variant of the three-laser technique developed for simultaneous detection of two species as demonstrated by Lucht (1987). As discussed in Chapter II, the first pump and the Stokes beams are visible laser beams with frequencies far from resonance

with the ultraviolet electronic transitions of C_2H_2, and the second pump beam is at a frequency at or near electronic resonance. This results in significant advantage over previous techniques in which both pump beams have the same wavelength and the pump and Stokes beams are both near electronic resonance. The ERE CARS technique offers enhanced selectivity owing to the requirement of simultaneous vibrational and electronic resonance for signal generation. In the detection of hydrocarbons such as C_2H_2, this advantage is even more amplified due to the overlap of the vibrational Raman resonances of various species, limiting the selective excitation of single species.

Acetylene has been selected as a test molecule to evaluate the applicability and potential of ERE CARS for concentration measurements of hydrocarbon molecules. It is a very important molecule in combustion processes, whether it is used directly as a fuel in flames or produced as an intermediate molecule during the hydrocarbon / air combustion processes. Measuring the acetylene concentration with good sensitivity by taking advantage of the excellent temporal and spatial characteristics of the ERE CARS technique would be quite valuable for understanding the chemical kinetics of hydrocarbon combustion. Acetylene plays an important role in the soot formation and growth mechanisms. Therefore, one of the main goals of this study is to make a preliminary assessment of the potential for the application of ERE CARS for acquiring acetylene profiles in sooting flames and high pressure flames. The ERE CARS technique offers excellent discrimination of the signal against the luminous background of these flames due to its laser-like signal. The influence of several experimental parameters on

the ERE CARS signal, including the UV probe wavelength and the pressure are of great interest for studying the fundamental physics of the ERE CARS technique.

The 1974 cm^{-1} υ_2 Raman transition of C_2H_2 was selected for both theoretical and experimental reasons. Herzberg (1945) explained the structure of the acetylene molecule as a linear molecule with five fundamental vibrations as illustrated in Fig. 3.1. Among the five modes, υ_1, υ_2 and υ_4 are Raman active and therefore are the only modes considered for Raman techniques such as CARS. The other two modes are Raman inactive. Comparing the three Raman active modes, Orduna et al. (1982) have measured Raman cross sections and depolarization ratios for each of the three modes. The υ_2 band at 1974 cm^{-1} was found to be the strongest of the three modes with a differential Raman cross section nearly eight times greater than for the nitrogen Q-branch. In addition to the strength of this band, the experimental system in the laboratory that was used for the NO ERE CARS required only slight modification for the C_2H_2 ERE CARS. The NO molecule was detected using a UV pump wavelength of approximately 236 nm and a Stokes wavelength of approximately 591 nm. To detect C_2H_2, only a small modification to these wavelengths and minor experimental changes were necessary. The UV wavelength used for the C_2H_2 ERE CARS experiments was between 232-242 nm. The UV energy was increased for higher wavelengths (> 236 nm) as the peak lasing wavelength of the LD 490 dye was approached. The Stokes beam for maximum ERE CARS signal intensity from the 1974 cm^{-1} band of C_2H_2 was 594 nm, again very close to the Stokes wavelength for NO ERE CARS.

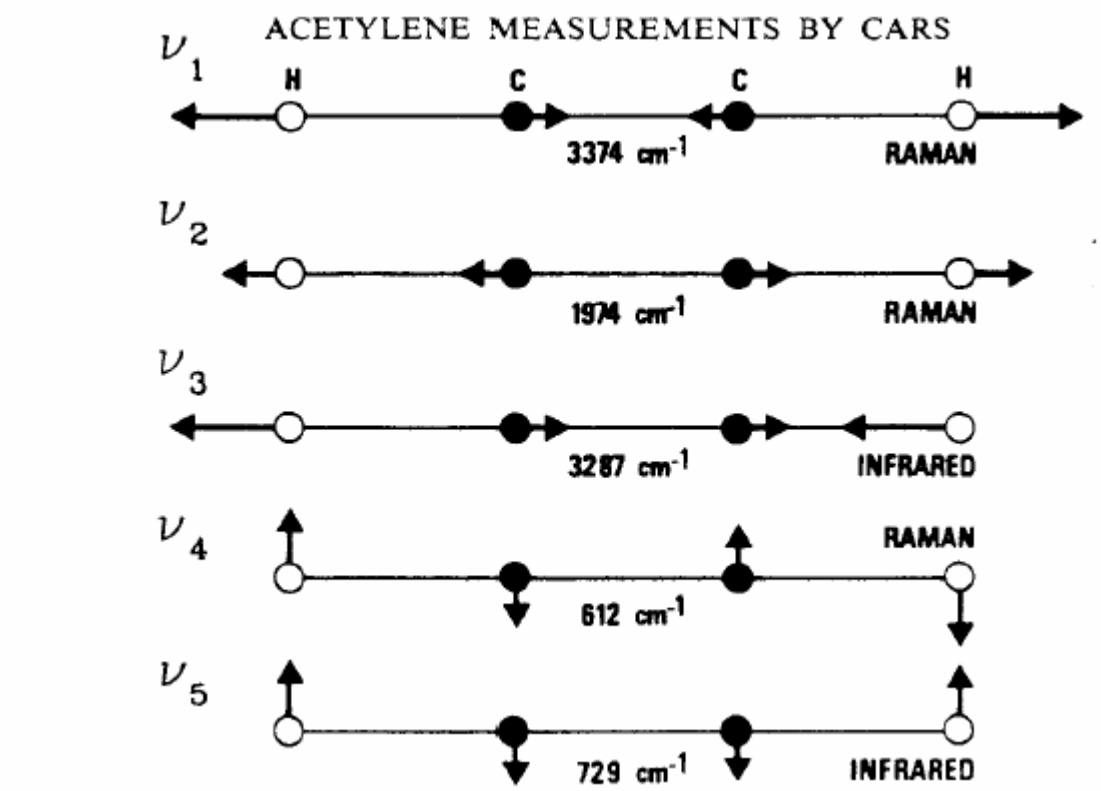

Fig.3.1. The vibrational modes of the acetylene molecule.

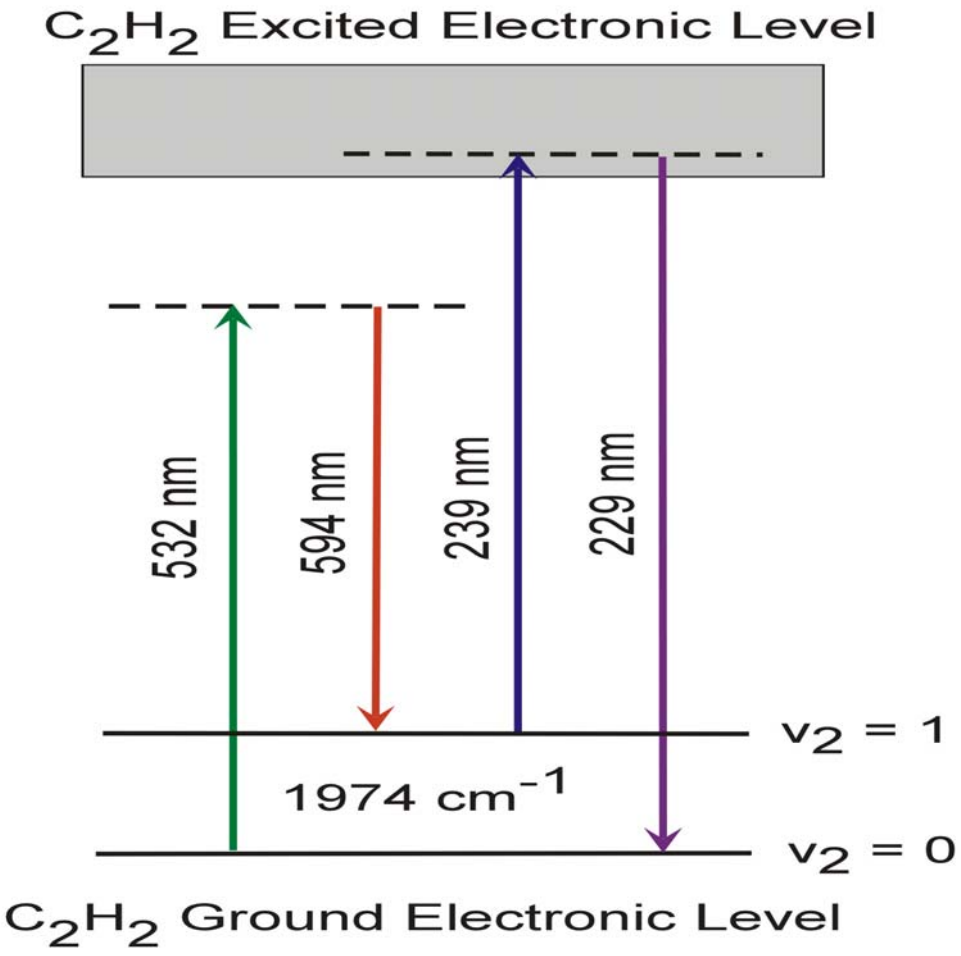

Fig.3.2. Energy level schematic diagram for the C_2H_2 ERE CARS process.

Both wavelength changes were easily accomplished with no modification in the optical system or alignment, proving the versatility of the ERE CARS technique and demonstrating the capability of measuring the concentration of multiple molecules with one optical arrangement.

3.2. Energy Diagram

An energy level schematic diagram for acetylene detection using the ERE CARS technique is shown in Fig. 3.2. The first pump beam is the second harmonic output of a Nd: YAG laser at a wavelength of 532 nm. The Stokes beam wavelength is approximately 594 nm and is generated using a 532-nm pumped narrowband dye laser. The UV probe beam is generated by frequency doubling the output of a 355-nm pumped narrowband dye laser. When the Stokes wavelength is tuned to a wavelength such that the difference between the frequency of the first pump beam and the Stokes beam is equal to the Raman transition of acetylene probed in this experiment at 1974 cm^{-1}, a Raman polarization is established in the medium. The UV probe beam is then scattered from this induced Raman polarization. When the UV wavelength is tuned to an electronic resonance of acetylene, the ERE CARS signal is generated. The wavelength of the ERE CARS beam is approximately 229 nm for a probe wavelength of 239 nm. The first pump beam and the Stokes beam are visible beams with frequencies far from resonance with the ultraviolet electronic transitions of C_2H_2. The second pump beam or the probe beam is at or near electronic resonance. The wide separation of the two pump beams frequencies distinguishes this experiment from previous ERE CARS experiments

which were performed with the same laser frequencies for both pump beams. In addition, the wide separation between the pump beam and Stokes beam wavelengths and the electronic resonance in this experiment is another distinction from previous experiments which were performed with these wavelengths at or near electronic resonance (Attal-Tretout et al., 1977; Doerk et al., 1997a; Attal-Tretout et al., 1990). One of the major advantages offered by these different wavelength features is the enhanced selectivity of the technique owing to the requirement of simultaneous vibrational and electronic resonance for signal generation. This is an especially important consideration for selective excitation of hydrocarbon species in regions where vibrational resonances from different species overlap.

3.3. Literature Review

Acetylene is a molecule of great importance in combustion processes and has therefore been the subject of extensive research. It is used as fuel, is an important intermediate combustion species in hydrocarbon oxidation mechanisms, and is thought to play a major role in soot formation and growth.

Herzberg (1945) outlined the different modes and structural features of acetylene as well as many of its spectral features. Orduna et al. (1982) measured Raman cross sections and depolarization ratios for different modes. Watson et al. (1982) photographed the A-X band system of acetylene with origin near 2400 angstroms in absorption with higher resolution than for studies that predated their research. They provided a detailed rotational analysis of bands in the 2470 – 2150 angstroms region,

involving the levels $n\upsilon''_4$ (n = 0-4) of the $X^1\Sigma_g^+$ state and $n\upsilon'_3$ (n = 0-3), and $\upsilon'_2 + n\upsilon'_3$ (n= 0-2) of the A^1A_υ (C_{2h}). They changed some of the previously established spectral line assignments based on their findings. The principal subbands with $\Delta K = \pm 1$, and the satellite subbands with $\Delta K = \pm 2$, 0 (due to axis-switching) and $\Delta K = \pm 3$ (due to axis-switching, asymmetry, and ℓ resonance) were included in a comprehensive least-squares fit. Rotational levels of all the ℓ components of the levels of υ''_4 were observed and the validity of the results was verified by its compliance with the theory of ℓ doubling and ℓ resonance of a linear molecule. The rotational structures of the vibrational levels of the nonlinear A state were fitted by Watson et al. (1982) with asymmetric top rotational constants A_υ, B_υ, C_υ and principal centrifugal constants D^J_υ, D^{JK}_υ and D^K_υ.

Robert W. Field and coworkers have made significant contributions to the study of acetylene spectroscopy. Abramson et al. (1984) observed clumps of narrowly spaced lines that appeared in the stimulated emission pumping spectrum of the acetylene $X\ ^1\Sigma_g^+$ state near 27900 cm^{-1}. They further note that all the lines in a given clump arise from transitions in levels with the same lower state J" value. They conclude that the fine structure within each clump is of a purely vibrational nature. This prompted Abramson et al. (1984) to further study this point, as rotationally resolved and assigned spectra at such high vibrational excitation had not been previously reported for a polyatomic molecule. They analyze the spacing between adjacent lines in several of these clumps and their analysis revealed that the lines followed a Wigner distribution rather than a Poisson distribution, a characteristic that is expected when chaotic behavior within a

molecule occurs. This opened the door to the possibility of applying one of the suggested criteria of quantum chaos to a real molecular spectrum.

J.K.G. Watson and coworkers continued on the research mentioned above. Van Craen et al. (1985) extended the studies of the high resolution absorption spectrum of the electronic transition of the acetylene molecule to the region between 2190 – 2050 Angstroms. The vibrational levels $n\upsilon'_3$ (n = 4-6), and $\upsilon'_2 + n\upsilon'_3$ (n = 3-5), and $\upsilon'_1 + n\upsilon'_3$ (n = 2, 3) of the A state were assigned and these levels together with another level not identified by the study were observed as upper states of vibrational progressions in the known $\upsilon''_4(\ \Pi_g)$ vibrational mode of the ground state. Detailed rotational analyses of these bands were performed. It was suggested that the rotational levels of each of these vibrational levels were perturbed by interactions with unidentified vibronic levels. This limited the possibility of extracting accurate values for the rovibrational constants and only approximate values were obtained.

Lucht et al. (1986) recognized the advantages that the CARS technique offers for the detection of hydrocarbon species, among them acetylene, in hostile media such as plasmas and sooting flames. Their approach is important to our study as well as their findings. They performed coherent anti-Stokes Raman scattering (CARS) measurements of acetylene in a laminar methane/ acetylene/ air flame. The acetylene concentration was determined from the ratio of the resonant acetylene CARS signal to the nonresonant background CARS signal. The resonant and nonresonant signals were detected separately on each laser shot by polarization analysis and a two-channel detection system. The flame temperature profile was determined from fits of nitrogen CARS

spectra and the experimental acetylene CARS spectra were compared with theoretical models and found to be in good agreement with theory. The measured CARS profiles indicate that as much as 2-3 percent acetylene is formed in the flame preheat region.

Yamanouchi et al. (1991) obtained dispersed fluorescence (DF) and stimulated emission pumping spectra (SEP) of acetylene originating from single rovibronic levels of the A^1A_u state. The spectra were measured with resolutions of 30 and 0.5 cm^{-1}, respectively, in order to examine the vibrational level structure of the electronic ground $X\ ^1\Sigma_g^+$ state. The spectra showed that below 14000 cm^{-1} the vibrational features in the acetylene DF spectra could be assigned to progressions in the trans bend, the CC stretch and one other vibrational mode. The spectroscopic constants associated with the spectra were consistent with the values reported in literature. The SEP spectroscopy revealed that the DF features, corresponding to single vibrational levels at low energy, are composed of many vibrational levels at high energy and are more adequately explained as groups of eigenstates among which a zero order FC bright state is distributed.

Taking advantage of newly recorded dispersed fluorescence spectra of acetylene and advances in developing a numerical pattern recognition technique which identifies groups of transitions in the spectra, O'Brien et al. (1998) assigned polyad quantum numbers to 134 vibrational levels of the $X^1\Sigma_g^+$ state of acetylene with internal energies from 3,000 to 15,000 cm^{-1}. No evidence for the breakdown of the polyad quantum numbers was observed.

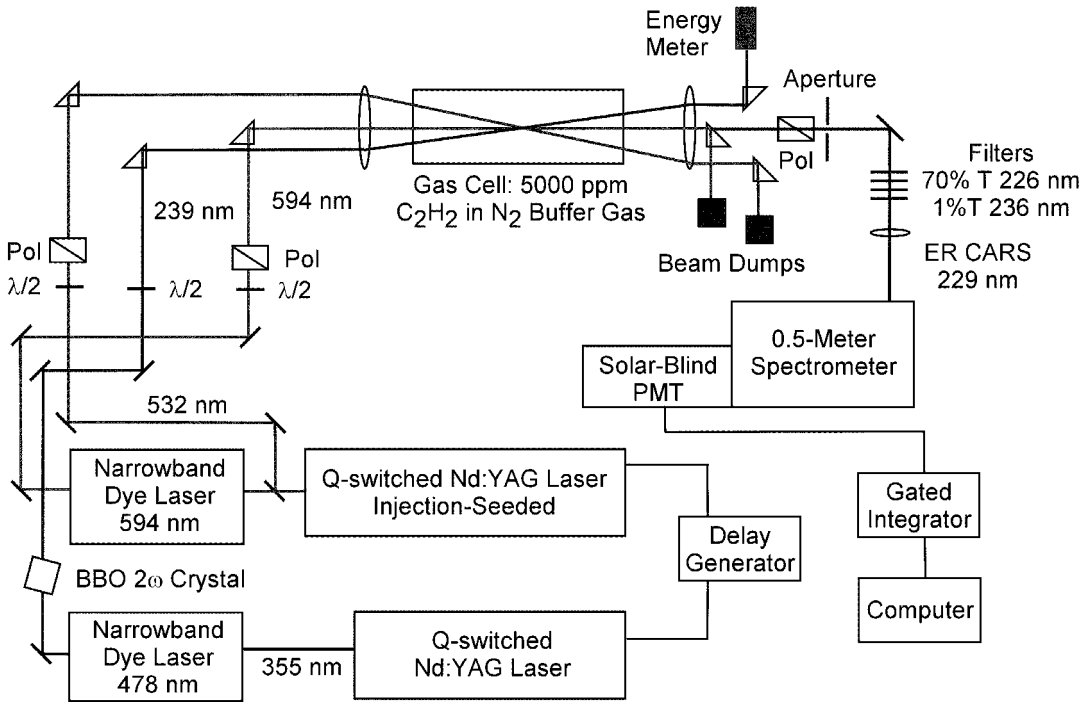

Fig.3.3. ERE CARS system for measurements of acetylene.

Watson (2001) calculated the relative intensities in the vibrational structure of the A^1A_u (C_{2h}) – $X^1\Sigma_g^+$ (D_{ooh}) electronic transition of acetylene. The large change in geometry and the change in normal coordinates between the two states were considered. The calculated intensities agreed quite well with those experimentally observed, lending confidence in the A-state harmonic potential. The strongest bands in the emission spectrum were for transitions to high levels of the ground state, for which anharmonicity is important. The calculations showed that the calculated emission intensities are quite sensitive to the form of the ground-state potential, which provides important data for future studies, such as the research presented in this thesis.

To detect acetylene in low-pressure propane and methane flames, Williams and Fleming (2002) used laser-induced fluorescence to record profiles of acetylene formed as an intermediate species in 10-Torr premixed propane and methane flames. In low – temperature regions of the flames, excitation spectra confirmed that acetylene was selectively detected. The spectra of acetylene overlap those of oxygen and nitric oxide on terms of both excitation and detection wavelengths, yet acetylene was detected with relatively little interference at 228 nm. This finding is important for our thesis research as this is approximately the same wavelength that the ERE CARS signal for acetylene is generated and detected. The fluorescence lifetime of acetylene for the flame conditions studied was found to be approximately 20 ns, much shorter than the radiative lifetime, due to high quenching rate for all colliders investigated. Another finding of Williams and Fleming (2002) was their inability to detect the LIF signal for acetylene in methane flames due to various factors that are eliminated in the ERE CARS technique.

Baum et al. (2003) investigated the analysis of acetylene in breath gas and developed a miniaturized, noninvasive instrument for its detection. The instrument relies on dispersive UV absorption spectroscopy as its measurement principle and is employed in an extractive (side-stream) configuration. The analyzer in this innovative instrument is used for fast, interference–free detection of acetylene, with signal-to-noise ratios in excess to 50. Comparison tests with a mass spectrometer using calibration gas samples gave an excellent correlation that validated the linearity and accuracy of the UV instrument developed. This development is important, yet does not provide an in-situ and real time measurements, a quality ERE CARS provides.

3.4. ERE CARS Experimental System for Acetylene Detection

The ERE CARS experimental system for detection of acetylene is shown in Fig. 3.3. The Nd: YAG lasers, the dye lasers, the optics, the detection systems, the computer controls, and the experimental arrangement and alignment of the laser beams are the same as in the experimental system for NO detection discussed in the previous Chapter. The only differences between the experiments are that the wavelengths of the Stokes beam and the UV probe beam are slightly different, and the detection wavelength of the ERE CARS signal is thus different as well. We shall therefore discuss the experimental system only briefly.

The laser source for the pump beam at 532 nm was a Continuum Model 9010 injection-seeded, Q-switched Nd: YAG laser with a repetition rate of 10 Hz, pulse length of approximately 7 ns, and pulse energy for the 532-nm output of approximately 750 mJ.

85% percent of the 532-nm output was used to pump a Continuum Model ND6000 narrowband, tunable dye laser to produce the Stokes beam (ω_2) at a wavelength near 594 nm with a frequency bandwidth of approximately 0.08 cm^{-1}. The 355-nm third-harmonic output of a Continuum Model 8010 Nd: YAG laser was used to pump a second Continuum Model ND6000 dye laser to produce tunable laser radiation at a wavelength of 470 nm to 490 nm; most measurements were performed with a probe beam wavelength near 239 nm. It is worth mentioning that the dye used, LD 490, has a maximum lasing energy when pumped with 355 nm at a frequency of about 243 nm. This resulted in higher UV beam energy for the acetylene ERE CARS experiments. The fundamental output of the dye laser was frequency-doubled to 239 nm using an INRAD Autotracker III with a beta barium borate (β-BBO) crystal to produce the pump beam at frequency ω_3 with an estimated frequency bandwidth of 0.2-0.3 cm^{-1}.

The CARS signal was generated using a three-dimensionally phase-matched arrangement. The pulse energies for the 532-nm, 594-nm, and 239-nm beams at the CARS probe volume were typically 30 mJ, 20 mJ, and 1 mJ, respectively. The CARS focusing lens had a focal length of 300 mm. After passing through the ERE CARS probe volume, the pump, Stokes, and CARS signal beams were recollimated using a 300-mm-focal-length lens. The 532-nm pump and Stokes beams were directed into beam dumps. The 239-nm pump beam was directed into a pyroelectric Joulemeter to measure the pulse energy. The ERE CARS signal was directed through apertures and four 45°-incidence, 215-nm dielectric mirrors. The 215-nm mirrors were used at 0° incidence and had approximately 70% transmittance at 229 nm but less than 1%

transmittance at 239 nm. These mirrors served as spectral filters and reduced significantly the background from the 239 nm scattered light. At higher ERE CARS wavelength, these mirrors reflected more of the ERE CARS signal intensity and therefore introduced uncertainties regarding the influence of increasing probe wavelength on the signal. The ERE CARS signal beam was then focused onto the entrance slit of a 0.5-m spectrometer, and a solar-blind-photomultiplier was used to detect the 229 nm ERE CARS signal. The ERE CARS signals and the ultraviolet pulse energies were recorded on a shot-by-shot basis using gated integrators while either the Stokes dye laser or the ultraviolet pump dye laser was scanned under computer control.

Polarization techniques were used to suppress the nonresonant four-wave mixing background signal as discussed in Chapter II. Both the 532-nm pump beam and the Stokes beams were linearly polarized with the polarization axis at 60 degrees to the vertical. The ultraviolet pump beam was vertically polarized. For this polarization arrangement the resonant CARS signal was generated with a nearly vertical polarization, while the nonresonant background was linearly polarized at 30 degrees to the vertical. An α-BBO polarizer was placed in the signal channel with its transmission axis perpendicular to the polarization of the nonresonant background. This resulted in a drastic reduction in the intensity of the nonresonant background. The ERE CARS signal intensity was also reduced, but the signal-to-noise ratio for the ERE CARS signal was significantly increased. The measurements reported here were performed using a calibrated gas mixture of 5000 ppm C_2H_2 in a buffer gas of N_2. The gas cell was approximately 0.3 m in length and was fitted with fused silica windows.

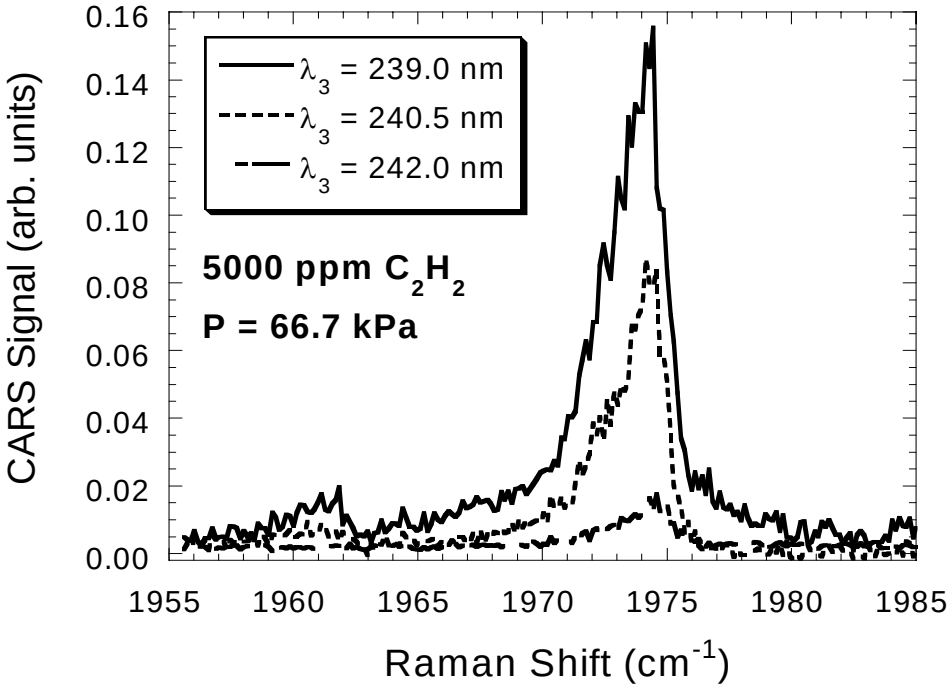

Fig.3.4. ERE CARS spectra of acetylene for different probe wavelengths.

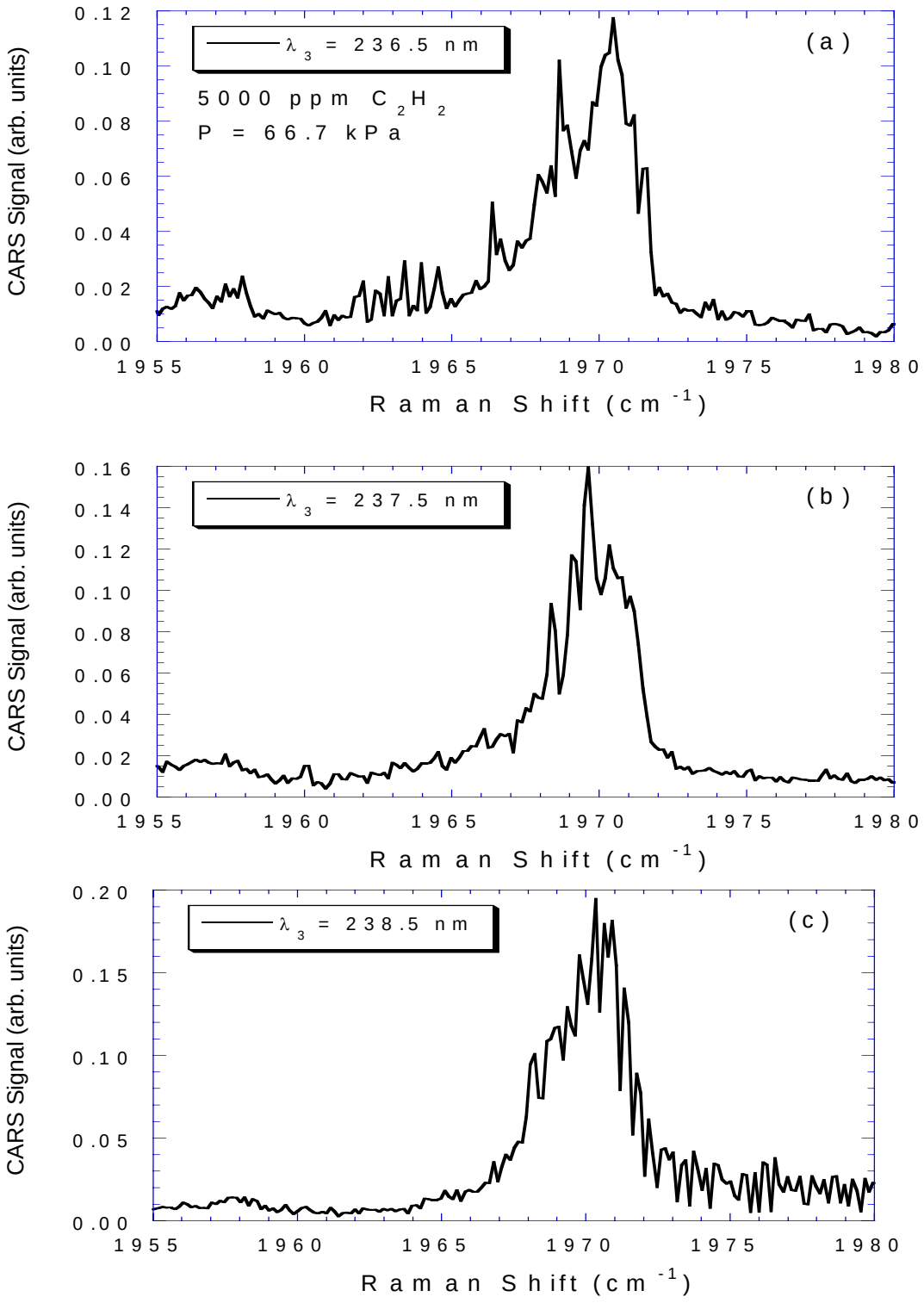

Fig.3.5. ERE CARS spectra of acetylene at three different probe wavelengths.

3.5. Experimental Results and Discussion

The primary objective of the experiments reported here was to investigate the effect of varying probe wavelength λ_3 on the shape and intensity of the C_2H_2 ERE CARS spectrum. The ERE CARS spectrum of C_2H_2 is shown in Fig. 3.4 for wavelengths of 239, 240.5, and 242 nm. The drop in intensity from λ_3 = 239 nm to λ_3 = 242 nm is clearly evident, although the shape of the spectrum is fairly similar for all three spectra. Some of the drop in intensity with increasing wavelength can be attributed to decreasing reflectivity of the mirrors in the signal channel. Mirror reflectivity curves show about 10-15 % increase in reflectivity for wavelengths higher than 229 nm, but most of the drop in intensity is because of the reduced electronic resonance effect as the wavelength λ_3 of the UV probe beam was increased. The electronic bands of acetylene are very broad but the transitions have significant intensity only below 240 nm, at least for room-temperature conditions. For the spectra shown in Fig. 3.4, for the probe wavelength at λ_3 = 239 nm the ERE CARS wavelength λ_4 = 228.2 nm and is very close to a very strong peak in the room-temperature absorption spectrum of acetylene. As discussed by Williams and Fleming (2002), the room-temperature absorption spectrum is complicated by transitions arising from low-lying vibrational levels, and the A-X electronic transition moments are much higher for excited vibrational levels in the X electronic state.

Fig. 3.5 shows the ERE CARS spectrum of acetylene for λ_3 = 236 nm, λ_3 = 237 nm, and λ_3 = 238 nm. As can be seen in Fig. 3.5, the shape of the spectrum varies as the probe wavelength is changed due to different electronic resonance interactions in the A-X electronic band. While the electronic resonance interaction is quite complicated for

acetylene because of the structure of the A-X band, the electronic resonance interaction will become stronger as the temperature of the medium increases because the electronic transition moment will increase for excited vibrational levels in the ground state.

The pressure dependence of the C_2H_2 ERE CARS signal was also investigated. As shown in Fig. 3.6, the ERE CARS signal increases approximately as the square of the pressure. This illustrates a very significant potential advantage of ERE CARS compared to laser-induced fluorescence (LIF) detection of minor species in high-pressure flames. For ERE CARS the signal is approximately proportional to the number density and thus increases significantly as pressure increases for a given mole fraction of the minor species, whereas at best the LIF signal will remain constant for a given minor mole fraction as the pressure increases.

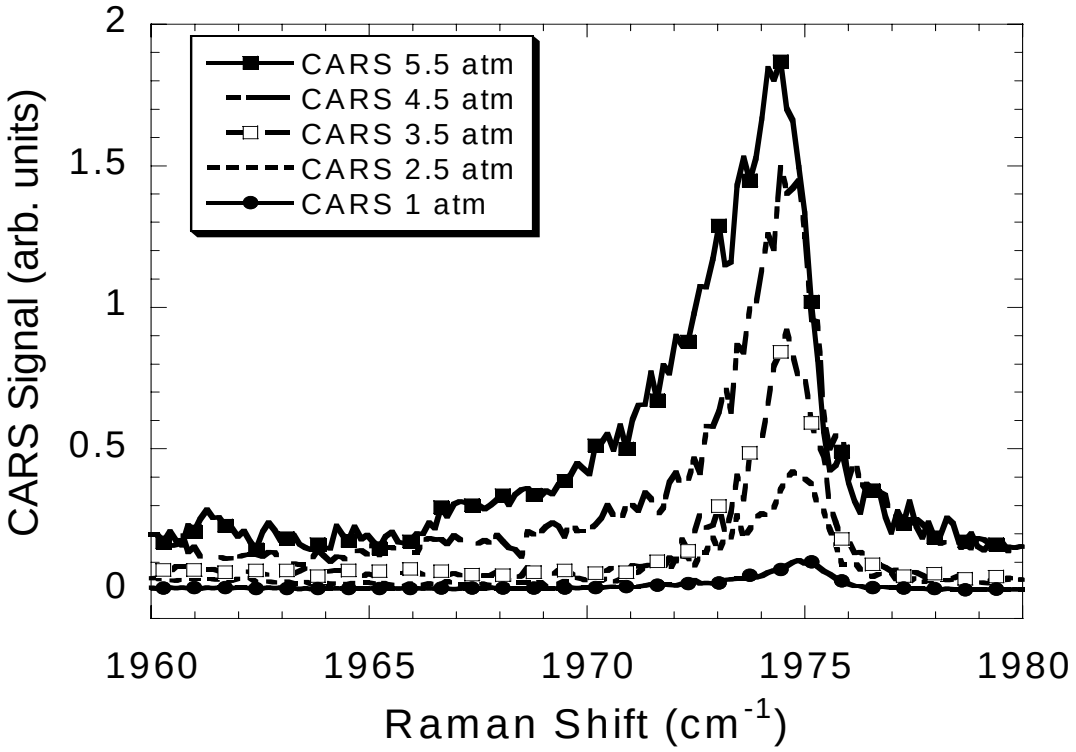

Fig.3.6. Pressure dependence of the acetylene ERE CARS spectra.

CHAPTER IV

DUAL-PUMP CARS FOR DETECTION OF DIPICOLINIC ACID

Dual Pump Coherent anti-Stokes Raman scattering (CARS) is used for detection of dipicolinic acid (DPA), a major component in the chemical composition of anthrax and other bacterial spores. A review of chemical and biological aspects of DPA is presented, followed by a brief summary of current methods to detect DPA. Both aerosol techniques and spectroscopic methods are reviewed. The experimental system for CARS detection of DPA is discussed. Experimental CARS spectra obtained for benzene and DPA are presented and analyzed. Two geometries of detection, forward and backward CARS detection, were investigated.

4.1. Motivation

DPA is a major component of anthrax bacterial spores. The anthrax attacks that followed the 9/11 atrocities called for more rapid, real-time and accurate methods for the detection of anthrax to avoid the disastrous consequences of anthrax attack. Ideally, real-time anthrax detection method would be incorporated in detection devices and used in post offices, governmental and military institution and other potential terror targets. In addition, the development of real-time anthrax detectors in battle fields has become an increasing need for troops. It proves to be a major challenge, as the spectroscopic technique should be able to detect the signal from DPA in a backward direction.

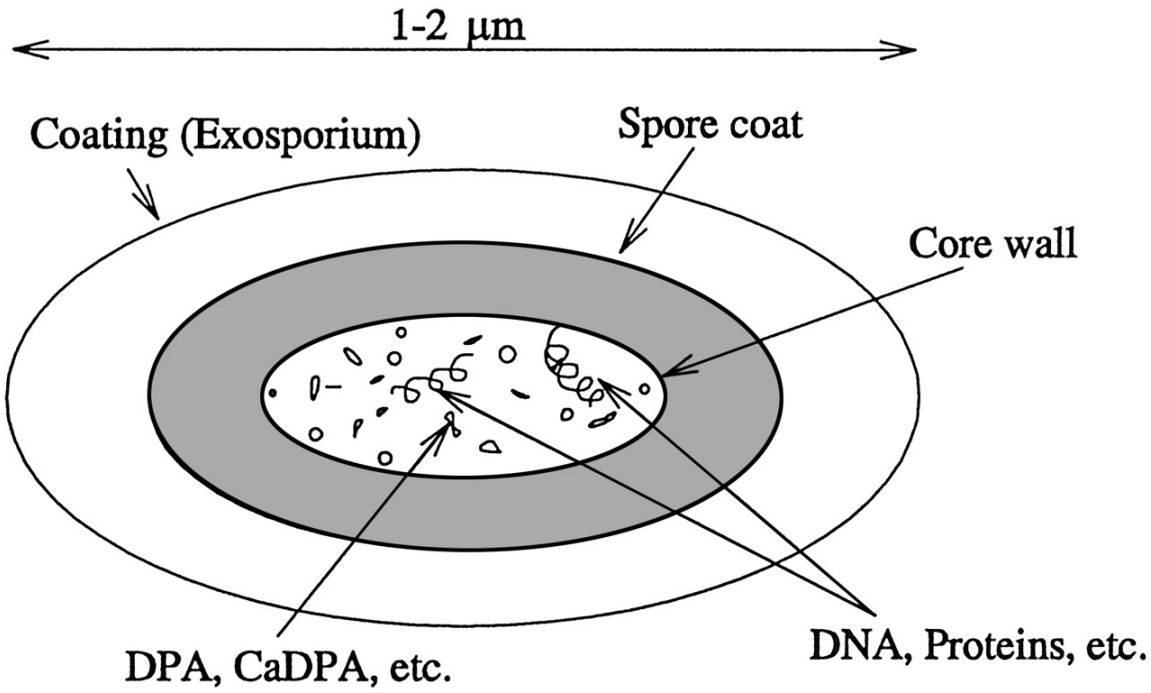

Fig.4.1. Sketch of bacterial spore (Scully et al., 2002). Reprinted with permission from "FAST CARS: Engineering a laser spectroscopic technique for rapid identification of bacterial spores" by Scully, M.O., Kattawar, G.W., Lucht, R.P., Opartny, T., Pilloff, H., Rebane, A., Sokolov, A.V., and Zubairy, M.S., 2002. *Proc. Natl. Acad. Sci.,* **99** (17), 10994-11001. Copyright 2002 by National Academy of Sciences.

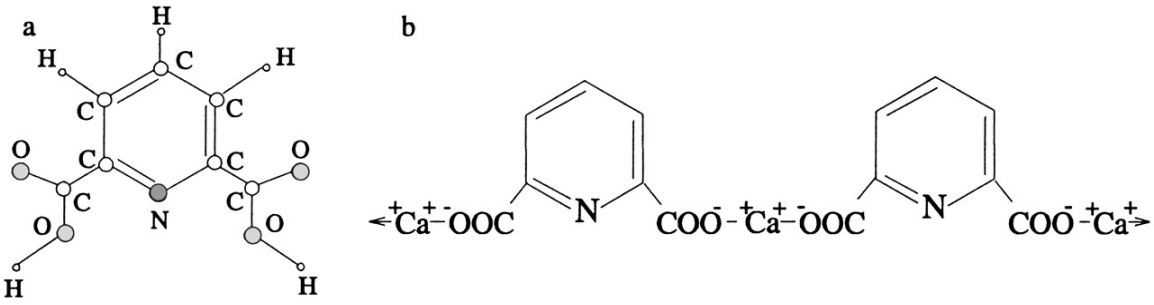

Fig.4.2. a) DPA b) Calcium – DPA complex (Scully et al., 2002). Reprinted with permission from "FAST CARS: Engineering a laser spectroscopic technique for rapid identification of bacterial spores" by Scully, M.O., Kattawar, G.W., Lucht, R.P., Opartny, T., Pilloff, H., Rebane, A., Sokolov, A.V., and Zubairy, M.S., 2002. *Proc. Natl. Acad. Sci.,* **99** (17), 10994-11001. Copyright 2002 by National Academy of Sciences.

The choice of CARS as the spectroscopic detection technique is based on the advantages that CARS offers over the currently existing techniques, as discussed in the review section of these methods. Both forward and backward CARS methods are discussed. CARS is the first step in identification and not only detection of DPA. Scully et al. (2002) presented the theory for using FAST CARS for identification of bacterial spores. The first step is to verify the applicability of this theory with CARS before applying the more complicated forms of CARS such as electronic-resonance enhanced (ERE) CARS.

4.2. Biological and Chemical Composition of DPA

A bacterial spore is depicted in Figure 4.1. It shows that DPA and its salts like Calcium-DPA are contained in the core and are in direct contact with the spore-specific DNA ribosomes and cell proteins. The approximate length of the spore is about 1.2 μm and the core is surrounded by the solid core wall and the spore coat. This structure is a key to the very long spore life, which is reported to extend to about 25 millions years (Black, 2002).

The role of DPA in these bacterial spores is the removal of water. This removal of water significantly reduces the destructive effect of heat on the bacterial cell. Heat destroys the DNA and proteins with aid of water. Because of the importance of this role, DPA and its salts contribute about 17 % of the dry weight of spores. Fig. 4.2a shows the chemical composition of DPA and Fig. 4.2b shows the composition of one of its salts, Ca-DPA. Two features are of specific importance for our study. DPA features a pyridine

ring that causes similarity in spectral features between Benzene and DPA. This fact has been used in our current study. For Ca-DPA, the Hydrogen ion in the O-C-O-H group is replaced by a Calcium ion.

4.3. Literature Review

4.3.1 Review of Non-Spectroscopic Methods for Anthrax Detection

This section is concerned with detection of anthrax and not specifically DPA, as the non-spectroscopic detection methods do not concentrate on a particular constituent of the biological agent as a marker. The end objective is the same in both cases. The methods reviews below concern bioaerosols in general, and can be applied to anthrax, which is usually present as a bioaerosol.

Such methods rely on collecting the bioaerosols under consideration and then allow them to settle directly into a culture that is easily accessible for detection by microscopic investigation. Hinds (1999) provides a good overview on the sampling process. Sampling of bioaerosols determines the presence of a certain bioaerosol and their number concentration. Sampling for bioaerosol particles employs many of the methods used for nonbioaerosol particles, but the analytical methods impose certain limitations on the sampling process. There are physical and biological aspects to bioaerosol sampling. The overview of the biological aspects involved in handling the bioaerosol was utilized in this present research with DPA, although direct exposure to anthrax spores was not in the scope of the study. The biological aspects require aseptic handling to prevent contamination and special attention to the survival of the biological

organisms during the process of sampling. Some studies show that the survival rate, which depends on the particular organism, the environment, the sample collection and analysis methods used, introduces a significant uncertainty into concentration measurements for the bioaerosol. The fraction of viable particles that survive the sampling and analysis process is estimated to be in the range between 0.1 and 0.001, as shown by Macnaughton et al. (1997). The high variation in the fraction of viable particles collected, interference with other particles, analytical sensitivity to underloading and overloading and the wide particle size range of interest are sources of considerable uncertainty. Additional reviews of sampling methods are found in publications by Nevalainen et al. (1993), Macher (1995) and Willeke and Macher (1998).

Bioaerosol sampling can be divided into three stages. The first stage involves the inlet collection, which is the same for bioaerosol and nonbioaerosol particles. The second stage is the collection and deposition of particles onto glass slides, a semisolid culture medium, or water. The third stage is biological analysis to identify the bioaerosol present and how much is present. Most bioaerosol analysis involves either examination with a microscope or growth in a culture medium followed by counting of colonies.

Multijet impactors have jets that impact directly onto the culture plates. This action spreads the collected particles over a wide area to prevent overloading. Single and multistage impactors are available with a range of cutoff diameters, but the shear forces that occurs in the high velocity jets and as a result of impact may cause loss of viability.

Impingers, which are a form of mutli-stage impactors but with the jet immersed in a liquid, are also used for bioaerosol collection. Liquid collection prevents desiccation, but the shear forces in the jet and in the turbulent liquid cause loss of viability. Water containing the collected organisms can be applied directly to the culture plates or can be diluted and applied to give the desired surface density.

Centrifugal samplers have a rotating paddle wheel, open to the environment on one end, with a stationary removable agar-coated plastic strip around the rim of the wheel. Air enters along the axis, and the particles contained in it are driven by centrifugal forces onto the collecting strip.

Membrane filters are also used to collect bioaerosol particles. The collected particles are then examined by an optical microscope, or they can be cultured by placing the filter, particle side up, on a culture medium. The filtration process causes significant desiccation of collected microorganism and loss of viability. This method of bioaerosol collection is used in highly contaminated environments.

The simplest technique for bioaerosol sampling would be to allow the bioaerosol to settle directly onto culture plates. The technique is not useful for quantifying airborne concentrations because, after culturing, the size of the initial particle cannot be determined.

The second stage relies heavily on impaction. The most common impactors are slit impactors, which impacts directly onto a culture medium. For bacteria and fungal spores, the culture medium, called agar, is a semisolid material containing water and nutrients that foster the growth of the viable particles that are collected. For viruses, cell

or tissue culture media are used. In many cases, the culture medium is mounted on a rotating disc to provide a history of collection.

The third stage of sampling, which involves depositing the particles on a plate to microscopically identify the bioaerosol, involves many considerations. The most important factor to consider is to provide the appropriate surface density for counting organism or colonies. If the loading is insufficient, there will be few counts and high statistical uncertainty. In microscopic counting of organisms, overloading causes overlap with nonbioaerosol particles, making identification difficult. Environmental samples usually have far more nonviable particles than viable particles. In counting colonies, overloading leads to three types of underestimation. First, if two of the same species are sufficiently close to each other, they will be counted as a single colony. Second, if two different species are close, one may inhibit the growth of the other. Finally, due to chemical nature, a nonbioaerosol particle may inhibit the growth of nearby viable particles. For a given sampler, the sampling time t to achieve the desired surface density s is calculated as $t = [s*A] / [C*Q]$, where A is the area onto which the particles are deposited, Q the sampler flow rate and C the average concentration of the bioaerosol.

Of particular interest is the study on aerosol-to-hydrosol transfer stages for use in bioaerosol sampling by Phan and McFarland (2004), in which a single-jet and multijet aerosol-to-hydrosol transfer stages (AHTSs) with cut points of 2 and 0.8 μm, were designed and its performances evaluated. The systems are intended to be used in series to transfer bioaerosol particles to transfer the biological particles of interest from aerosol state to hydrosol state in near real time. The AHTSs were used using polystyrene solid

and oleic acid liquid aerosol particles to determine their collection efficiencies, achieving efficiencies well above 90% for most size ranges. The various tests that were conducted indicated the need for a surfactant addition to the collection liquid to prevent losses of particulate matter from hydrosol to internal surfaces of AHTSs. The optimum concentration of Tween 20 into distilled water was determined to be near 0.1%. Preliminary bioaerosol testing was performed with a single jet unit using 5.2 μm AD clusters of BG spores, and with the multijet unit using both 0.8 μm AD single spores and 4.2 μm AD clusters of spores. Results showed unrealistic collection efficiency, which indicates that a different testing procedure should be used.

4.3.2 Review of Laser – Based Methods for Detection of Bioaerosol

Previous research dealing with detection and identification of bioaerosols through laser-based techniques is reviewed in this section. These methods are usually combined with methods for sizing and collection of aerosols.

Seaver et al. (1999) described an instrument developed to monitor the biological fraction of an aerosol. The instrument simultaneously sizes individual particles in a flowing air stream and then measures total fluorescence of the particles following excitation at 266 nm. Laboratory data show that measurements of these two parameters enable discrimination between different types of bacterial species. Field measurements are discussed in which bacterial samples were aerosolized and subsequently detected 800 m downwind. The apparatus has an optical chamber in which a stream of air with entrained biological particles is admitted through a 0.2 μm cutoff filter to produce a

well-defined jet. A 780-nm diode laser is directed perpendicular to the air stream so that it intersects with particles in the air stream. The scattered 780-nm laser light is collected by a reflector and collimated onto a photodiode. When the scattered light signal exceeds an adjustable threshold, a pulsed UV laser is triggered. The 266-nm laser radiation is generated by a frequency quadrupled Nd: YAG laser. With a proper delay, the UV beam is used to irradiate the particles. The 266-nm laser excitation produces fluorescence from constituents of the bioaerosol such as DNA, DPA and tryptophan. A color filter is used to block the 266 nm radiation. While the approach was partially successful to distinguish between some species, it could not distinguish between all species due to the presence of common constituents in all species. But more significantly, as in most biological fluorescence techniques, the complicated spectra are hard to analyze and quantify.

Cheng et al. (1999) described a similar apparatus for aerosol generation to investigate fluorescence spectra of bioaerosols and pollen. The system included an aerosol generator, chamber, aerosol monitoring instrumentation, and LIF detection system. The aerosol generators, chamber, and monitors were housed in an enclosure with the exhaust vented through a filtration system. Bacterial aerosols were generated from using a nebulizer. The aerosol chamber was designed with the aid of a computational fluid dynamics code to optimize the generation of aerosol beams with a well-defined geometry for reproducible fluorescence measurements. The aerosol chamber had four windows for optical access. Contours of measured fluorescence signals showed the expected peak related to tryptophan at a fluorescence wavelength of 330 nm, and four bacterial species in the aerosol exhibited very similar spectra. The fluorescence cross

sections were reproducible to within a factor of 5. Again, the fluorescence technique provided little information about a specific bacterial species and interference was still a problem.

Manoharan et al. (1990) probed Bacillus subtilis and three other bacterial spores at four different wavelengths with UV resonance Raman spectroscopy. With 251 nm excitation, bacterial nucleic acid spectra were obtained selectively. Nucleic acids also are strongly excited at 244-nm light while at that wavelength aromatic amino acid spectra just begin to be detected. Aromatic amino acid spectra were observed exclusively at 231 nm appears along with some new strong nucleic acid peaks with 222 nm excitation. While this study is significant in its attempt to target DPA as its probe molecule, the large difference in spectral characteristics, due to potential selective excitation of various UV absorption cell components, puts this laser technique in a disadvantage as a detection method for DPA. On the other hand, the results obtained also suggest that absorbing bacterial markers across the spectrum can be selectively excited to give rise to characteristic resonance Raman bacterial spectral fingerprints as a basis for rapid identification. This feature, if coupled with a laser diagnostic method that eliminates the disadvantages of scattering and fluorescence techniques like CARS, is the basis for our research.

Ghiamati et al. (1992) extended the research on aqueous solutions of DPA and Calcium DPA by probing endospores of three different bacterial spores using UV resonance Raman spectroscopy. The spores were detected at four different wavelengths and were compared with vegetative cells for normalization. At 222,231, and 251 nm the

spectra of endospores and their corresponding geminated spores show only modest differences. At 242 nm excitation, substantial differences are observed. Difference spectra obtained at 242 nm by subtracting spectra of germinated spores of Bacillus cereus from spectra of their corresponding endospores are attributed entirely to dipicolinate. It seems that this variation between different wavelength excitations can be attributed to large differences in the amounts and composition of proteins and nucleic acids. Ghiamati et al. (1992) showed that the 242 nm excitation is a significant transition in DPA for it can selectively and sensitively detect calcium dipicolinate in spores. The resonance enhancement at 242 nm is associated with the pyridine ring.

Carmona (1979) studied the vibrational spectra and structure of crystalline dipicolinic acid and calcium dipicolinate trihydrate at 100K by recording Raman Spectra of DPA and its salts in the spectral region extending from 0 to 4000 cm^{-1}. The solutions of DPA were saturated to avoid hydrolysis of the salt. The comparison of the vibrational spectra of the acid and its salts was quite useful. Some of the frequencies of the vibrational features remain almost unchanged for the different species and those that shift substantially are useful in understanding the nature of molecular association present in the solid state of these materials. The comparison is helpful in assigning band characteristics to different groups like the OH group and the pyridine ring. The latter in particular proved very valuable in the CARS research discussed in this dissertation. The benzene-like Raman transition of DPA and its salts due to the presence of the pyridine ring in the molecule was probed in our CARS experiment.

4.3.3 Review of Raman Spectroscopic Techniques for Solids and Solutions

Crystals of DPA were produced and probed using CARS technique in this thesis research. The advantages of CARS over other techniques were previously discussed, and the previous research dealing with spectroscopy for solids was reviewed.

Suzuki et al. (1968) first obtained polarized Raman spectra of single crystals of naphthalene and anthracene using an argon ion laser as an excitation light source. Pronounced effects of polarization were found for the Raman lines in the crystal spectra. The spectroscopic data was compared with theoretical models for the calculation of vibrational frequencies. The vibrational modes responsible for the lattice vibrational Raman lines were found to be described by rotational oscillations about the three principal axes of the molecule. Using the same technique, the effects of temperature variations the vibrational Raman lines of the lattice were studied. The frequencies obtained at different temperatures were used to evaluate the mean square amplitudes of the rotational oscillations of the molecules in the crystal lattice.

Following on the above research, Bree and Kydd (1970) recorded infrared and Raman spectra of single crystal samples of naphthalene-d_8 over the entire energy range of the fundamental vibrations. The depolarization ratios for the Raman lines in carbon tetrachloride and benzene solutions were obtained. The data was used to assign the frequencies of the molecular fundamental vibrations. The data were compared to force-field calculations and were found to be in good agreement.

Zinth et al. (1982) used a transient stimulated Raman process to coherently excite the Raman-active vibrational modes. They probed liquid cyclohexane and four new

Raman lines were observed in the frequency range they investigated. After the transient stimulated Raman process was initiated, a subsequent delayed probe of relatively long duration interacted with the freely relaxing vibrations. The resolution of the spectra was degraded by scattering. The paper by Zinth et al. (1982) describes the problems associated with probing liquid solutions, such as scattering and background interference of the background.

Decola et al. (1980) investigated the lineshape of a vibrational transition of naphthalene crystal at 1.6 K using four-wave mixing techniques with two narrow band lasers at ω_1 and ω_2. The lineshape of the CARS signal from the 1385 cm^{-1} totally symmetric mode was well described by the Lorentzian lineshape over the complete range and the vibrational relaxation time of the excitation was measured.

An early study of molecular structure using CARS was performed by Dlott et al. (1982). The temperature dependence of the decay of vibrational excitations in naphthalene was investigated. At temperatures less than 40 K, the vibrational relaxation is dominated by spontaneous emission of phonons. Above this temperature, high frequency phonons induce dephasing. There was a significant discrepancy between the measured vibrational frequencies than in previous studies. This discrepancy is attributed to impurities in the samples used in the previous studies. The temperature-dependent contribution to the linewidth was characterized by a simple activation energy.

Wen et al. (1991) extend the use of CARS to polycrystalline and opaque solids, which is of direct relevance to our study of DPA crystals. In addition, they measured the CARS signal in the backscattering geometry, which has been demonstrated as well in

our research. They used a three-color picosecond CARS technique in backscattering geometry. The advantage of using three-color CARS is its insensitivity to the sample morphology, which did not raise any problems for our DPA CARS research. Wen et al. (1991) studied time-dependent vibrational dephasing from opaque polycrystalline solids at low temperatures. A quantative treatment of the limiting time response of the experimental apparatus was performed. Measurements of vibrational dynamics in low-temperature carbon disulfide indicated that the polycrystalline samples were homogeneous on a microscopic level as was the case for the large single crystals used in other research. Raman line broadening in a sample of naphthalene in which strain was induced intentionally by grinding and compression is investigated as well. The CARS signal was easily discerned against the nonresonant background and scattered light by the proper use of interference optics and choice of the detection instruments. The measurements of CS_2 CARS spectra revealed the advantage of using the backscattering geometry for rough materials or powders.

4.3.4 Previous Spectroscopic Research on Benzene

CARS experiments for liquid benzene were conducted as a preliminary step in our measurements of DPA CARS for the purpose of fine tuning and adjustment of the experimental system. DPA has a benzene-like ring in its chemical structure, as shown before, and as such benzene can be used as a model molecule for this experiment. In addition to the above mentioned advantages, benzene is a well characterized molecule that has been extensively studied.

Callomon et al. (1966) examined the 260-nm electronic resonance in benzene with absorption spectroscopy. The rotational fine structure was analyzed by comparison with theoretical contours. Improved values for several fundamental spectroscopic constants were obtained and some vibrational assignments were revised. The rotational and vibrational spectra recorded in this study made it certain that the equilibrium configurations of the carbon skeleton in benzene are exactly planar and hexagonal in both the ground and excited states.

Raman techniques have been used extensively to probe the benzene molecule. Gillen and Griffiths (1972) analyzed the Raman line shapes and ^{2}D NMR relaxations as functions of temperature, and the highly anisotropic nature of the molecular reorientation was evident. It was concluded that the rotation about the symmetry axis appeared to be consistent with a slightly damped free rotation model of diffusion, whereas the rotational motion perpendicular to the C_6 axis was best interpreted in terms of a small step Brownian rotation model. These findings were important because the interpretation of molecular reorientation in liquid benzene had been largely unsatisfactory up to this study because isotropic reorientation was assumed.

Griffiths et al. (1974) used detailed measurements of Raman line shapes and linewidths to study collision-induced intermolecular vibrational energy transfer process in liquid benzene. The lifetimes of molecules in the upper vibrational level of the υ_2 Raman transition in benzene were evaluated using frequency and time measurements. Varying the absolute number of benzene-benzene collisions through dilution with C_6D_6 the lifetime of the υ_2 transition was altered.

Tanabe and Jonas (1977) reported the Raman line shapes of totally symmetric bands, υ_1 and υ_2 and five degenerate bands as a function of pressure from 50 bar to 4 kbar and over a temperature range from 30-120 degrees Celsius. They used a crude model to estimate the vibrational relaxation width for the degenerate Raman bands and concluded that the vibrational relaxation contributes differently to the total width of the individual bands. For all bands measured the vibrational relaxation time increased with pressure but the effect of varying the temperature was different for each individual band.

Dugan et al. (1988) also used CARS and coherent Stokes Raman spectroscopy (CSRS) to probe liquid benzene. A new class of detuning oscillations in the THZ domain was reported. Vibrational dephasing rates were measured in neat benzene, benzene-d_6 and in a binary mixture where frequency beating oscillations difference are convolved with the detuning oscillations.

Joo and Albrecht (1991) performed femtosecond time-resolved CSRS measurements of benzene-h_6 and benzene-d_6. Binary mixtures of both species were investigated for two different polarization geometries. The reorientational correlation time of benzene and the vibrational dephasing time for the υ_1 ring breathing mode were measured. Bohr difference frequency beats were resolved between the υ_1 band of protonated benzenes and deuterated benzenes that were present in neat liquids.

Joo and Albrecht (1993) probed liquid benzene using femtosecond time-resolved CARS at room temperature and at 6.5 degrees Celsius. The υ_1 ring-breathing modes of neat benzene-h_6 and benzene-d_6 were probed. The dephasing dynamics at early stages were measured with the ultrafast time resolution owing to the use of femtosecond lasers.

Deviations from the conventional exponential decay were reported and the data analyzed using a Kubo line shape. The correlation time and the rms magnitude of the Bohr frequency modulation were determined for the process responsible for the vibrational dephasing. A spinning motion was suggested as the stochastic process responsible for the vibrational dephasing in benzene and neat liquids.

4.4. Theoretical Basis

This current research is based on a theoretical study by Scully et al. (2002). In this study the potential use of CARS technique for detecting DPA was discussed. Scully et al. (2002) identified the major problem of the different resonance fluorescence techniques as being the inherent lack of advanced signal processing techniques. This leads to significant difficulties in identifying specific organisms from the fluorescence technique because of non-distinguishable emission spectra. It is postulated that resonant Raman spectroscopy is more promising for spore-specific identification. However, for resonance Raman spectroscopy, the interference of the background with the weak signal necessitates long collection times. Therefore, the optical probing of the biological particle is not instantaneous. This disadvantage can be overcome by increasing the resonant Raman signal strength and thereby reduce the probing time of the particle. This can be achieved through the CARS technique. In this research, we have realized the first steps towards such technique by performing visible CARS of DPA.

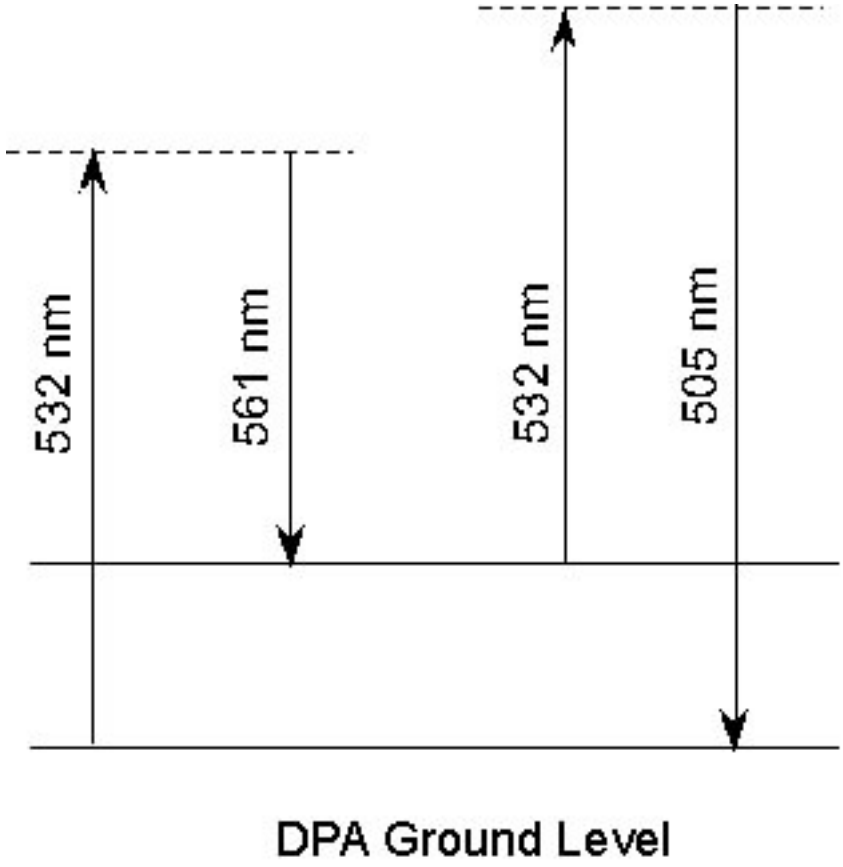

Fig.4.3. Energy level schematic diagram for the DPA CARS process.

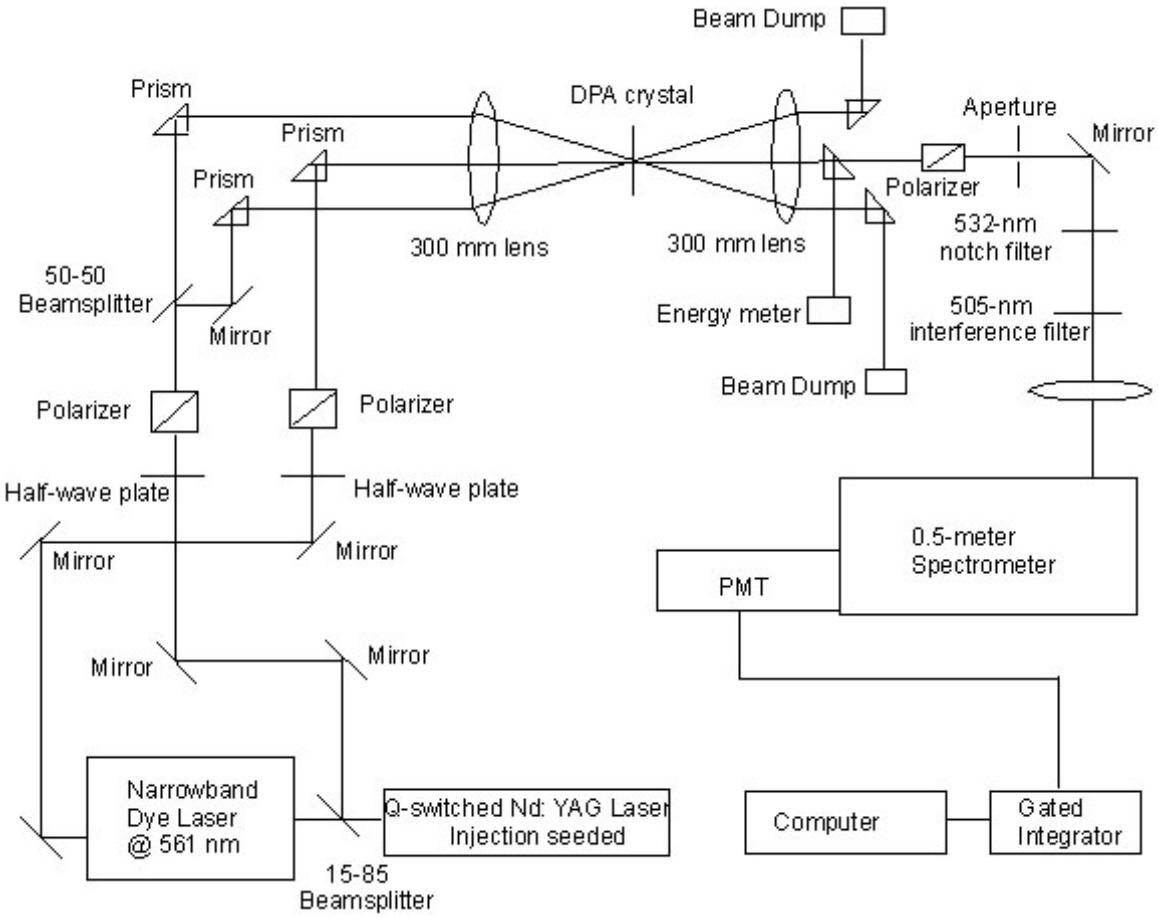

Fig.4.4. Experimental system for the DPA CARS measurements. For the benzene CARS measurement a cell of pure liquid benzene was placed in the CARS probe volume.

Figure 4.3 is a schematic energy level diagram of the coherent anti-Stokes Raman scattering (CARS) system for the detection of DPA. The Raman polarization in the medium is established when the Stokes laser is tuned so that the frequency difference between the first pump beam and the Stokes laser is tuned to a Raman resonance of the DPA molecule. The second pump beam then scatters from the induced Raman resonance to produce the CARS signal.

4.5. Forward Scattering CARS for DPA

4.5.1 Experimental System for Forward Scattering CARS System

The CARS system for DPA and benzene in a forward CARS scattering collection configuration is shown in Figure 4.4. The CARS spectrum of the 990 cm^{-1} ring-breathing transition in pure liquid benzene was recorded to calibrate the experimental system and optimize the system alignment. DPA was detected using the same experimental system. The wavelength of the Stokes beam was changed to match the 998 cm^{-1} transition of DPA.

The pump source for the 532-nm pump beam (ω_1) was a Continuum Model 9010 injection-seeded, Q-switched Nd: YAG laser with a repetition rate of 10 Hz, pulse length of approximately 7 ns, and 532-nm pulse energy of approximately 750 mJ. The 532-nm beam was also used to pump a Continuum Model ND 6000 narrowband, tunable dye laser to produce the Stokes beam (ω_2) at a wavelength near 560 nm with a frequency bandwidth of approximately 0.08 cm^{-1}. The energy of the 532-nm beam was split using an 85-15 beam splitter, with the higher energy beam being directed into the dye laser.

The dye solution used for the dye laser was prepared from a solution of Rhodamine 590 in Methanol. The output beam of the dye laser had a pulse energy of approximately 10 mJ. The 532-nm beam, after the first beam splitter, was passed through a delay line to ensure that the pump and Stokes beams were temporally well-overlapped in the probe volume. The 532-nm beam energy was further divided by a 50-50 beam splitter and directed by mirrors and prisms into the probed media. The pulse energies for both the 532-nm beams and the 560-nm beam energies were controlled by combinations of half-wave plates and polarizers. The control of the energy of the beams, which were overlapped at their beam waist and focused on a fragile DPA crystal or in a cell with liquid benzene, was absolutely crucial for the success of the experiment and for safety considerations relating to benzene flammability. The DPA samples, prepared by precipitation from a DPA solution in water, degraded rapidly when subjected to intense laser irradiation. Increasing the lifetime of the DPA samples proved important in the early stages of the experiment to determine the optimal wavelength for the Stokes beam at the centerline of the DPA transition, as some drifts from the nominal dye laser wavelength were experienced. When acquiring DPA spectra, the increased lifetime of the DPA samples enabled extended measurements of spectra. In addition to the maximum attenuation provided by the combination of half-wave plates and polarizers inserted in the path of the 532-nm beam and Stokes beam, it was necessary to operate the Nd: YAG laser with a non-optimal Q-switch delay relative to the flashlamp pulse in order to lower further the pulse energies of the CARS beams at the DPA crystal. The

pulse energies for the 532-nm and 560-nm beams at the CARS probe volume were estimated to be on the order of few microjoules.

The pump and Stokes beam were focused into the CARS probe volume using a lens with a focal length of 300 mm. Optimal overlap was achieved using a 100 μm pinhole, through which the pump and Stokes beam were directed. After passing through the CARS probe volume, the pump, Stokes and CARS signal beams were recollimated using a 300-mm-focal-length lens. The 532-nm pump and the Stokes beams were then directed into beam dumps. Significant scattering of the beams was experienced when they passed through the DPA samples or benzene, and this scattering interfered with the CARS signal. A 532-nm notch blocking filter was placed in the CARS signal channel, together with a 505-nm interference filter (CARS signal wavelength), to minimize scattered light. The interference filter passed 12% of the CARS signal and had a 10 nm bandwidth, but this reduction in CARS signal intensity was necessary to avoid scattered light interference with the DPA spectrum. The 505-nm CARS signal was directed through apertures and focused using a 150 nm lens onto the entrance slit of a 0.5-m spectrometer.

The spectrometer was not scanned synchronously with the dye laser wavelength. The exit slit was operated throughout the experimental measurements at maximum width to provide the widest possible detection bandwidth; this was possible only because the suppression of the scattered light using filters was very effective. A photomultiplier tube (PMT) (Hamamatsu R1516) was used to detect the 505-nm CARS signal at the exit of the spectrometer. The CARS signal was divided by the dye laser energy on a shot-by-

shot basis to account for the fluctuation of the dye laser energy and its influence on the CARS signal. The Stokes dye laser was scanned under computer control in an interval long enough to capture the 998 cm^{-1} DPA or 990 cm^{-1} benzene transition, and a Labview program was used to record the CARS spectrum. The wavelength of the Stokes dye laser was scanned in different step sizes for various scans, averaging over a different number of laser shots at each position, and the length of the scan interval varied as well. These parameters in data acquisition procedure were influenced chiefly by the need to extend the lifetime of the DPA crystal and to obtain meaningful results. The Stokes beam and the 532-nm beams were blocked alternatively at the end and the beginning of the scan to provide an estimate of the contribution of the non-resonant signal to the spectrum.

The benzene cell used is shown in Fig. 4.5. Benzene filled the volume between two BK-7 glass windows held in place by two aluminum rings. Liquid benzene was fed through a side inlet pipe. Leakage through the windows was prevented through the use of Teflon O-rings, chosen for their excellent resistance to corrosion by benzene. The benzene cell was mounted on a translational stage to move its position relative to the overlap of the beams and thus to obtain maximum benzene CARS signal.

DPA crystals were prepared by dissolving powdered DPA in distilled water. Because of the poor solubility of DPA in water at room temperature, the mixture was heated to 100 °C and kept at this temperature until the DPA powder was entirely dissolved. The solution of the DPA in water was then cooled in an insulated chamber. After preparing the initial sample, DPA flakes with good crystalline structure were used as seed crystals and were inserted into the solution at this stage.

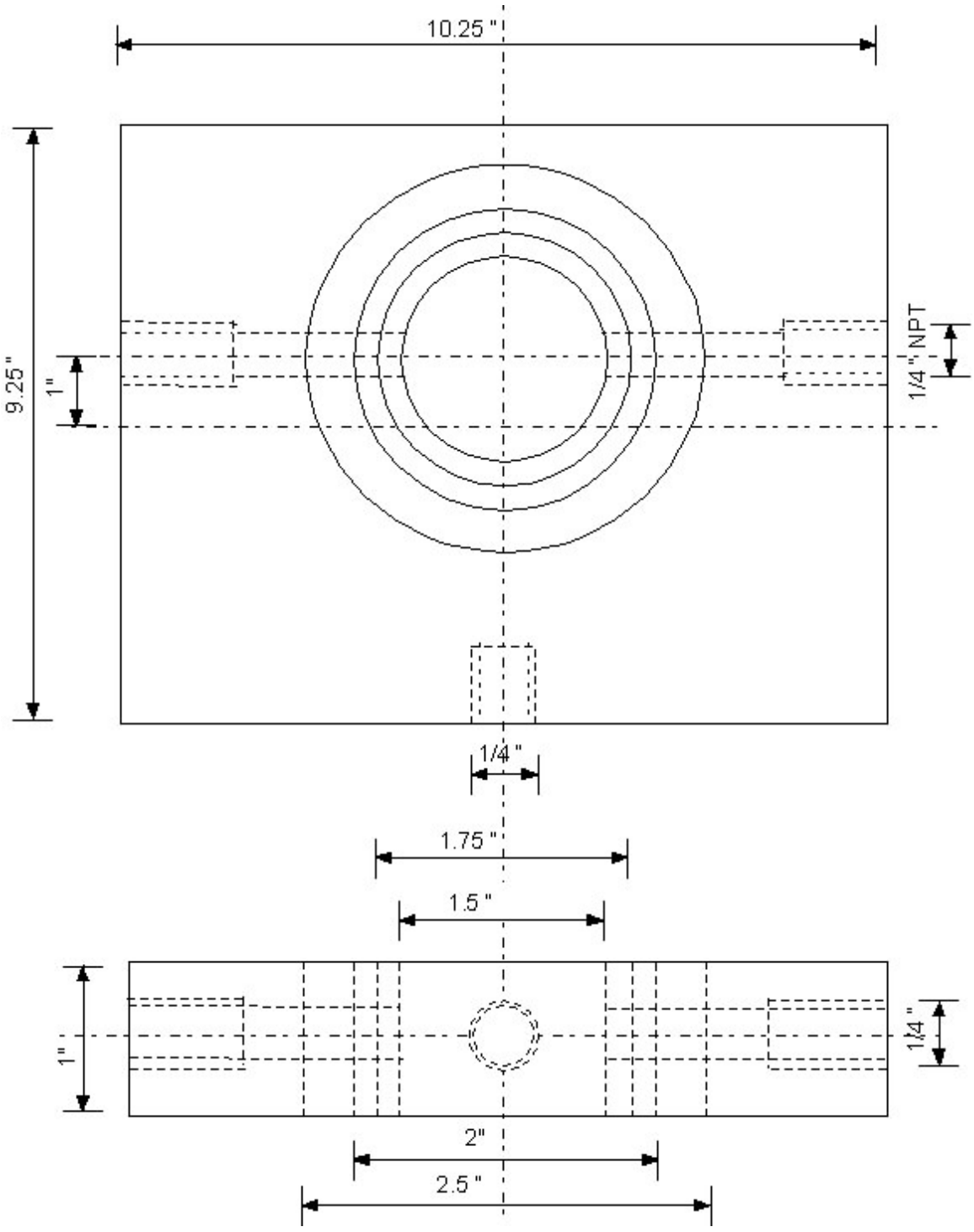

Fig.4.5. Aluminum Cell for the Benzene CARS measurements.

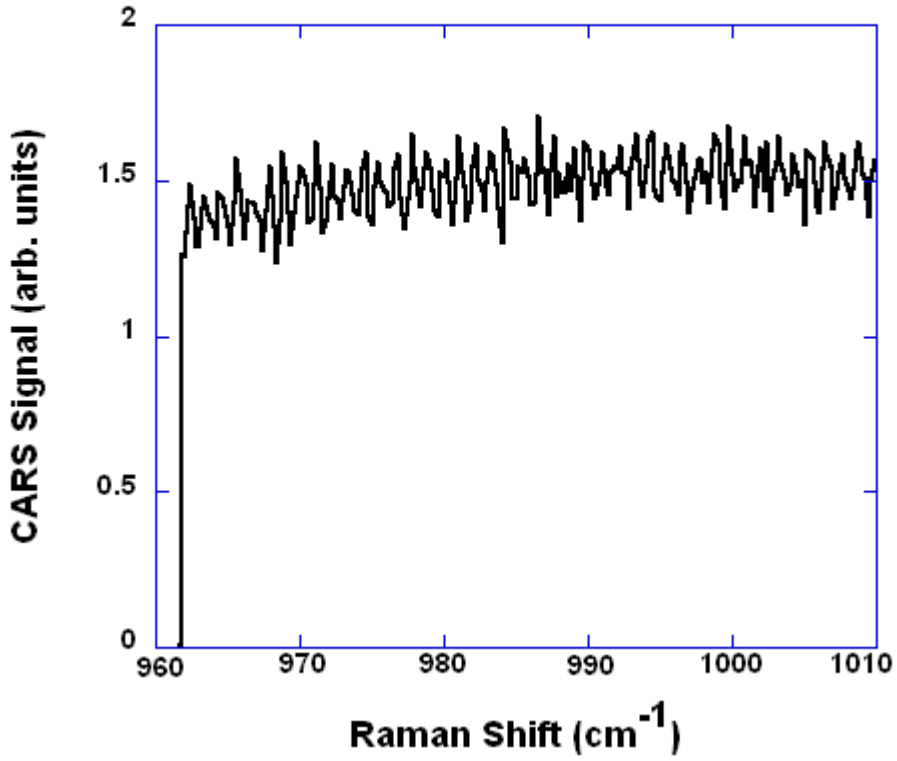

Fig.4.6. Nonresonant background signal recorded by placing a glass plate in the CARS probe volume. The sharp signal decrease at 982 cm^{-1} is an indication of the extent of the spectrometer bandpass.

As cooling continued, DPA flakes were observed to grow from the solution. The seed crystals, when used, slightly improved the light transmission properties of the DPA crystals. The flakes that exhibited the best light transmission properties, had no or few cracks on visual inspection and were large enough to be mounted at on a translation stage were selected. These were then placed in the CARS probe volume. The thickness of the DPA crystals used for the forward CARS experiment was approximately 500 microns. Single CARS spectra were recorded with the sample at a given position with respect to the beam overlap position. The samples were then translated to another position to record another spectrum as the DPA crystal usually deteriorated as the result of the laser irradiation.

4.5.2 Experimental Results for Forward Scattering CARS

The spectral response of the CARS system was first tested by placing a glass slide in the CARS probe volume. The resulting nonresonant background spectrum is shown in Fig. 4.6. The drastic increase in signal is an indication of the spectral bandpass of the 0.5-m spectrometer. Once the dye laser was scanned so that the CARS signal was within the spectral bandpass, the system response was nearly constant for the entire spectrometer bandpass. Determining the bandpass of the spectrometer was necessary to verify that resonances of DPA shown below in the DPA CARS spectra are real resonances and not non-resonant signals. The Stokes dye laser power is constant to better than 10% over the scanning range shown in Fig. 4.6. The dye laser was scanned using a step size of 0.01 nm/s and were averaged over 30 shots at each spectral position.

This scanning speed provided the optimum conditions to capture the various features of the DPA spectrum while maintaining the DPA crystal quality and lifetime for the longest possible lifetime.

The CARS spectra of polycrystalline DPA and pure liquid benzene are shown in Fig. 4.7. The ring-breathing Raman transition of the pyridine ring in DPA appears at 998 cm^{-1} in agreement with experimental Raman measurements of Carmona (1979), who performed Raman measurements on crystalline DPA samples held at a temperature of 100 K. The shape of the CARS spectrum that we have recorded for the 998 cm^{-1} transition is remarkably similar to the spectrum recorded by Carmona, even though our DPA spectrum was recorded at room temperature. The shoulder to the low-Raman-shift side of the 998 cm^{-1} transition that is evident in the DPA spectrum shown in Fig. 4.7 is also evident in the spectrum shown by Carmona (1979). The full-width-at-half-maximum of the 998 cm^{-1} CARS transition is approximately 4 cm^{-1}, and the peak is shifted by approximately 8 cm^{-1} from the peak of the equivalent transition in benzene. It is also noteworthy that the nonresonant background from the DPA spectrum is essentially negligible.

Fig. 4.8 and Fig. 4.9 are two different spectra of DPA acquired at two different experimental runs to show consistency of the results and their repeatability. It is evident from Fig. 4.8 and Fig. 4.9 that the resonance appears consistently at 998 cm^{-1}. The intensity of the signal varied with the quality of the DPA crystals used and the thickness of the crystal at the CARS probe volume.

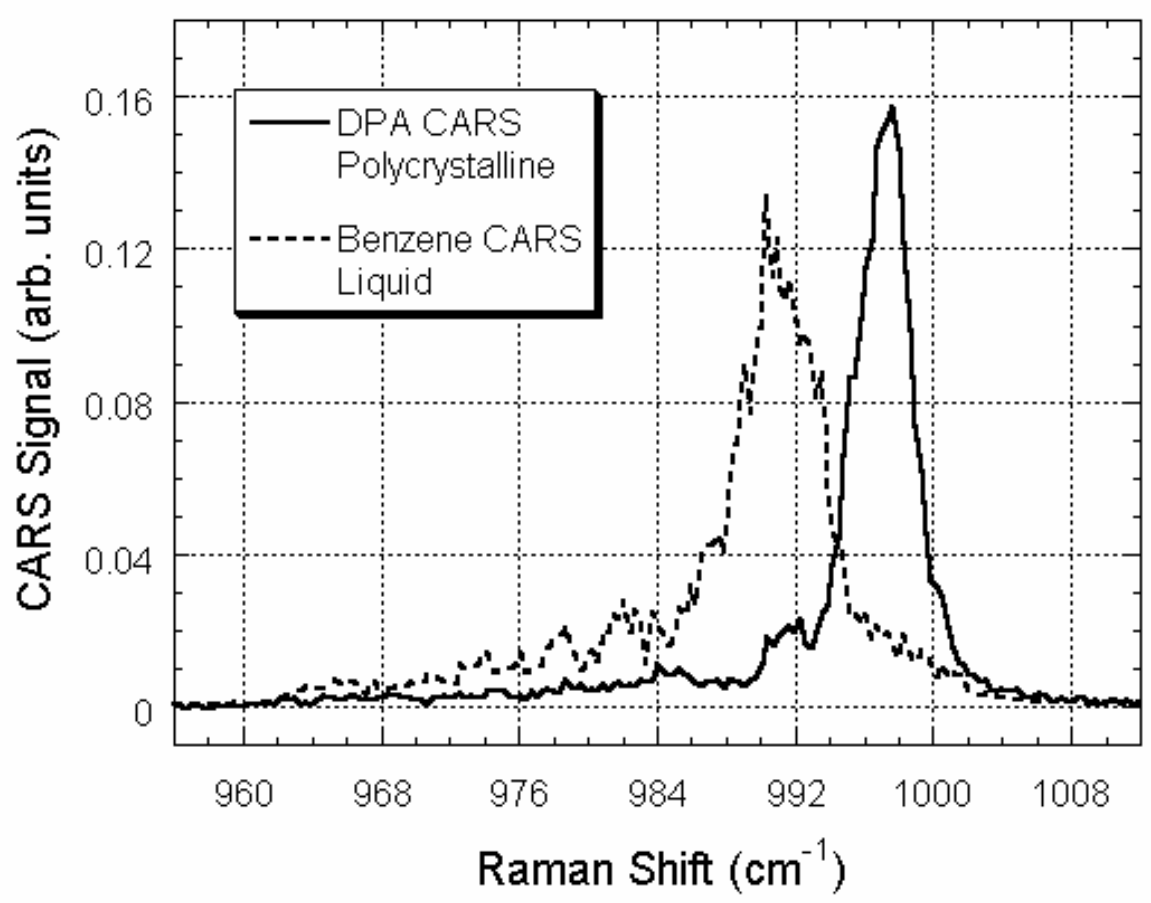

Fig.4.7. CARS signals recorded from polycrystalline DPA and pure liquid benzene.

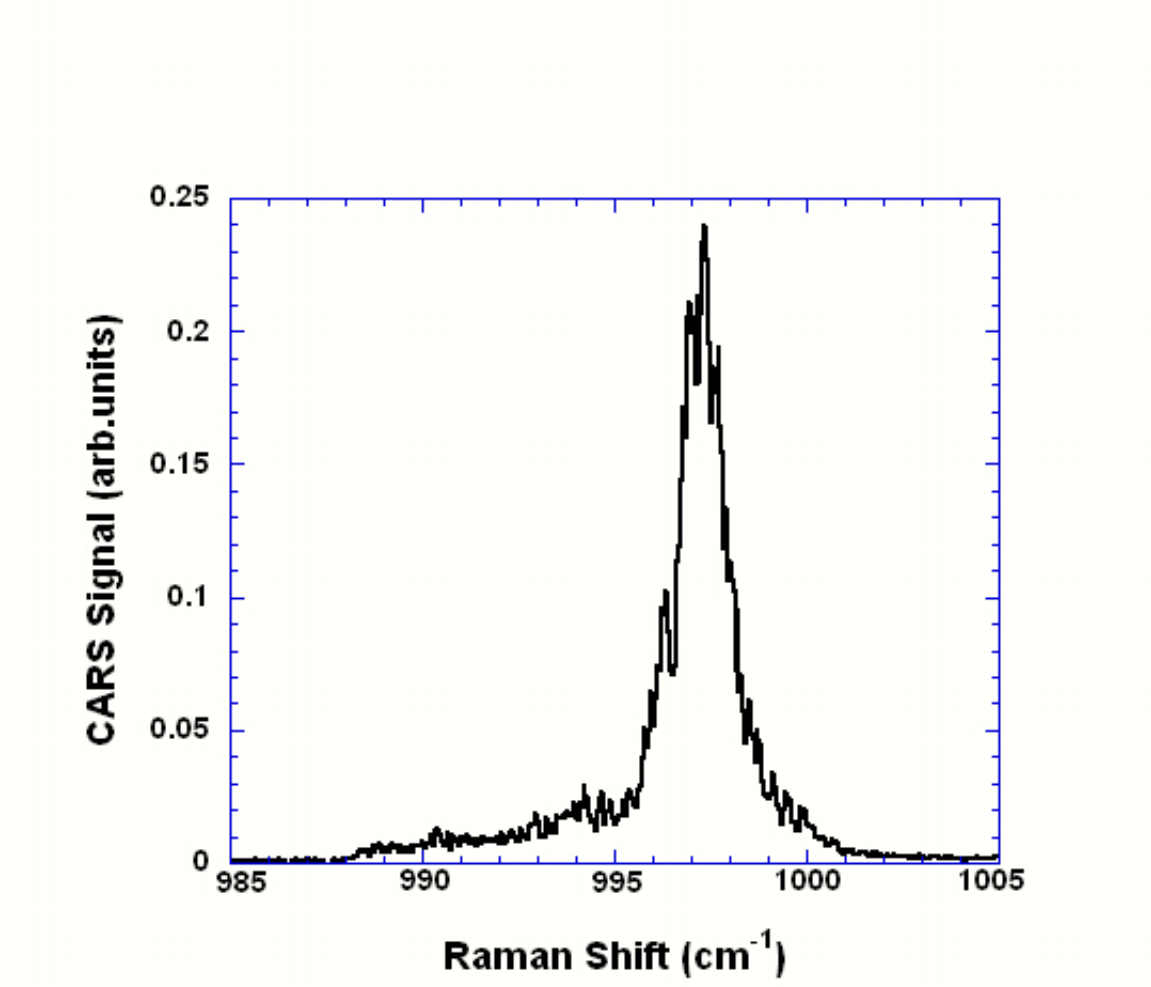

Fig.4.8. CARS signal recorded from polycrystalline DPA.

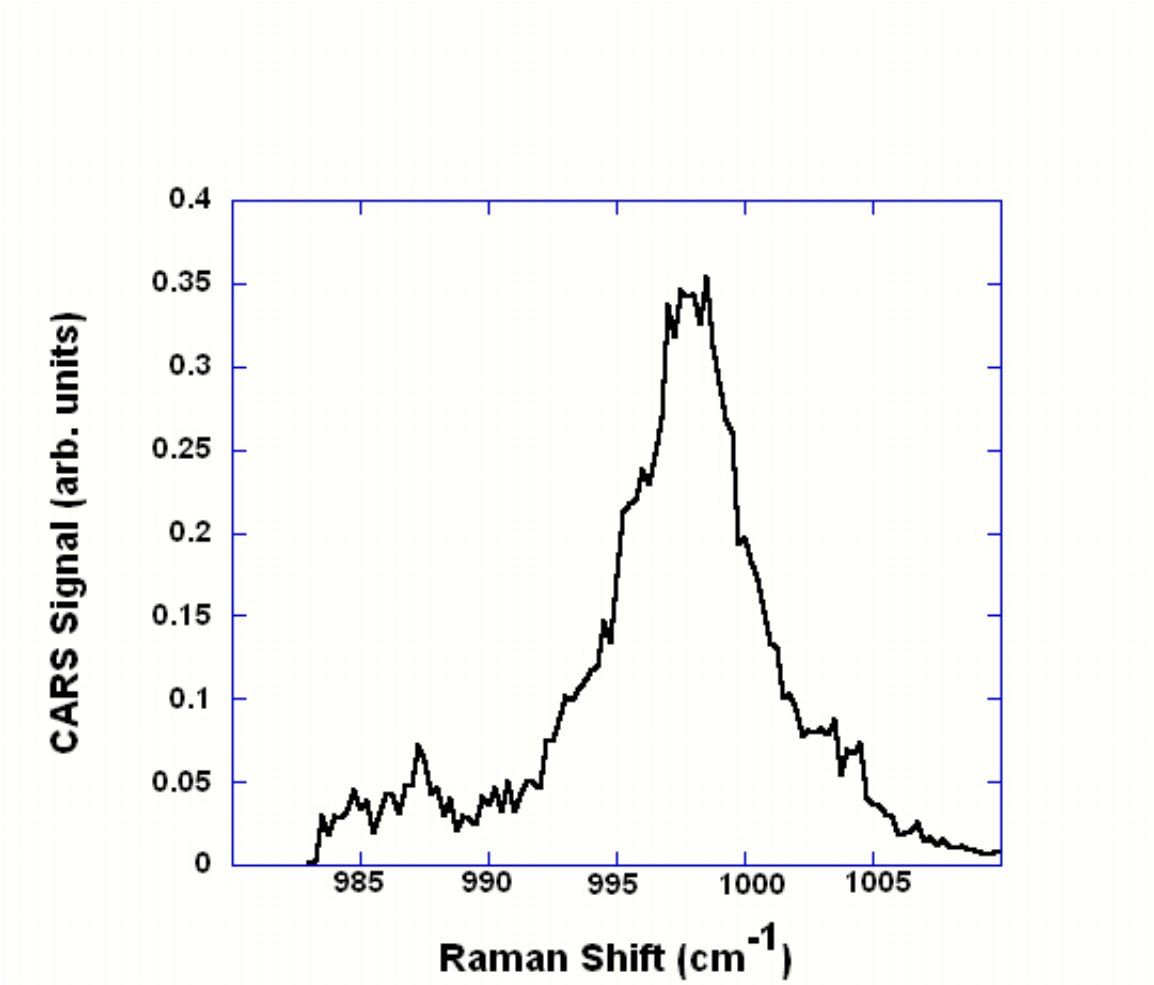

Fig.4.9. CARS signal recorded from polycrystalline DPA. Consistency in main spectral features evident when compared with Fig.4.8.

4.6. Backward Scattering CARS for DPA

Experimental results obtained for the DPA CARS technique with the signal collected in a backscattering configuration is discussed in this section. The experiments were performed using two types of crystals obtained from different solutions. The motivation for detecting the DPA CARS crystal in backward direction was the need to explore the possibility of developing military portable sensors that would be able to detect the presence of an anthrax cloud at different distances to protect the soldiers from biological warfare.

4.6.1 Theoretical Model

Solutions of DPA in dymethylformamide (DMF) produced solid, opaque DPA crystals with milky appearance. These crystals have the shape of parallelepiped dimensions of a few millimeters. The crystal exhibits numerous cracks, scratches and irregularities when observed under the microscope. These irregularities scatter light strongly in different directions. The second type of crystal that was used are the flakes discussed section 4.5.1. They are modeled as monocrystals attached to each other, and each monocrystal has a size bigger than the optical wavelength. The model used addresses both types of crystals and the CARS signal by adjusting the parameters of roughness for each case.

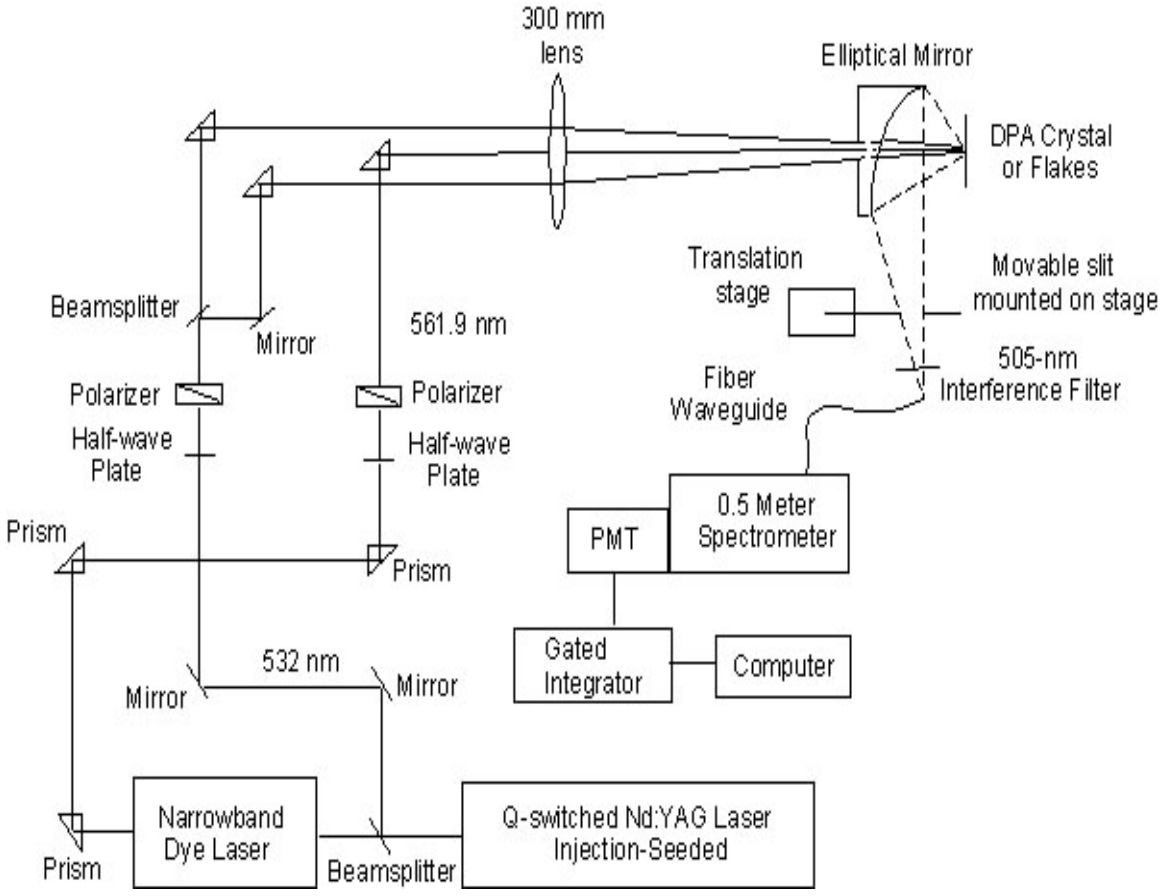

Fig.4.10. Experimental system for DPA detection in backward CARS configuration.

The DPA crystals are modeled as a stack of crystals with rough surfaces, for which the random grating model, discussed by Rim et al (1990), Voronovich (1994) and Nieto-Vesperinas (1990), can be used. The rough surface is described by random height $z = \xi (x, y, z)$, where x and y are the Cartesian coordinates along the Cartesian plane. The number of interfaces and characteristic spatial size of them is different for each type of crystalline medium used in the experiment. Hanna et al. (2005) provides a detailed discussion of the theoretical model used for comparison.

4.6.2 Experimental System-Backscattering CARS Detection of DPA

The experimental system for the backscattering CARS technique used for the detection of DPA is shown in Fig. 4.10. The source for the 532-nm pump beam used in the CARS experiment was a Continuum Model 9010 injection-seeded, Q-switched Nd: YAG laser with a repetition rate of 10 Hz, pulse length of approximately 7 ns and a pulse energy for the 532-nm output of approximately 700 mJ. The same 532-nm output of the Nd: YAG laser was used to pump a narrow-band Continuum Model ND6000 tunable dye laser to produce the Stokes beam at a wavelength of 561 nm. The Stokes beam has a frequency bandwidth of approximately 0.08 cm^{-1}. The pump and Stokes beams passed through multiple reflections by mirrors and prisms to be guided to the probe volume. The probe volume consisted of either thin, brittle polycrystalline DPA flakes obtained by precipitation of heated DPA solution in water or from solid DPA crystals obtained from precipitation of DPA solution in Dimethylformamide (DMF). It was crucial in these experiments to control the power of the pump and Stokes beam

when taking a CARS spectrum of DPA because the crystals and flakes would degrade rapidly when subjected to intense laser fields. Therefore, the energy of each beam was controlled using a combination of half wave-plates and polarizers and the lasers were operated at a non-optimal Q-switch delay relative to the flashlamp pulse for further attenuation. The pulse energies of the pump beams at 532-nm and the Stokes beam around 561-nm at the CARS probe volume were about 0.9 mJ and 0.3 mJ, respectively.

The CARS focusing lens had a focal length of 300 mm. The waist of the beams at the probe volume was approximately 100 microns. The beams passed through a hole in an ellipsoid Aluminum mirror. The DPA sample and the facet of an optical fiber waveguide were placed at the conjugated points of the mirror. The backscattered CARS signal from the DPA crystal second surface as well as scattered 532-nm and 561-nm radiation was collected by the optical fiber. To separate the backscattered CARS signal guided into the fiber from the other sources, a 505-nm narrow band interference filter with 10-nm bandwidth was placed at the inlet fiber tip. The other end of the fiber waveguide was directed onto the entrance slit of a 0.5-m spectrometer. The backscattered CARS Signal was detected using photomultiplier tube (PMT) (Hamamatsu R 1516) at the spectrometer exit slit. The CARS signal was recorded on a shot-by-shot basis using a gated integrator while the Stokes dye laser wavelength was scanned through a Labview program.

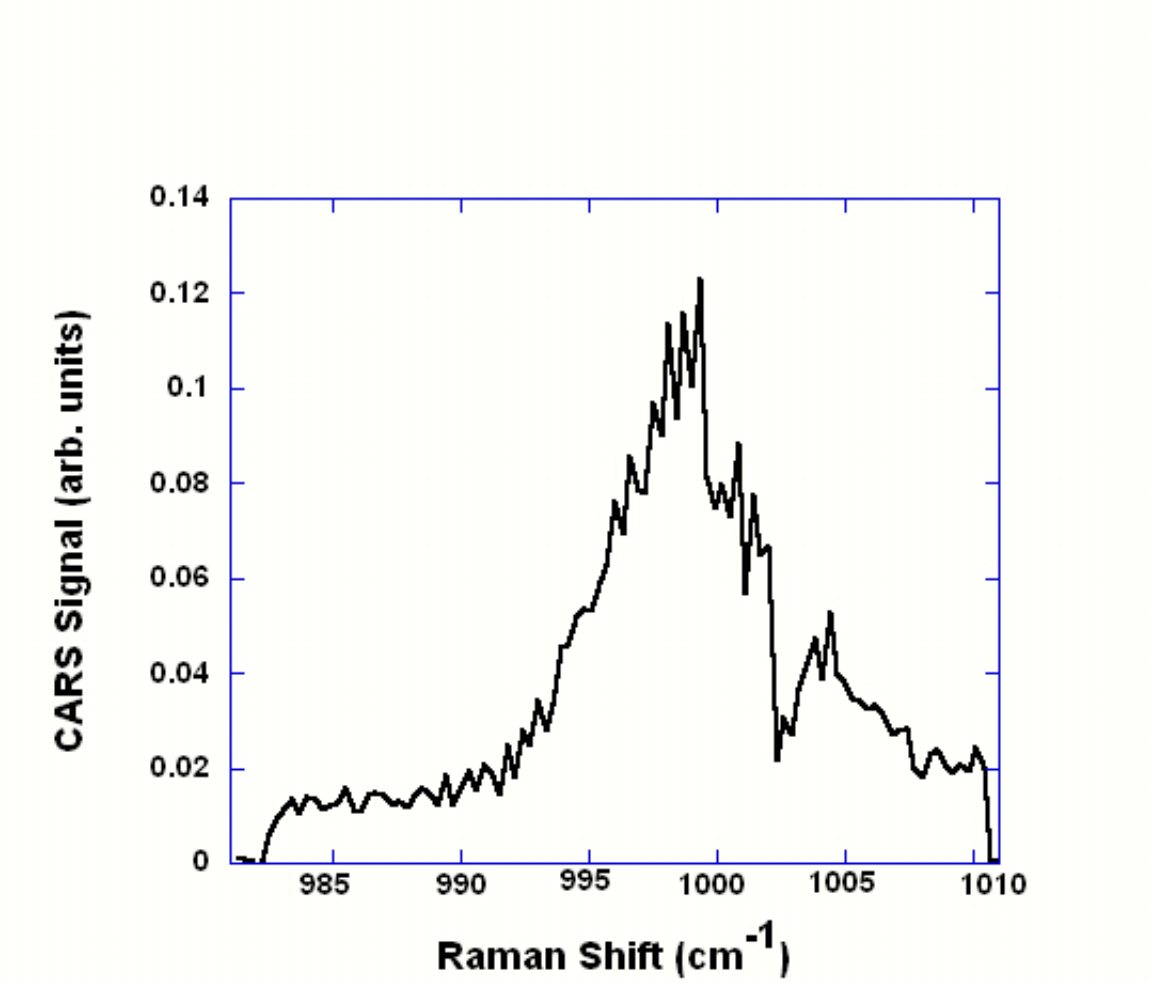

Fig.4.11. DPA spectrum acquired by backscattering CARS configuration using DPA flakes.

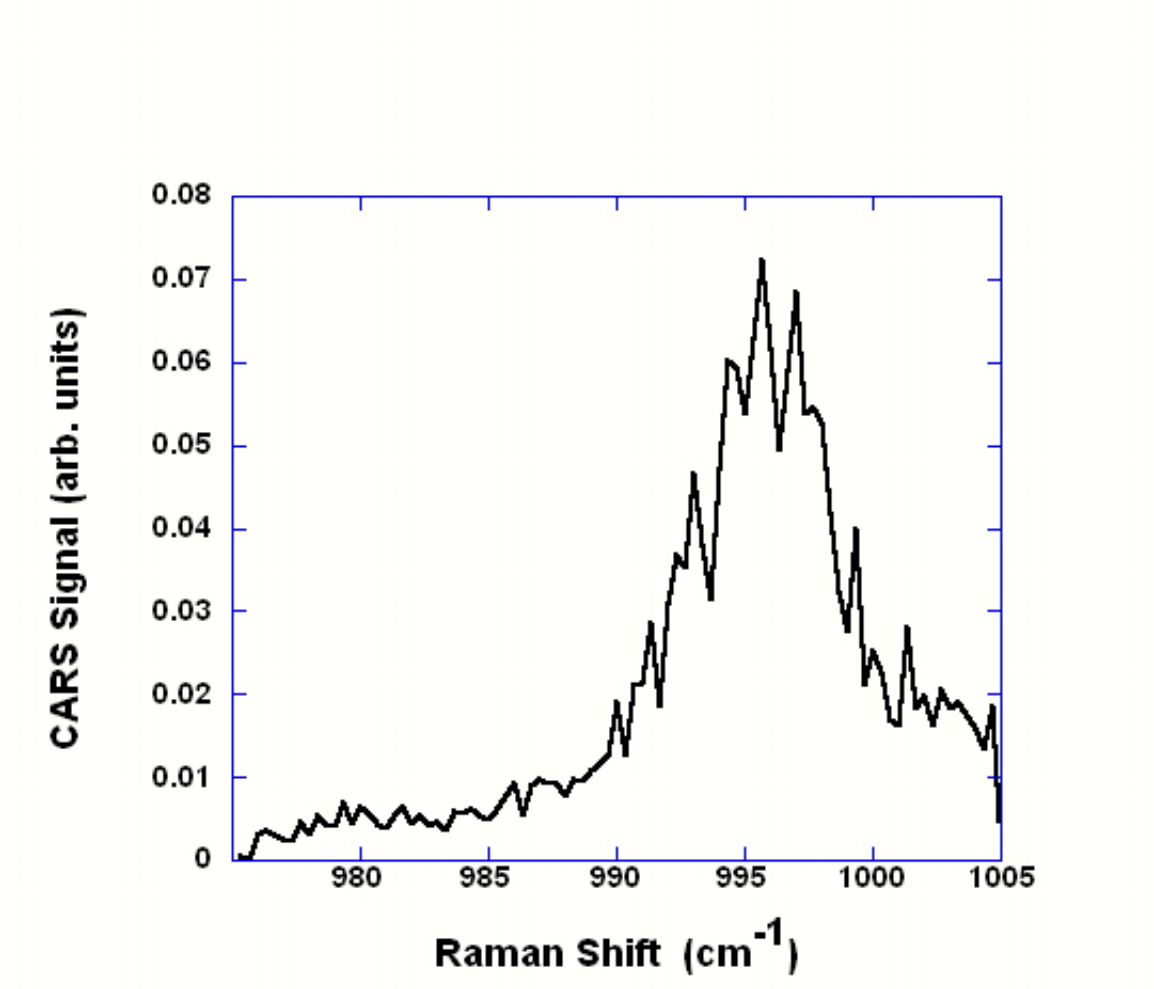

Fig.4.12. DPA spectrum acquired by backscattering CARS configuration.

4.6.3 Experimental Results for DPA CARS in Backscattering Configuration

Figure 4.11 and Figure 4.12 show CARS spectra acquired using the CARS system in backscattering configuration. The scans were performed on two different days to ensure consistency and repeatability. The spectrum features a peak at the same spectral location as for the forward scattering CARS configuration at a Raman shift of 998 cm^{-1}. The intensity of the CARS signal in Fig. 4.11 is much higher than for the other scans, which can be attributed to the quality of the crystal used and the wide collection angle of the single provided by the elliptical aluminum mirror. The general features of the DPA spectra are similar to the forward scattering CARS spectra obtained before.

The angular spatial distribution of the CARS signal collected by the aluminum mirror was investigated and angular scans obtained were modeled using the theory in Hanna et al. (2005) to verify its validity. The spatial distribution was measured using a movable and adjustable rectangular slit placed between the ellipsoid mirror and the fiber. The slit size was 1.5 mm in horizontal direction and was moved in steps of 1.5 mm across the fiber entrance. This corresponds to an angular resolution of 0.017 rad. The main limiting factor for the angular resolution was the need to maintain a reasonable signal-to-noise ratio.

The backscattered radiation was examined in two regimes. In the non-linear regime, the CARS signal was collected using the experimental system described above. The three beams were focused on a spot on the DPA crystal. In the linear regime, the Stokes beam and one of the 532-nm beams were blocked and the other 532-nm was

focused on the same spot where the CARS signal was detected. To detect the 532-nm radiation, the spectrometer was tuned to this wavelength and the 505-interference filter in front of the fiber was removed. The spatial distribution scan in Fig. 4.13 was taken using DPA crystals precipitated from a DPA in DMF solution, while to obtain the data shown in Fig. 4.14 various DPA flakes from heated DPA in water solution were used. To ensure repeatability, both non-linear and linear regimes were probed several times, and for each different DPA crystal two representative cases are shown. In Fig. 4.13, the linear and non-linear regimes exhibit nearly the same scattering features, and this is more evident in Fig. 4.14. This is due to the fact that in both regimes, the scattered radiation results from non-homogeneous spots in the crystals.

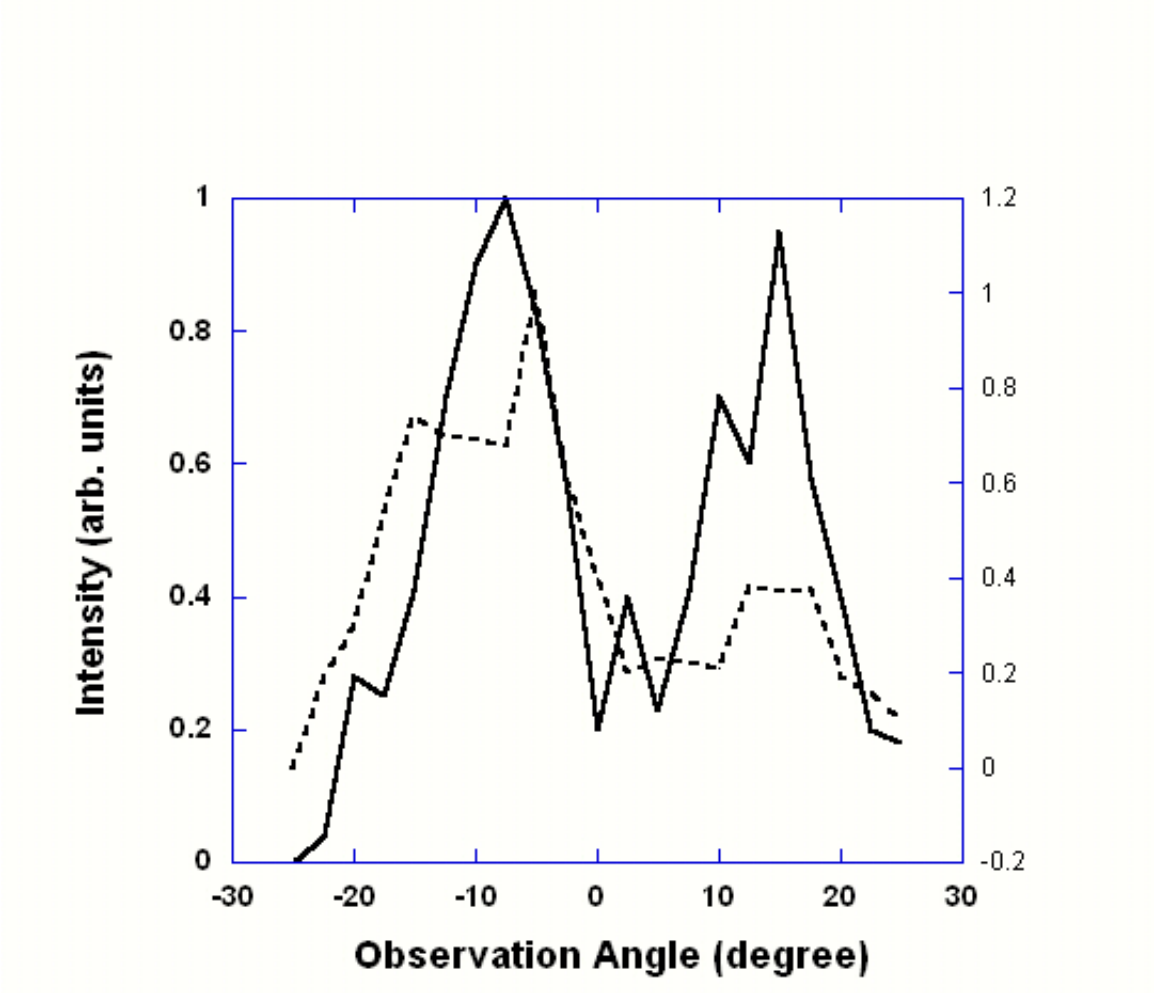

Fig.4.13. Intensity of scattered light (arbitrary units) vs. observation angle. Data taken for a milky crystal. The angular dependence of scattered green light (a) and CARS signal (b) (Hanna et al., 2005).

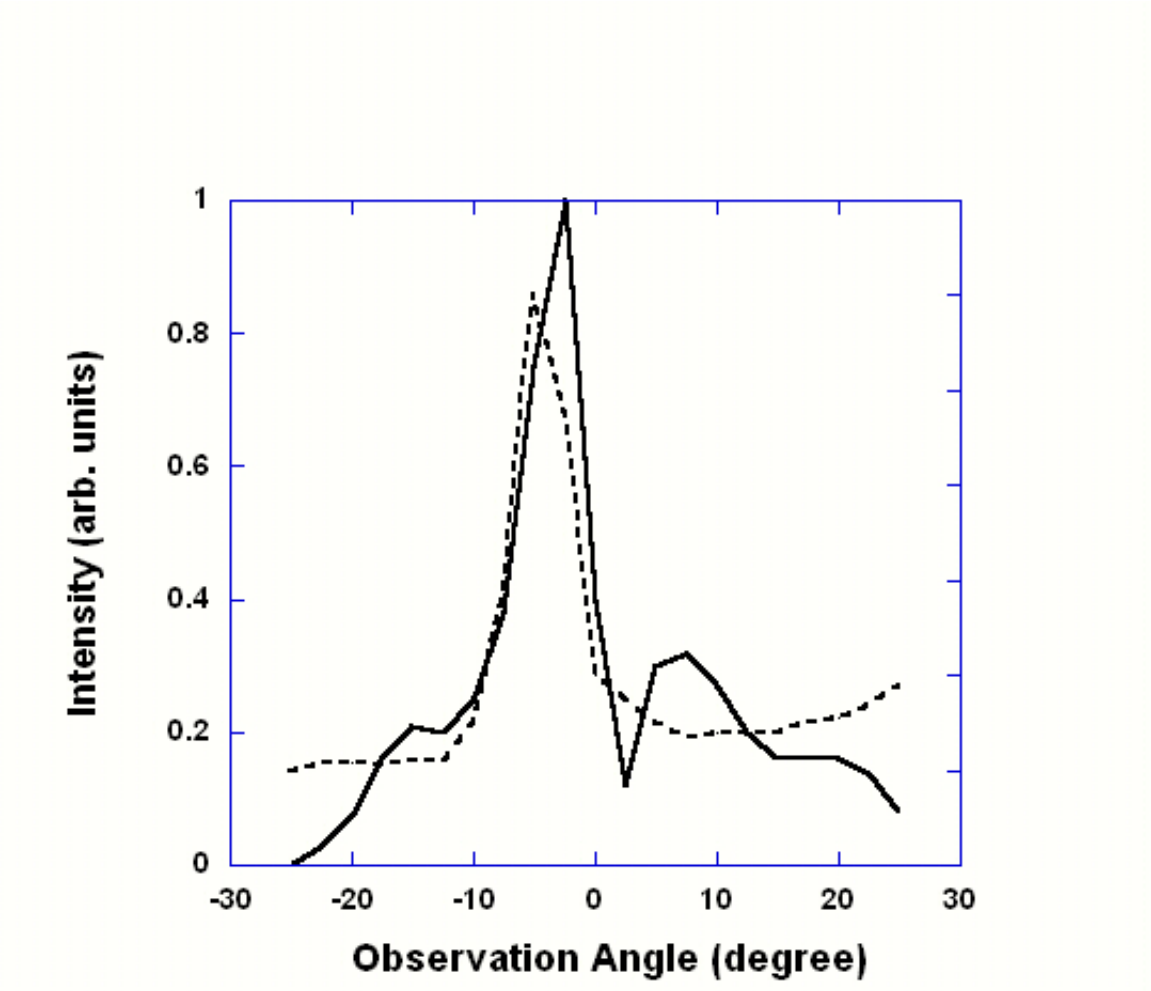

Fig.4.14. Data taken with DPA flakes. The angular dependence of scattered green light (a) and CARS signal (b) (Hanna et al., 2005).

CHAPTER V

CONCLUSIONS AND RECOMMENDATIONS

The investigation of the electronic–resonance-enhanced coherent (ERE) anti-Stokes Raman scattering (CARS) technique for detection and measurement of nitric oxide (NO) and acetylene (C_2H_2) concentration is described in this dissertation. The use of coherent anti-Stokes Raman Scattering for the detection of dipicolinic acid (DPA) is also discussed as the first step for application of ERE CARS for DPA.

5.1. Nitric Oxide

5.1.1. Summary of Results for Nitric Oxide ERE CARS Spectroscopy

In the development and application of the ERE CARS technique to nitric oxide, there were three main objectives as outlined in Chapter II. The first was the design and assembly of the ERE CARS experimental system to perform spectroscopic measurements of NO. Second, the system was to be tested and the experimental parameters refined as a step towards its application to hydrocarbons and DPA. Finally, the experimental results were to be compared with numerical results obtained by modification of the CARSFT computational code for electronic resonance enhancement. Consistent with the objectives, the results are summarized below.

In low pressure region, we have demonstrated the detection of ERE CARS signals from NO in concentrations as low as 100 ppm. Spectral scans were obtained with

fixed Stokes frequency as the ultraviolet pump frequency was varied, and with fixed ultraviolet pump frequency as the Stokes frequency was varied.

The experimental system parameters were improved and experimental complications from different sources such UV scattered light interference and nonresonant background contributions to the spectra obtained were minimized.

In low-pressure region, good agreement between theory and experiment was obtained for both scan methods, either the Stokes beam scans or the UV pump beam scans. The numerical results revealed strong saturation of the ultraviolet transition as the bandwidth for the ultraviolet pump laser was increased to a value of 6 cm^{-1} to obtain good agreement between the experiment bandwidth and theoretical width of resonance lines.

At high NO pressure, the experimental results were complicated by the multimode operation of the injection seeder in the Continuum model 9010 Nd: YAG laser. The inconsistency of the seeder was monitored. Scans with minimum multimode interference were presented. They show excellent spectral resolution and well-defined spectral features.

5.1.2. Recommendations for Future Work Based on NO ERE CARS Results

To continue the development of the ERE CARS technique, many venues could be pursued, with the NO molecule and with other molecules. Some recommendations are presented in this section.

The use of the ERE CARS technique allows us to separate clearly the process by which the Raman coherence is induced in the medium from the ERE process where the Raman coherence is probed with the second pump. This separation simplifies considerably the theoretical modeling of the ERE process, and may enable sensitive, selective detection of small polyatomic molecules and flames.

The high-pressure scans for NO should promise for application of the ERE CARS technique to measure NO concentrations in high-pressure flames, yet definitive conclusions could not be obtained due to multimode operation of the seeder and its interference with the spectra. High – pressure scans are recommended with stable laser operation. Numerical modeling with the modified CARSFT code is recommended as well for high – pressure spectroscopy.

The multimode characteristics of the narrow–band dye lasers used to generate the ultraviolet pump beam and Stokes beam introduced minor, yet undesirable, complications in the spectra. A single–mode ultraviolet source, such as an injection-seeded optical parametrical oscillator (OPO) will eliminate these effects. In addition, the experimental complications attributed to the continuous decline of the ultraviolet pump energy due to decay of the LD 490 dye would be overcome with the development of an OPO.

The development of a single-mode laser source to replace the multimode ultraviolet source will enhance the detection limit greatly. A laser source is developed by R.P. Lucht and coworkers in the School of Mechanical Engineering at Purdue University. A β-BBO optical parametric generator system is seeded at the idler

wavelength with distributed feedback diode laser. The system was tested for single-mode operation and has produced a tunable, pulsed laser radiation at seed wavelengths of 460 nm. The system can be configured to generate signal and idler radiation over the wide ranges by using suitable diode laser for injection-seeding the β-BBO at different seed or idler wavelength.

5.2. Acetylene

5.2.1. Summary of Results for Acetylene ERE CARS Spectroscopy

The transition from nitric oxide to acetylene detection was accomplished by changing the wavelength of the Stokes beam to probe the 1974 cm^{-1} υ_2 Raman transition of C_2H_2. The ultraviolet pump wavelength was varied between 232 nm and 242 nm to generate the ERE CARS signal.

The detection of acetylene using the ERE CARS technique was demonstrated. Very high signal-to-noise ratios were obtained from a calibrated room-temperature mixture of 5000 ppm C_2H_2 in a buffer gas of nitrogen.

The dependence of the spectral line shape and intensity on the probe wavelength was investigated. Below an ultraviolet wavelength of 239 nm, the peak intensity of the ERE CARS spectrum was fairly constant but the shape of the spectrum changed as the ultraviolet wavelength was shifted. The change in the shape of the spectra is due to different electronic resonance interactions in the A-X electronic band. For wavelengths higher than 239 nm, the intensity decrease was rapid. This decrease in signal can be mainly attributed to the reduced electronic resonance effect as the ultraviolet wavelength

increased. In addition, the fifth harmonic YAG mirrors used as spectral filters have an increasing reflectivity for the ERE CARS signal wavelength in this range.

The pressure dependence of the acetylene ERE CARS signal was investigated as well. The ERE CARS signal increased approximately as the square of the pressure. This illustrates a significant advantage of the ERE CARS technique compared to laser-induced-fluorescence (LIF) detection of minor species in high-pressure flames. The ERE CARS signal is approximately proportional to the number density and thus increases significantly as pressure increases, whereas the LIF signal remains constant for the same minor species mole fraction as the pressure is increased.

5.2.2. Recommendations for Future Work Based on C_2H_2 ERE CARS Results

The successful detection of acetylene using the ERE CARS technique indicates the potential of this technique in many areas. Many other hydrocarbon species such as C_3H_8 and diatomic species such as OH and O_2 can be potentially detected using the same technique. In addition, acetylene detection in high-pressure flames using the ERE CARS and LIF techniques will provide an assessment of the potential advantages of ERE CARS over competing laser diagnostic techniques.

Application of the ERE CARS technique to high temperature media should be investigated closer. While the electronic resonance interaction is quite complicated for acetylene because of the structure the A-X band, the electronic resonance interaction will become stronger as the temperature of the medium increases because the electronic transition moment will increase for excited vibrational levels in the ground state as

explained by Williams and Fleming (2002). As such, with higher signal-to-noise ratios, the complicated electronic and Raman spectra of acetylene could be investigated in detail.

5.3. Dipicolinic Acid

5.3.1. Summary of Results for Dipicolinic CARS Spectroscopy

The detection of dipicolinic acid (DPA) using CARS was demonstrated. The 998 cm^{-1} Raman transition of DPA was detected in the forward and backward experimental configurations to assess the applicability of this technique in biological warfare applications for anthrax detection. This transition has very characteristic and sharp spectral features and shows great promise for selective detection of bacterial endospores. In addition, the detection of this transition is facilitated by its benzene-like behavior due to the structure of DPA. This makes the calibration of the experimental system easier by detecting the strong signal of benzene first and then DPA.

The DPA crystals were prepared by precipitation of DPA crystals from a solution in water. The flakes produced were inspected visually and the most transparent crystals that exhibited the minimum number of cracks was used in the CARS probe volume. The lifetime of the DPA crystals under intense laser radiation was short and required the reduction of the laser beams energy to well below 1 mJ to extend the lifetime. Together with reducing the number of experimental scans averaged at each wavelength and the number of steps during the dye laser wavelength scans, it helped to extend the crystal lifetime to survive the scans.

In the backward experimental configuration for DPA detection, the strong scattering of the CARS signal on rough interfaces between crystal layers in the polycrystalline medium was collected by an elliptical aluminum mirror and focused into a fiber optical waveguide. The angular distribution of the scattered CARS signal on the aluminum mirror was determined and used to determine the characteristic spatial size of inhomogeneities of the crystal.

5.3.2. Recommendations for Future Work Based on DPA CARS Results

The successful detection of various molecules such as NO and C_2H_2 using ERE CARS and the experience gained with the experimental system should be invested in detecting DPA using ERE CARS. Having detected DPA with two 532-nm pump beams and a 561-nm Stokes beam in a "normal" CARS experiment, the experimental considerations for DPA CARS spectroscopy are better understood.

Preparing DPA crystals by precipitation from DPA solution in dimethylformamide (DMF) showed promising results. Instead of flakes, solid crystals were obtained and showed promise in extending the lifetime of the crystal. Many parameters such as the thickness and surface quality can be more controlled with these crystals. The crystal with better qualities should be used for ERE CARS for DPA detection. The results obtained in the backward configuration can be applied to improve LIDAR system performance.

REFERENCES

Abramson, E., Field, R.W., Imre, D., Innes, K.K., and Kinsey, J.L. (1984) Stimulated emission pumping of acetylene: Evidence of quantum chaotic behavior near 27900 cm^{-1} of excitation? *J. Chem. Phys.,* **80** (6), 2298 -2300.

Alnis, J., Gustafsson, U., Somesfalean, G., and Svanberg, S. (2000) Sum-frequency generation with a blue diode laser for mercury spectroscopy at 254 nm. *Appl. Phys.,* **76**, 1234-1236.

Anderson, T. (2003) The development and application of a diode-laser-based ultraviolet absorption sensor for nitric oxide. Master's Thesis, Texas A&M University, College Station, TX.

Anderson, T.N., Lucht, R.P., Barron-Jimenez, R., Hanna, S.F., Caton, J.A., Walther, T., Roy, S., Brown, M.S., Gord, J.R. Critchley, I., and Flamand, L. (2005) Combustion exhaust measurements of nitric oxide with an ultraviolet diode-laser-based absorption sensor. *Appl. Opt.,* **44** (8), 1491-1502.

Attal-Tretout, B., Shnepp, O.O., and Taran, J-P. (1977) Resonant CARS in I_2 vapor. *Opt. Comm.,* **24**, 77-82.

Attal-Tretout, B., Schmidt, S., Crete, E., Dumas, P., and Taran, J-P. (1990) Resonance CARS of OH in high pressure flames. *Quant. Spectrosc. Radiat. Transf.,* **43** (5), 351-364.

Barrett, J.J., and Begley, R.F. (1981) Photoacoustic Raman spectroscopy of gases. In Harvey, A.B. (Ed.) *Chemical Applications of Nonlinear Raman Spectroscopy*. Academic Press, New York, pp. 89-169.

Baum, M.M., Kumar, S., Lappas, A.M., and Wagner, P.D. (2003) Measurement of acetylene in breath by ultraviolet absorption spectroscopy: Potential for noninvasive cardiac output monitoring. *Rev. Sci. Instru.*, **74** (6), 3104-3110.

Bessler, W.G., Schulz, C., Lee, T., Shin, D.I., Hofmann, M., Jeffries, J.B., Wolfrum, J., and Hanson, R.K. (2002) Quantitative NO-LIF imaging in high-pressure flames. *Appl. Phys. B,* **75**, 97-102.

Black, J. (2002) *Microbiology: Principles and Explorations*. Wiley, New York.

Bree, A., and Kydd, R.A. (1970) Vibrational spectra and assignment of naphthalene-d_8. *Spectochimica Acta,* **26**A, 1791-1803.

Callomon, J.H., Dunn, T.M., and Mills, I.M. (1966) Rotational analysis of the 2600 angstrom absorption system of benzene. *Philosophical Transactions of the Royal Society of London. Series A, Mathematical and Physical Sciences,* **259** (114), 499-532.

Carmona, P. (1979) Vibrational spectra and structure of crystalline dipicolinic acid and calcium dipicolinate trihydrate. *Spectrochimica Acta*, **36**A, 705-712.

Chang, A.Y., DiRosa, M.D., and Hanson, R.K. (1992) Temperature dependence of collision broadening and shift in the NO A ← X (0, 0) band in the presence of argon and nitrogen. *J. Quant. Spectrosc. Radiat. Transfer,* **47**(5), 375-390.

Charleston-Goch, D., Chadwick, B.L., Morrison, R.J, Campisi, A., Thomsen, D.D., and Laurendeau, N.M. (2001) Laser-induced fluorescence measurements and modeling of nitric oxide in premixed flames of $CO+H_2+CH_4$ and air at high pressures. *Combustion and Flame*, **125**, 729-743.

Cheng, Y.S., Barr, E.B., Fan, B.J., Hargis, P.J., Rader, D.J., O'Hern, T.J., Torczynski, J.R., Tisone, G.C., Preppernau, B.L., Young, S.A., and Radloff, R.J. (1999) Detection of bioaerosols using multiwavelength UV fluorescence spectroscopy. *Aerosol Science and Technology,* **30**, 186-201.

Colls, J. (2002) *Air Pollution*. 2nd edition, Spon Press, New York.

Cooper, C.S., and Laurendeau, M. (2000) Quantitative measurements of nitric oxide in high-pressure (2-5 atm), swirl stabilized spray Flames via laser-induced fluorescence. *Combustion and Flame,* **12**, 175-188.

Corner, L., Gibb, J.S., Hancock, G., Hutchinson, A., Kasyutich, V.L., Peverall, R., and Ritchie, G.A. (2002) Sum frequency generation of 309 nm using a violet and a near-IR DFB laser for detection of OH. *Appl. Phys. B,* **74**, 441-444.

Decola, P.L., Hochstrasser, R.M., and Trommsdorf, H.P. (1980) Vibrational relaxation in molecular crystals by four-wave mixing: Naphthalene". *Chem. Phys. Lett.,* **72** (1), 1-4.

Demtroder, W. (1996) *Laser Spectroscopy*. 2nd Edition, Springer-Verlag, New York.

Deng, L., Garrett, W.R., and Payne, M.G. (1997) Pressure dependence of the ac Stark shifts in nitric oxide: resonant multiphoton spectroscopy without space charge. *Chem. Phys. Lett.,* **271**, 15-18.

Dlott, D.D., Schosser, C.L., and Chronister, E.L. (1982) Temperature-dependent vibrational dephasing in molecular crystals: A picosecond CARS study of naphthalene. *Chem. Phys. Lett.,* **90** (5), 386- 390.

Doerk, T., Jauernik, P., Handrich, S., Phelzer, B., and Uhlenbusch, J. (1995) Resonance enhanced CARS applied to the CH radical. *Opt. Comm*., **118**, 637-647.

Doerk, T., Hertl, M., Phelzer, B., Handrich, S., Jauernik, P., and Uhlenbusch, J. (1997a) Resonance enhanced coherent anti-Stokes Raman scattering and laser-induced fluorescence applied to CH radicals: A Comparative study. *Appl. Phys. B,* **64**, 111- 118.

Doerk, T., Ehlbeck, J., Jedamzik, R., Uhlenbusch, J., Hoeschele, J., and Steinwandel, J. (1997b) Application of coherent anti-Stokes Raman scattering (CARS) technique to the detection of NO. *Appl. Spectrosc.,* **51**(9), 1360-1368.

Druet, S.A., Attal, B., Gustafson, T.K., and Taran, J.P. (1978) Electronic resonance enhancement of coherent anti-Stokes Raman scattering. *Phys. Rev. A,* **18**, 1529-1557.

Druet, S.A., and Taran, J.P. (1981) CARS spectroscopy. *Prog. Quant. Elec.,* **7**, 1-71.

Dugan, M.A., Melinger, J.S., and Albrecht, A.C. (1988) Tetrahertz oscillations from molecular liquids in CSRS/CARS spectroscopy with incoherent light. *Chem. Phys. Lett.,* **147** (5), 411-419.

Ebata, T., Mikami, N., and Ito, M. (1983) Highly excited states of nitric oxide studied by two-color double resonance spectroscopy. *J. Chem. Phys.,* **78** (3), 1132-1139.

Eckbreth, A.C. (1995) *Laser Diagnostics for Combustion Temperature and Species*. 2nd Edition, Gordon and Breach, Amsterdam, The Netherlands.

Fujimoto, J.G., and Yee, T.K. (1983) Diagrammatic analysis of the third order nonlinear optical processes. *IEEE J. Quant. Elec.,* **QE-19**, 861-872.

Furlong, E.R., Mihalcea, R.M., Webber, M.E., Baer, D.S., and Hanson, R.K. (1999) Diode-laser sensors for real-time control of pulsed combustion system. *AIAA J.,* **37**, 732-737.

Ghiamati, E., Manoharan, R., Nelson, W.H., and Sperry, J.F. (1992) UV resonance raman spectra of bacillus spores. *Applied Spectroscopy,* **46** (2), 357-364.

Gillen, K.T., and Griffiths, J.E. (1972) Molecular reorientations in liquid benzene: Raman line shapes and ^{2}D NMR relaxations. *Chem. Phys. Lett.,* **17** (3), 359-364.

Griffiths, J.E., Clerc, M., and Rentzepis, P.M. (1974) Intermolecular energy transfer in liquid benzene: Raman spectra, linewidth measurements, picosecond spectroscopy, and vibrational relaxation times. *J. Chem. Phys.,* **60** (10), 3824-3830.

Gustafson, E.K., McDaniel, J.C., and Byer, R.L. (1982) High-resolution continuous-wave coherent anti-Stokes Raman spectroscopy in a supersonic Jet. *Opt. Lett.*, **7**, 434-436.

Hancock, G., Kasyutich, V.L., and Ritchie, G.D. (2002) Wavelength-modulation spectroscopy using a frequency-doubled current-modulated diode laser. *Appl. Phys. B,* **74**, 569-575.

Hanna, S.F., Barron-Jimenez, R., Anderson, T.N., Lucht, R.P., Caton, J.A., and Walther, T. (2002) Diode-laser-based ultraviolet absorption sensor for nitric oxide. *Appl. Phys. B,* **75**, 113-117.

Hanna, S.F., Kulatilaka, W.D., Arp, Z., Opartny, T., Scully, M.O., Kuehner, J.P., and Lucht, R.P. (2003) Electronic-resonance-enhanced (ERE) coherent anti-Stokes Raman scattering (CARS) spectroscopy of nitric oxide. *Appl. Phys. Lett.,* **83** (9), 1887-1889.

Hanna, S.F., DuBois, J.R., and Lucht, R.P. (2004) Electronic-resonance-enhanced coherent anti-Stokes Raman spectroscopy of acetylene. *Third Technical Meeting of the Central States Section of the Combustion Institute,* March 2004, Austin, TX.

Hanna, S.F., Lei, W., Sariyanni, Z.E, Kalugin, N., Lucht, R., Sautenkov, V., Sokolov, A., Rostovtsev, Y., and Scully, M.O. (2005) Observation of coherent anti-Stokes scattering signal in phase-mismatched direction." *Journal of Optical Society of America B,* accepted for publication.

Herzberg (1945) *Infrared and Raman Spectra of Polyatomic Molecules*. Van Nostrand Reinhold Co., New York.

Hinds (1999) *Aerosol Technology: Properties, Behavior, and Measurement of Airborne Particles*. 2nd Edition, Wiley, New York.

Huo, W.M., Gross, K.M., and McKenzie, R.L. (1985) Optical Stark effect in the two-photon spectrum of NO. *Phys. Rev. Lett.,* **54** (10): 1012-1015.

Joo, T., and Albrecht, A.C. (1991) Time-resolved coherent Stokes Raman spectroscopy (CSRS) of benzene. *Chem. Phys. Lett.,* **177** (1), 4-10.

Joo, T., and Albrecht, A.C. (1993) Femtosecond time-resolved coherent anti-Stokes Raman spectroscopy of liquid benzene: A Kubo relaxation function analysis. *J. Chem. Phys.,* **99** (5), 3244-3251.

Kessler, W.J. and Sonnenfroh, D.M., Upschulte, B.L., and Allen, M.G. (1997) Near-IR diode lasers for in-situ measurements of combustor and aero engine emissions. *33rd*

AIAA/ASME/SAE/ASEE Joint Propulsion Conference, Paper AIAA 97-2706, July 1997, Seattle, WA.

Khadiya, N., and Glumac, N.G. (2001) Catalytic removal of NO from post-flame gases in low pressure stagnation-point flames over platinum. *Combustion and Flame,* **125**, 931-941.

Koplow, J.P., Kliner, D.V., and Goldberg, L. (1998) Development of narrow-band, tunable, frequency-quadrupled diode laser for UV absorption spectroscopy. *Appl. Opt.,* **37**, 3954-3960.

Kosterev, A.A., Molinovsky, A.L., Tittel, F.K., Gmachl, C., Capasso, F., Sivco, D.L., Baillargeon, J.N., Hutchinson, A.L., and Cho, A.Y. (2001) Cavity ringdown spectroscopic detection of nitric oxide with continuous-wave quantum-cascade laser. *Appl.Opt*., **40**, 5522-5529.

Laane, J., and Kiefer, W. (1980) Interference effects in the high resolution CARS spectra of gases. *J. Raman Spectrosc*., **90** (6), 353-360.

Lempert, W., Rosasco, G.J., and Hurst, W.S. (1984) Rotational collisional narrowing in the NO fundamental Q branch, studied by cw stimulated Raman spectroscopy. *J. Chem. Phys.,* **81** (10), 4241-4245.

Lucht, R.P., Farrow, R.L., and Palmer, R.E. (1986) Acetylene measurements in flames by coherent anti-Stokes Raman scattering. *Combust. Sci. and Tech.,* **45**, 261-274.

Lucht, R.P. (1987) Three-laser coherent anti-Stokes Raman scattering measurement of two species. *Opt. Lett.,* **12** (2), 78-80.

Lucht, R.P., Velur, V.N., Carter, C., Grinstead, K., Gord, J., Danehy, P., Fietchner, G., and Farrow, R. (2003) Dual-pump coherent anti-Stokes Raman scattering temperature and CO_2 concentration measurement. *AIAA J.,* **41** (4), 679-685.

Luque, J., and Crosley, D.R. (1999a) Transition probabilities and electronic transition moments of the $A^2\Sigma^+$-$X^2\Pi$ and $D^2\Sigma^+$-$X^2\Pi$ systems of nitric oxide. *J. Chem. Phys*., **111** (16), 7405-7415.

Luque, J., and Crosley, D.R. (1999b) *LIFBASE: Database and Spectral simulation Program (Version 1.5)*. SRI International Report MP 99-009, Stanford Research Institute, Menlo Park, CA.

Macher, J.M. (1995) Sampling airborne microorganisms and aeroallergens. In Cohen, B.C., and Hering, S.V. (Eds.) *Air Sampling Instruments*, 8th ed., American Conference of Governmental Industrial Hygienists, Cincinnati, OH.

Macnaughton, S.J., Jenkins, T.L., Alugupolli, S., and White, D.C. (1997) Quantitative sampling of indoor air biomass by signature lipid biomarker analysis: Feasibility studies in a model system. *Am. In. Hyg. Assoc. J.,* **58**, 270-277.

Manoharan, R., Ghiamati, E., Dalterio, R.A., Britton, K.A., Nelson, W.H., and Sperry, J.F (1990) UV resonance Raman spectra of bacteria, bacterial spores, protoplasts and calcium dipicolinate. *Journal of Microbiological Methods,* **11**:1-15.

Marowsky, G., Gierulski, A., and Dick, B. (1986) Experimental study of vibrational and pure rotational coherent anti-Stokes Raman scattering (CARS) in molecular hydrogen. *Appl. Phys. B*, **39**, 47-53.

Menzel, L., Kosterev, A.A., Curl, R.F., Tittel, F.K., Gmachl, C., Capasso, D.L., Sivco, J.N., Baillargeon, J.N., Hutchinson, A.L., Cho, A.Y., and Urban, W. (2001) Spectroscopic detection of biological NO with quantum cascade lasers. *Appl. Phys. B*, **72**, 859-863.

Mihalcea, R.M., Baer, D.S., and Hanson, R.K. (1998) A diode-laser absorption sensor system for combustion emission measurements. *Meas. Sci. Technol*. **9**, 237-338.

Naik, S.V., and Laurendeau, N.M. (2002) Quantitative laser-saturated fluorescence measurements of nitric oxide in counter-flow diffusion flames under sooting Oxy-fuel conditions. *Combustion and Flame,* **12**, 112-119.

Nevalainen, A., Willeke, K., Liebhaber, F., and Pastuszka, J. (1993) Bioaerosol sampling. In Willeke, K., and Baron, P.A., (Eds.) *Aerosol Measurements.* Van Nostrand Reinhold, New York.

Nibler, J.W., and Knighten, G.V. (1979) Coherent anti-Stokes Raman spectroscopy. In Weber (Ed.) *Raman Spectroscopy of Gases and Liquids*. Springer-Verlag, Berlin, pp. 253-299.

Nieto-Vesperinas, M. (1990) *Scattering in Volumes and Surfaces*. North Holland, Amsterdam.

O'Brien, J.P., Jacobson, M.P., Sokol, J.J., Coy, S.L., and Field, R.W. (1998) Numerical pattern recognition analysis of acetylene dispersed fluorescence spectra. *J. Chem. Phys.,* **108** (17), 7100-7113.

Oh, D.B., and Stanton, A.C. (1997) Measurement of nitric oxide with an antimonide diode laser. *Appl. Opt.,* **36**, 3295-3297.

Orduna, F., Domingo, C, Montero, S., and Murphy, W.F. (1982) Gas phase Raman intensities of C_2H_2, C_2HD and C_2D_2. *Mol. Phys*., **45**, 64-82.

Palmer, R.E. (1989) *The CARSFT Computer Code for Calculating Coherent anti-Stokes Raman Spectra: User and Programmer Information*. Sandia National Laboratories Report SAND89-8206.

Paul, P.H. (1997) Calculation of transition frequencies and rotational line strengths in the γ-Bands of nitric oxide. *J. Quant. Radiat. Transf.,* **57** (5), 581-589.

Phan, H.N., and McFarland, A.R (2004) Aerosol-to-hydrosol transfer stages for use in bioaerosol sampling. *Aerosol Science and Technology,* **38** (4), 300-310.

Piper, L.G., and Cowles, L.M. (1986) Einstein coefficients and transition moment variation for the NO ($A^2\Sigma^+$ -$X^2\Pi$) transition. *J. Chem. Phys.,* **85**(5), 2419-2422.

Pott, A., Doerk, T., Uhlenbusch, J., Ehlbeck, J., Hoeschele, J., and Steinwandel, J. (1998) Polarization-sensitive coherent anti-Stokes Raman scattering applied to the detection of NO in a microwave discharge for reduction of NO. *J. Phys. D,* **31**, 2485-2498.

Pratt, S.T. (1989) Pressure dependence of the ac Stark effect in nitric oxide. *Phys. Rev. A,* **39** (9), 4877-4879.

Prior, Y. (1984) A complete expression for the third-Order susceptibility ($\chi^{(3)}$) – perturbative and diagrammatic approaches. *IEEE J. Quant. Elec.,* **QE-20**, 37-42.

Ray, G.I., Anderson, T.N., Caton, J.A., Lucht, R.P., and Walther, T.H. (2001) OH sensor based on ultraviolet, continuous-wave absorption spectroscopy utilizing a frequency-quadrupled, fiber-amplified external-cavity diode laser. *Opt. Lett.,* **26**, 1870-1872.

Regnier, P.R., and Taran, J.P.E. (1974) On the possibility of measuring gas concentrations by stimulated anti-Raman scattering. *Appl. Phys. Letts*., **23**, 240-242.

Rahn, L.A., Zych, L.J., and Mattern, P.L. (1979) Background-free CARS studies of carbon monoxide in a flame. *Opt. Comm.,* **30** (2), 249-252.

Rim, Y.H., Haus. J.W., and Schroeder, J. (1990) Forward and backward scattering of light in inhomogeneous media. *Phys. Rev. A,* **42** (4), 2385- 2400.

Scully, M.O., Kattawar, G.W., Lucht, R.P., Opartny, T., Pilloff, H., Rebane, A., Sokolov, A.V., and Zubairy, M.S. (2002) FAST CARS: Engineering a laser spectroscopic technique for rapid identification of bacterial spores. *Proc. Natl. Acad. Sci.,* **99** (17), 10994-11001.

Seaver, M., Eversole, J.D., Hardgrove, J.J., Cary, W.K., and Roselle, D.C. (1999) size and fluorescence measurements for field detection of biological aerosols. *Aerosol Science and Technology*, **30**, 174-185.

Sonnenfroh, D.M., and Allen, M.G. (1997) Absorption measurements of the second overtone band of NO in ambient and combustion gases at 1.8-μm room temperature diode laser. *Appl. Opt.,* **36**, 7970-7977.

Suzuki, M., Yokoyama, T., and Ito, M. (1968) Polarized Raman spectra of naphthalene and anthracene single crystals. *Spectrochimica Acta,* **24** A, 1091-1107.

Tanabe, K., and Jonas, J. (1977) Raman study of vibrational relaxation in liquid benzene-d_6 at high pressure. *J. Chem. Phys.,* **67** (9), 4222-4228.

U.S. EPA Office of Air Quality Planning and Standards (2000) *National Air Pollutant Emission Trends, 1900-1998*. U.S. Environmental Protection Agency Report EPA-454/R-00-002.

Van Craen, J.C., Herman, M., Colin, R., and Watson, J.K.G. (1985) The A-X band system of acetylene: Analysis of medium-wavelength bands, and vibration-rotation constants for the levels $n\upsilon'_3$ (n = 4-6), and $\upsilon'_2 + n\upsilon'_3$ (n = 3-5), and $\upsilon'_1 + n\upsilon'_3$ (n = 2, 3). *J. Mol. Spectrosc.*, **111**, 185-197.

Vaught Engineering Incorporation (1999) Low-NOx Measurement: *Gas Turbine Plants. Final Report on Review of Current Measuring and Monitoring Practices*. ASME International, Center for Research and Technology Development Report CRTD Vol.52.

Voronovich, A.G. (1994) *Wave Scattering from Rough Surfaces*. Spring-Verlag, Berlin.

Wang, D.X., Haridass, C., and Reddy, S.P. (1996) The gamma ($A^2\Sigma^+ - X^2\Pi_r$) system of the nitric oxide isotopomers. *J. Mol. Spectrosc.,* **175**, 73-84.

Watson, J.K.G, Herman, M, Van Craen, J.C., and Colin, R. (1982) The A-X band system of acetylene: Analysis of long-wavelength bands, and vibration-rotation constants for the levels $n\upsilon''_4$ (n = 0-4), $n\upsilon'_3$ (n = 0-3), and $\upsilon'_2 + n\upsilon'_3$ (n = 0-2). *J. Mol. Spectrosc.,* **95**, 101-132.

Watson, J.K.G. (2001) Calculated vibrational intensities in the A-X electronic transition of acetylene". *J. Mol. Spectrosc.,* **207**, 276-284.

Wen, X., Chen, S., and Dlott, D.D. (1991) Time-resolved three-color coherent Raman scattering applied to polycrystalline and opaque solids". *Journal of Optical Society of America B.,* **8** (4), 813-819.

Willeke, L., and Macher, J.M. (1998) Air sampling. In Macher, J.M. (Ed.) *Bioaerosols: Assessment and Control*, American Conference of Governmental Industrial Hygienists, Cincinnati, OH.

Williams, B.A., and Fleming, J.W. (2002) Laser-induced fluorescence detection of acetylene in low-pressure propane and methane flames. *Appl. Phys. B.,* **75**, 883-890.

Wysong, I.J., Jeffries, J.B., and Crosley, D.R. (1989) Laser-induced fluorescence of O ($3p^3P$), O_2, and NO near 226 nm: photolytic interferences and simultaneous excitation in flames. *Opt. Lett.,* **14** (15), 767-769.

Yamanouchi, K., Ikeda, N., Tsuchiya, S., Jonas, D.M., Lundberg, J.K., Adamson, G.W., and Field, R.W. (1991) Vibrationally highly excited acetylene as studied by dispersed fluorescence and stimulated emission pumping spectroscopy: Vibrational assignment of the feature states. *J. Chem. Phys.,* **95** (9), 6330-6342.

Yarkoni, E., and Prior, Y. (1984) Exact and approximate expressions for $\chi^{(3)}$ in CARS diagnostics measurements. *IEEE J. Quant. Elect.,* **QE-20**, 43-47.

Zinth, W., Nuss, M.C., and Kaiser, W. (1982) A new Raman technique of superior spectral resolution. *Chem. Phys Lett.,* **88** (3), 257-261.

VITA

Sherif Fayez Hanna was born on January 18, 1974, in Bonn, Germany, to Fayez and Nadia Hanna. He attended the German School in Cairo, Egypt from 1978 to 1992. In 1991, he received the DAAD merit award by the German International Academic Institute for academic excellence. After graduating from the German High School in 1992 with highest honors on the national level, he attended Cairo University from 1992 till 1997. He earned a B.Sc. in Mechanical Engineering in July 1997, graduating top of class with graduation appreciation of distinction with highest honors. He was the recipient of the Cairo University scholarship for academic excellence from 1992 – 1997, the DAAD merit award for outstanding academic achievement in 1995 and EGAT merit award in 1997 for his outstanding graduation project. After graduation, Sherif worked as an assembly line manager in Proctor and Gamble from Sep.1997 till Dec. 1998. In 1999, he attended Texas A&M University where he joined the Laser Diagnostics Laboratory. He obtained his M.S. degree in December, 2001 and his Ph.D. degree in August, 2005. His research advisor throughout his M.S. and Ph.D. research was Professor Robert P. Lucht. His work has concentrated on investigating the physics of different laser diagnostics techniques, both theoretically and experimentally, and development of industrial sensors for detection of various molecules. He developed a sensor for detection of nitric oxide that currently in the process of being patented. In addition, he worked as a teaching assistant in spring and summer of 1999 and spring of 2005, teaching senior level thermodynamics and heat transfer. He currently resides in 77 Finch Avenue, Apt. #746B, North York, Ontario M2N 6H8, Canada.